UNIVERSITY OF SOUTHAMPTON

CARBON-BASED NEGATIVE ELECTRODES FOR LI-ION BATTERIES

ADAM HARDING WHITEHEAD BA GRSC

DOCTOR OF PHILOSOPHY

FACULTY OF SCIENCE

CHEMISTRY

APRIL 1997

UNIVERSITY OF SOUTHAMPTON

ABSTRACT

FACULTY OF SCIENCE

CHEMISTRY

Doctor of Philosophy

CARBON-BASED NEGATIVE ELECTRODES FOR LI-ION BATTERIES

By Adam Harding Whitehead

It appears likely that the increasing demand for high energy density, high power density, rechargeable power sources will be met, at least partly, by batteries with lithium-insertion electrodes. This research was aimed at elucidating the irreversible electrode processes and factors influencing the cycling kinetics of carbon-based Li-ion battery negative electrodes.

Monolithic electrodes were used as model systems to examine: the reactivity of plated lithium metal towards prospective electrode backing materials and electrolytes, film formation in solutions of $LiAsF_6$ and $LiCF_3SO_3$ in ethylene carbonate (EC)/ diethyl carbonate (DEC) or propylene carbonate (PC) on polarised glassy carbon, film formation and intercalation into the edge and basal planes of oriented pyrolytic carbon electrodes and the kinetics of lithium intercalation into graphite from a $LiCF_3SO_3$/ EC/ DEC electrolyte.

A Fourier transform impedance technique was developed, to examine electrode processes during galvanostatic cycling, and demonstrated on graphite and coke powder electrodes in PC-based electrolytes.

Pulsed galvanostatic cycling was used to explore the relationships between reversible electrode capacity and binder concentration, irreversible capacity and conductivity additive, and insertion capacity and stack pressure.

The kinetics of lithium-graphite phase interconversion were examined by X-ray diffraction. The relationship between insertion kinetics and the insertion/ extraction profile was examined through dx/dV vs. V plots, in heated $LiCF_3SO_3$/ EC and $LiCF_3SO_3$/ EC/ DEC electrolytes.

Contents

Acknowledgements

I would like to thank:

Dr John Owen for his supervision and incisive, constructive comments; Dr Emmanuel Eweka for distilling the solvents and for his eternal patience; Prof. Josh Thomas and Dr Kristina Edström for their hospitality, assistance and trust with regards to their X-ray equipment; Dr Martin Hardgrave, Dr Ningling Rao and Dr Steen Yde-Anderson for their time and encouragement; Dr James Rohan and Mr Mark Perkins for helpful discussions of all things lithium; Mr Mike Pilling and Mr Nick Gray for continually updating all of the computer software; Dr Ian Brotherston for assistance with moving detector XRD measurements; Mr Alistair Clark for SEM images; Mr Chris Middleton for modelling a telephone box so convincingly.

I would like to thank for material assistance:

the EC Joule III project for funding; GS Inorganics Ltd. for Lonza carbon samples; Cabot Carbons for carbon black samples; Danionics A/S for their hospitality and many samples, including EPM rubber and coke powder electrodes.

For just being there:

Miss Gill Vernon, Dr Saccha Johnson, Dr Steve Nugues, Mr Steve Perkins, Dr Simon Kilvington, Mr Nick Houlton and the rest of you ...

For being, wherever you are:

Mr Xu Ming, Mr Remi Aubree, Dr J.P. Raincoat , Bill & Ben, ...

A. Whitehead

A.H. Whitehead

April 1997

Abbreviations

SI units have been used throughout with their standard abbreviations. The following abbreviations have also been used:

α gradient between insertion and relaxation transients

ν scan rate

ζ cycling efficiency

η overpotential

Θ i) x-ray glancing angle ii) angle of optical illumination

λ wavelength

μ chemical potential

σ standard deviation

ε permittivity

τ time constant for diffusion

ρ_{area} mass per unit area

ω angular frequency

12-crown-4 1, 4, 7, 10-tetraoctacyclododecane

A i) Ampere ii) Area iii) Beer-Lambert absorption coefficient

a a variable

Å Angström, 1 Å $\equiv 10^{-10}$ m

AA standard battery size

AAA standard battery size

AC alternating current

ADC analogue to digital converter

b a variable

B full-width half-maximum of an X-ray diffraction peak

C i) standard battery size ii) Coulomb iii) number of components iv) capacitance v) charge rate, corresponding to completely charging a cell in one hour at 100 % efficiency

chap. chapter

CPE	constant phase element
ct	charge transfer
d	dieletric film thickness
D	i) standard battery size ii) rate of diffusion
d_x	interlayer spacing
DEC	diethyl carbonate
dl	double layer
DOD	depth of discharge
E	i) energy ii) potential
EC	ethylene carbonate
EPM	ethylene propylene copolymer
Eqn.	equation
f	frequency
F	i) degrees of freedom ii) Farad
f.s.	full scale
FCx	type of coke powder with x micron maximum particle size
Fig.	figure
FRA	frequency response analyser
FT	Fourier transform
FTIR	Fourier transform infra-red
FWHM	full-width half-maximum
GIC	graphite intercalation compound
i	current
I/O	input/ output
j	current density
KSx	type of graphite powder with x micron maximum particle size
L	crystallite size
l	diffusion length
m	i) milli- ii) metre iii) mass iv) refractive index
M	mole dm^{-3}
MAAx	type of graphite powder with x micron maximum particle size
mAh	milliampere-hour ≡ 3.6 C
n	i) harmonic index ii) number of measurements iii) order of a

constant phase element

NHE normal hydrogen electrode

Ni-Cd nickel-cadmium battery

NMP 1-methyl-2-pyrrilodinone

OCV open circuit voltage

OPC oriented pyrolytic carbon

P i) number of phases ii) proportion of active material

PC propylene carbonate

PP3 standard battery size

ppm parts per million

PSD position sensitive detector

PSU power supply unit

PTFE polytetrafluoroethylene

PVDF polyvinyldiene fluoride

q charge

Q charge per unit area

Q charge per unit mass

R i) resistance ii) gas constant

RTP room temperature and pressure

s i) second ii) Laplace 'frequency' term

SFGx type of graphite powder with x micron maximum particle size

SLI starting, lighting and ignition

t i) time ii) crystallite thickness

T temperature

triglyme triethylene glycol dimethyl ether

UV/ vis ultra-violet/ visible

V voltage

vs. versus

w/o percentage by weight

Wh Watt-hour ≡ 3.6 kJ

x insertion coefficient, for Li_xC_6, a minimum of 372 mAh g^{-1} of inserted charge would be required for x to increase by 1

XC72 type of carbon black

XRD	X-ray diffraction
y	normalised insertion coefficient
Y_0	constant phase element prefactor
Z	impedance
Z'	resistance
Z''	reactance
ZEV	zero-emmission vehicle
Z_w	Warburg impedance

Chapter 1

Introduction

1.1 Batteries and Cells

" ... and we obtain that magnificent instrument of philosophic research, the voltaic battery." [1]

1.1.1 Demand: The Battery Market

Electrochemical power sources are a vital component in a wide range of devices, with a worldwide market exceeding 10^{10} pounds sterling/ year [2].

The large range of batteries and cells may be considered by size:

i) The smallest power supplies are often in the form of primary (non-rechargeable) button or coin cells. Button cells, available in a wide range of sizes (typically 1.5 - 6 mm high, with a diameter of 5 - 20 mm [3]), are employed in cameras, watches, hearing aids and other low-power equipment. A button cell with a high ratio of diameter to height may be known as a coin cell. One typical application of 500 μm high coin cells is in 'smart' cards [4]. Other small primary power supplies have found medical applications in implantable defibrillators, drug infusion pumps and pacemakers [5] (Fig. 1.1). However, possibly the smallest cells are 'microcells' envisaged for use as on-chip backup power supplies [6]. A prototype lithium secondary microcell has been developed with an overall thickness of 10 μm [7].

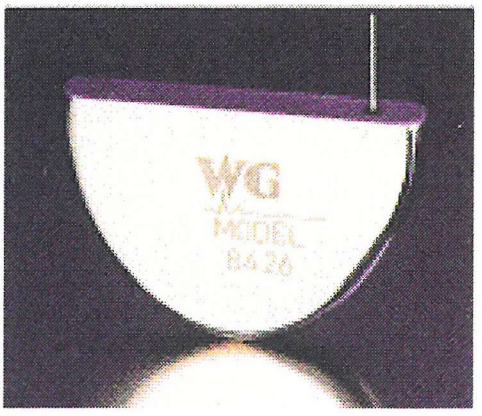

Figure 1.1 - Pacemaker cell (picture with permission of Wilson Greatbatch Ltd.)

ii) The most common primary battery/ cell types (Table 1.1) are used to power torches, radios, remote controls and other portable electronic equipment. Some rechargeable (secondary) devices are available as direct replacements for these primary cells. It may be noted that lithium cells cannot generally be used as replacements for AAA to D size batteries, as their operating voltages are significantly greater than 1.5 V (Table 1.2). One exception is an AA sized lithium-iron sulphide cell developed by Eveready that operates at about 1.6 V [8].

Table 1.1 - Common battery/ cell dimensions and nominal voltages [9]

Size	Diameter / mm	Height / mm	Voltage / V
AAA	10.5	44.5	1.5
AA	14.3	50.0	1.5
C	25.7	49.6	1.5
D	33.5	60.7	1.5
PP3	16.8 x 26.2	48.4	9

The world-wide market for these types of power supply is large; one major supplier reported sales of 3×10^9 units/ year [9].

iii) The largest common types of chemical power supply (that is with a volume larger than PP3 but smaller than 10 dm^3 [10]) are almost exclusively secondary (rechargeable) batteries. The biggest markets for this size of batteries are to provide power for the starting, lighting and ignition (SLI) systems of cars, boats and other vehicles.

iv) Secondary batteries are also used as power 'buffers' for some power generating stations to meet peak electricity demand more readily, and as a back-up in case of generator failure. A complex of 1032 lead-acid batteries in California is capable of delivering 10 MW and storing 40 MWh [11] . On a smaller scale; some buildings rely on batteries, as a more reliable alternative to diesel generators (chap. 1.1.3), for emergency power. In a similar vein some submarines carry lead-acid batteries that are capable of discharging at 1000 A for one hour [1].

New markets for secondary batteries are being created; notably for the purpose of powering portable electronic devices (e.g. notebook computers and phones [12]) and

vehicle propulsion: Californian, clean-air regulations are aimed at introducing an increasing number of zero-emission vehicles (ZEVs) in place of fossil-fuel powered ones [13, 22]. Secondary batteries are also envisaged for medical use with the next generation of implantable devices, such as gas and pressure sensors, micro-robots and micro-transmitters [14].

1.1.2 Supply: Primary and Secondary Technologies

The open-circuit voltage (OCV) and, in part at least, the cost and maximum theoretical energy density of the cell is determined by the electrode chemistries. A number of common cell chemistries are listed below (Table 1.2 - note '↔' denotes reversible reaction).

It can be seen from Table 1.2- that a wide range of reactions has been exploited to produce cells that fulfil different criteria. For example, zinc has been widely used in small primary cells due to its low cost, compatibility with aqueous electrolytes and mechanical properties [15]. Primary cells based on lithium have been found to lose little charge over long periods at open circuit (< 1.5 % capacity loss *per annum* at 20 °C, compared to ~ 5 % for zinc alkaline cells [16]).

Some cell chemistries are peculiar to specialist applications. Thermal batteries [1], for example, employ an electrolyte that is solid at room temperature, giving the cell a very low self-discharge rate. To enable the cell to operate the electrolyte is melted, by means of a pyrotechnic device. The cells may operate only once for a short period of time (10 s - 1 h) and are generally designed for military use.

Table 1.2 - Common battery chemistries with open-circuit voltages

Overall cell reaction	OCV / V	Comments
$Zn + 2MnO_2 + 2NH_4Cl \rightarrow 2MnO.OH + Zn(NH_3)_2Cl_2$	1.5	Zinc-carbon (Leclanché) cell, the standard primary cell [15]
$4Zn + ZnCl_2 + 8MnO_2 + 8H_2O \rightarrow 8MnO.OH + ZnCl_2.4Zn(OH)_2$	1.5	Zinc chloride cell [17], a replacement for zinc carbon technology
$2Zn + 2MnO_2 + H_2O \rightarrow 2MnO.OH + 2ZnO$	1.55	Alkaline cells [18], a replacement for zinc carbon
$2Zn + 4OH^- + O_2 \rightarrow 2ZnO_2^{2-} + 2H_2O$	1.4	Zinc-air cell [17], a high power density primary cell
$2Li + 2SO_2 \rightarrow Li_2S_2O_4$	2.8 - 2.9	High potential, button cells
$2Li + I_2 \rightarrow 2LiI$	2.8	Used in pacemaker cells
$4Li + FeS_2 \rightarrow 2Li_2S + Fe$	1.6 - 2.2	Used in thermal batteries (LiCl/ KCl electrolyte) [19]
$4Li + 2SOCl_2 \rightarrow LiCl + SO_2 + S$	3.6	Lithium-thionyl chloride, for military applications [1]
$Pb + PbO_2 + 2H_2SO_4 \leftrightarrow 2PbSO_4 + 2H_2O$	2.15	Lead-acid cell
$Cd + 2H_2O + 2NiOOH \leftrightarrow 2Ni(OH)_2 + Cd(OH)_2$	1.2	Ni-Cd batteries, alternative to lead acid secondaries
$Li_xHosta + Hostb \leftrightarrow Hosta + Li_xHostb$	3 - 4	Li-ion
$2Na + NiCl_2 \leftrightarrow Ni + 2NaCl$	2.6	Zebra cell, used for automotive traction [20]
$6Ni(OH)_2 + LaNi_5 \leftrightarrow 6NiOOH + LaNi_5H_6$	1.3	Nickel-metal hydride cell [21], alternative to the lead-acid

It may be noted that primary-cell anode materials tend to be low density, electronegative metals (for example zinc and lithium). However, until recently,

secondary batteries have predominantly been used in applications where the need for high power and reliable performance over many cycles has outweighed the need for high energy density - thus denser, less electronegative metals (e.g. lead and cadmium) have been acceptable as negative electrode materials. Much work is currently being directed towards the commercial realisation of high energy density secondary batteries.

The new generation of high-power secondary batteries include nickel-metal hydride, sodium-sulphur, sodium-nickel chloride (zebra cell) and Li-ion. The projected energy densities and costs (based on 10,000 - 40,000 units/ year) of prospective ZEV batteries are shown in Table 1.3.

Table 1.3 - Projected ZEV battery cost and energy density [22]

Technology	Projected energy density / Wh kg^{-1}	Projected cost (normalised to lead-acid)
Advanced lead-acid	50	1
Nickel-cadmium	60	2 - 2.5
Zebra	100	1.5 - 2.5
Nickel-metal hydride	120	1.7 - 2.5
Li-ion	140	≤ 1.5
Sodium-sulphur	140	1.7 - 3.7

Li-ion is predicted to compare well, in terms of energy density and cost, with other ZEV battery technologies, particularly when it is noted that the 'high temperature' systems (zebra and sodium-sulphur) require high-performance thermal enclosures which provide a continuous drain on the battery, even when the ZEV is not in use. Another advantage of Li-ion batteries is that they are not expected to exhibit the 'memory effect' of nickel-cadmium batteries [8]. A nickel-cadmium cell 'memorises' the depth of discharge (DOD) at which it was recharged. During the subsequent discharge the cell voltage drops, by about 100 mV [23], at the memorised DOD.

Safety concerns over lithium cells have been partly allayed by the use of lithium insertion compounds in place of metallic lithium [10, 24] (chap. 1.2.2). Such concerns should be partly offset by the low toxicity of carbon-based lithium negative electrodes with respect to lead (lead-acid cells), nickel (nickel-cadmium, nickel-metal hydride and

zebra cells) and cadmium (nickel-cadmium cells) and the greater reactivity of metallic sodium (sodium-sulphur cells).

1.1.3 Competition: Alternative Technologies

Self-contained chemical cells may be considered to be in competition with other technologies in two distinct areas, namely electricity generation and energy storage.

Electricity generation:

i) Coal, oil and hydrocarbon gases may be combusted to liberate heat. The heat may be used to boil water, producing steam which can drive a steam turbine, thus generating electricity. This is the principle behind conventional power stations. Smaller generators, for producing electricity in remote areas, are often powered by petrol or diesel fuel.

The combustion energy from petrol, diesel, natural gas and wood is often used without conversion to electricity, for example in the internal combustion engine, or wood-burning stove. Upon combustion these fuels liberate carbon dioxide, which may have a detrimental environmental effect in large quantities, by contributing to the 'greenhouse effect' [25 - 28]. Other combustion products, especially from coal, are much less desirable, for example soot particles (carcinogenic) [85], polycyclic hydrocarbons (carcinogenic), heavy metals (toxic) and sulphur and nitrogen oxides (harmful and acidic). It may also be noted that, with the exception of wood, these fuels are not renewable in the short term (< 100 years).

ii) fuel cells are being considered for vehicle propulsion [86] and generating station use [29]. A fuel cell electrochemically oxidises a fuel (typically hydrogen, methane or methanol) at the anode and reduces oxygen at the cathode to produce electricity (Eqn. 1.1). The oxidation is inherently 'cleaner' than the combustion processes outlined above, although carbon-based fuels still release CO_2.

$$2CH_3OH + 3O_2 \rightarrow 2CO_2 + 4H_2O \quad OCV \sim 1.2\ V \qquad \textbf{Equation 1.1}$$

In comparison to secondary chemical cells high current densities may be obtained (~ 1 A cm^{-2}) and the cells may be 'recharged' rapidly (as with a petrol-driven vehicle). However, the cells run at elevated temperatures (60 - 100 °C for solid polymer fuel cells,

900 - 1000 °C for solid oxide fuel cells) which present some engineering difficulties and ~ 15 minutes warm-up time in the higher temperature cells [29]. Another technical difficulty is the poisoning of the catalytic surfaces of the anodes by impurities and combustion intermediates. Despite these drawbacks 4.5 MW prototype fuel cell generating plants are being tested in New York and Japan [11].

In order to make an accurate comparison of the maximum power densities of fuel cells and chemical cells it must be noted that fuel cells require fuel storage tanks, pumping gear and possibly air compressors and after-burners, whereas chemical cells are completely self-contained. When used in ZEVs, chemical cells may be partially recharged be using a generator to slow the car in place of conventional brakes. However, the overall efficiency of a fuel cell could not be increased by the use of a similar device.

iii) Photovoltaic cells convert light to electricity. They are already used in many low power appliances. They have also found much use in isolated stand-alone devices that are required to operate for long periods of time, especially remote telecommunications repeater units [30]. Photovoltaic devices are often coupled to batteries to provide a continuous power supply irrespective of the level of illumination (Fig. 1.2).

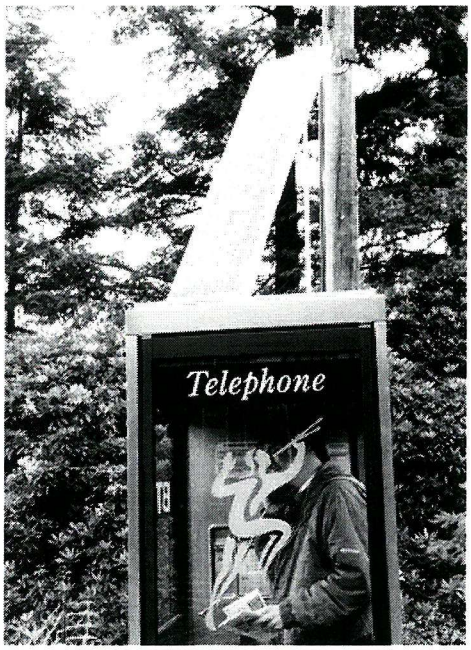

Figure 1.2 - telephone powered by a combined photovoltaic panel (above the telephone kiosk) / storage battery (not shown) system

iv) Solar energy has been harnessed by parabolic dish type reflectors which focus sunlight onto a boiler, generating temperatures up to 1500 °C, to power a generator, thus

producing electricity [31]. Solar energy is more often used directly for domestic water heating by using flat bed, solar pond and vacuum tube collectors.

v) Windmills have been used for several hundred years to convert the kinetic energy of air to a more beneficial form, for example the motion of a grinding wheel. The modern equivalent of the windmill is the aerogenerator [32], which generates electricity from the wind. Aerogenerators have been built for small-scale use (typically < 1 kW, designed for use on yachts and for remote farming communities [33]) to 4 MW devices (as in Wyoming, USA). The small-scale use of aerogenerators requires coupling to an energy storage device, due to the intermittent nature of the electricity generation.

Energy Storage:

i) Solar energy [11] may be stored as heat in specially designed pits, tanks or caverns, often containing materials with high heat capacities, to meet private or communal heating needs over several months.

ii) Flywheels [11] have been considered for use in transportation devices [84], as spinning reserves for national electricity grids and for high power research tests. However, the use of flywheels in domestic vehicles may be limited by safety considerations and the relatively rapid energy loss (when compared to chemical cells) through air resistance and friction in the bearings.

The maximum energy that may be stored in a flywheel is limited by the design stress and density of the flywheel material: a 10 MWh flywheel constructed from Kevlar ™ fibre/ epoxy composite laminates may be predicted to have a mass of 130 tonnes (77 Wh kg^{-1}) , whereas 1220 tonnes of mild steel would be required to store the same amount of energy (8 Wh kg^{-1}). At present, the maximum energy densities obtained for flywheels are below those predicted for Li-ion ZEV batteries (Table 1.3).

iii) Pumped storage stations [11] may be used to supplement national electricity grids at times of high demand and be re-charged from the grid at off-peak times. Pumped storage stations operate by allowing water, from an upper reservoir, to pass through high pressure turbines to generate electricity. Water is pumped back to the upper reservoir by reversing the direction of the turbines to use them as pumps. A station at Dinorwig in North Wales is capable of rising to 80 % of its maximum output power (1.8 GW) in 11 s. However, the use of such stations is restricted by the need for rare geographical features.

iv) Supercapacitors bear many similarities to chemical cells, except that the charge is stored through non-faradaic electrode processes. For an ideal capacitor the OCV is directly proportional to the charge stored, Eqn. 1.2.

$$V = \frac{q}{C} \qquad \textbf{Equation 1.2}$$

where q = charge stored, C = capacitance, V = open-circuit voltage

The energy, E, stored in an ideal battery or capacitor is given generally by Eqn. 1.3 [34].

$$E = \int_{q=0}^{q_{max}} V\,dq \qquad \textbf{Equation 1.3}$$

For an ideal chemical cell in the 'charged' state, the OCV should be independent of the amount of charge stored. Thus the energies stored in an ideal battery, E_{bat}, or capacitor, E_{cap}, are given explicitly by Eqn. 1.4 and Eqn. 1.5.

$$E_{bat} = V.q \qquad \textbf{Equation1.4}$$

$$E_{cap} = \frac{V.q}{2} \qquad \textbf{Equation 1.5}$$

Electrolytic capacitors are based on utilisation of the electrolytic double-layer. By using very high surface area electrode materials (1000 - 2000 $m^2\ g^{-1}$ carbons) they may be charged and discharged rapidly, giving rise to high power densities and very high cycle-lives. However, the energy densities are as low as $\leq$ 20 Wh kg^{-1} [34], which are significantly below the projected energy densities of ZEV chemical cells (Table 1.3).

Pseudocapacitors employ faradaic redox reactions at the electrodes to either deposit or desorb a monolayer of atoms (particularly of hydrogen). The energy densities (up to 30 Wh kg^{-1}), cycle lives (> 10^5 cycles) and power densities (1 - 1000 kW kg^{-1}) of these devices lie between those of electrolytic capacitors and chemical cells [35]. The use of supercapacitors will probably be restricted to applications that require high-power sources (for example pulsed laser sources) and sinks (to remove power supply voltage 'spikes').

It may be concluded that Li-ion rechargeable batteries may offer a high energy density, low toxicity alternative to existing primary and secondary battery technologies.

They may also be expected to find application in the new markets of ZEVs and possibly to store energy generated from intermittent, renewable sources (wind and solar energies).

1.2 Lithium Secondary Batteries

Lithium has many attractive properties as a negative electrode material; including a large negative electrode potential (-3.05 V vs. NHE [36]), low molar mass per electron transferred on oxidation and tolerable mechanical properties. These factors have led to the use of lithium in several types of primary cells (chap. 1.1.2). Two types of lithium secondary cells are currently being developed: the lithium metal cell and Li-ion (or rocking-chair [37] or shuttlecock [38]) cell. Both types of cell are based on a positive electrode insertion matrix and aprotic electrolyte. The Li-ion cell uses a negative insertion matrix in place of the metal.

1.2.1 Intercalation Chemistry

Intercalation is the process by which guest species are inserted between the layers of a host lattice without significantly affecting the structure or composition of the host. However, the host generally swells slightly on intercalation. The swelling may be quite marked, as is found for the insertion of an octadecylamine bilayer into tantalum disulphide, which causes the host layer spacing to increase from 6.05 Å to 55.6 Å [39]. Intercalation compounds may be synthesised by three general methods [40]:

1) Direct reaction, e.g.

$$\mathbf{0.25\ Co(\eta\text{-}C_2H_5)_2 + VSe_2 \leftrightarrow VSe_2\{Co(\eta\text{-}C_2H_5)_2\}_{0.25}}$$ 130 ^{O}C in toluene

$$\mathbf{xLiI + V_2O_5 \rightarrow Li_XV_2O_5 + x/2\ I_2}$$ 25 ^{O}C in acetonitrile

2) Ion exchange, e.g.

$$\mathbf{Na_XTiS_2 + xLiPF_6 \rightarrow Li_XTiS_2 + xNaPF_6}$$ 25 ^{O}C in dioxalane

3) Electrochemical intercalation, e.g.

$$xLi^+ + V_2O_5 + xe^- \leftrightarrow Li_xV_2O_5$$ 25 °C in propylene carbonate

It is the third type of reaction that makes intercalation compounds of interest as electrode materials. In contrast to metallic lithium, intercalation materials can offer a well-defined surface that changes little as charge is passed. This may be advantageous in limiting parasitic, film-forming reactions; as electrodes, at potentials close to that for lithium plating, are known to react with many electrolytes [41 - 43].

An important consideration for insertion electrodes is the potential range over which insertion occurs, as this will govern the cell voltage. For a lithium insertion electrode, when no net current is flowing the electrode potential, E, with respect to Li/Li^+ is given by:

$$E = \frac{-\mu_{Li}}{F}$$ **Equation 1.6**

where μ_{Li} is chemical potential of the inserted lithium, which is equal to the sum chemical potentials of the inserted lithium ions and associated electrons [44]:

$$\mu_{Li} = \mu_{(Li^+,e^-)} = \mu_{Li^+} + \mu_{e^-}$$ **Equation 1.7**

For a single non-stoichiometric insertion phase Li_xHost, in which all of the insertion sites are of equal energy, two limiting cases may be imagined; in which the chemical potential is exclusively dependent upon either ionic or electronic terms. The maximum degree of insertion, x_{max} may be limited by either the number of ionic insertion sites or the number of accessible electronic states. For a host material with a large number of possible insertion sites but a limited number of electronic states that may be readily populated then the fermi-level of the host material will be dependent on the degree of insertion. If it is assumed that there is an empty electronic band which is narrow and of constant width a dimensionless quantity, y_{el}, may be defined such that:

$$y_{el} = \frac{x}{x_{max}}$$ **Equation 1.8**

and the chemical potential will be given by:

$$\mu_{Li} = \mu^{O}_{Li,Host} + RT\ln\left(\frac{y}{1-y}\right) \qquad \textbf{Equation 1.9}$$

where $y = y_{el}$ and $\mu_{Li} = \mu_{Li}^{O}$ when $y = 0.5$.

Alternatively, if the maximum degree of insertion is limited by the number of insertion sites and the electronic density of states is high around the fermi-level then Eqn 1.9 may still be applied with $y = y_{ion}$ and y_{ion} is given by:

$$y_{ion} = \frac{x}{x_{max}} \qquad \textbf{Equation 1.10}$$

However, generally there will be some contribution to the chemical potential from both ionic and electronic terms and also from ion-ion interactions. Eqn 1.11 has been proposed by Armand [45] on the assumption that there is an ion-ion interaction energy which has a linear dependence on y_{ion}.

$$\mu_{Li} = \mu^{O}_{Li} + z.y_{ion}E_{Li-Li} + nRT\ln\left(\frac{y_{ion}}{1-y_{ion}}\right) \qquad \textbf{Equation 1.11}$$

Where z is the lithium co-ordination number, $E_{Li\text{-}Li}$ is the ionic repulsion energy, and n = 1 or 2 depending on number of factors limiting the insertion (i.e. ionic or electronic or ionic and electronic limitation).

Taking $y = y_{ion}$ and $E^{O} = -\mu_{Li}^{O}/F = 0.10$ V vs. Li/Li^{+} a theoretical curve for a single non-stoichiometric phase (Fig. 1.3) was constructed according to Eqn. 1.9.

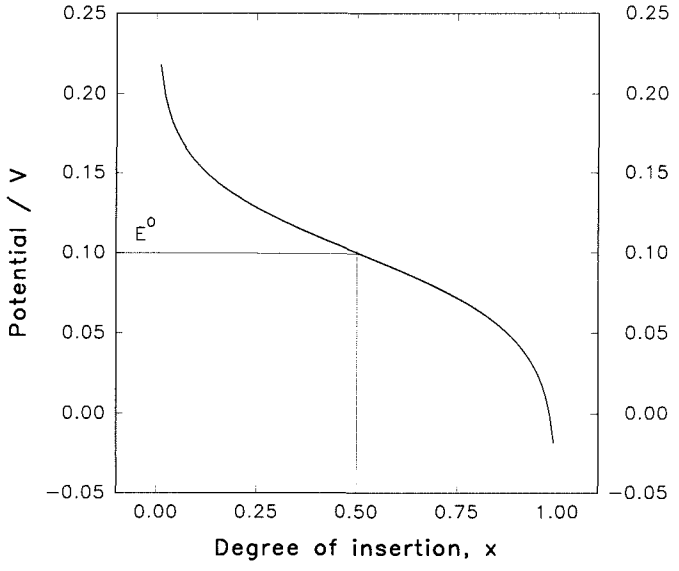

Figure 1.3 - Theoretical potential profile for a single non-stoichiometric phase

However, some insertion materials exhibit more than one phase during intercalation. If two non-stoichiometric phases are adjacent in the phase diagram such that there is a region of overlap where one phase becomes more thermodynamically stable a potential insertion curve may be constructed by using Eqn 1.9 (Fig. 1.4). This is known as a pseudo two phase insertion process [46].

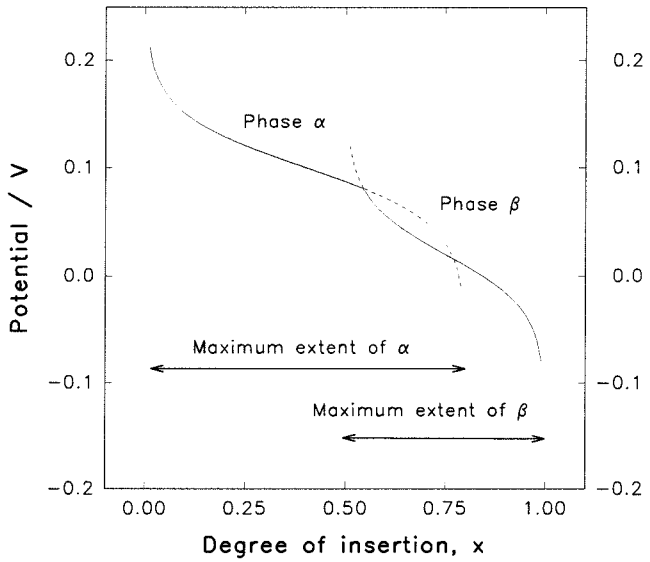

Figure 1.4 - pseudo-two phase theoretical potential curve

In a 'true' two phase system there may consist of two phases with different compositions and very narrow composition ranges. A compound of 'intermediate' composition would in actuality be an appropriate mixture of the two phases.

For two phases to coexist at equilibrium within an electrode the chemical potential of lithium in each phase must be equal. The number of degrees of freedom, F, may be determined according to the phase rule (Eqn 1.12):

$$F = C - P + 2 \qquad \textbf{Equation 1.12}$$

Where C is the minimum number of components needed to describe the system completely and P the number of coexisting phases. Thus, for a system in which there are two coexisting phases, $Li_{x1}Host$ and $Li_{x2}Host$, P = 2, C = 2 (Li and Host) implying that F = 2. Therefore μ_{Li} would be independent of the relative proportions of the phases if the temperature and pressure were held constant (Fig 1.5).

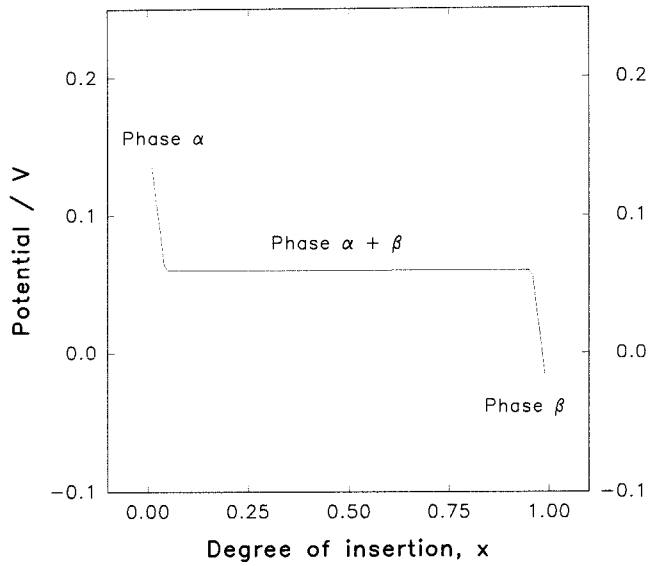

Figure 1.5 - Theoretical potential curve for a two phase system

To maximise the cell voltage electrodes would be chosen with the maximum practical difference in free-energies of intercalation. Ideally cell voltage should be independent of the state of discharge (chap 1.1.3), thus the chemical potential of inserted lithium should vary as little as possible with lithium concentration in the electrodes (two phase behaviour). Further criteria for practical cell design are that it should be possible to charge and discharge the cell many times, efficiently, at an acceptable rate. Therefore, electrodes should intercalate lithium reversibly with minimal charge loss to parasitic reactions. It is also desirable to have a high rate of lithium diffusion in the electrodes, in order to maximise the optimum charging and discharging rates of the cell.

Many materials have been considered for the positive electrode, Table 1.4.

Table 1.4 - potentials of lithium cell positive electrode materials.

Positive Electrode Material	Potential at Half Charge / V vs. Li/Li^+
$Li_{0-1}Mn_2O_4$ (λ-MnO_2)	4.0 [47 - 49]
$Li_{0-1}MnO_2$ (γ-MnO_2)	2.9 [48, 49]
$Li_{0-1}NiO_2$	3.5 [47, 48]
$Li_{0-1}CoO_2$	4.0 [48 - 50]
$Li_{0-1}MoS_2$	1.7 [50]
$Li_{0-1}TiS_2$	2.1 [50]

Of the possible negative electrode materials for use in Li-ion batteries much attention has focused on the use of carbons or modified carbon electrodes.

1.2.2 Carbon

Several forms of carbon have been shown to permit intercalation of lithium. These may be summarised as:

i) Graphite - a crystalline allotrope of carbon that may be synthesised (or found naturally) with an ABAB hexagonal structure (Fig. 1.6), although it often contains a fraction of ABC rhombohedral sequences [51].

Graphite is a relatively inexpensive material which is readily available on a multi-tonne scale. Depending on the particle size and purity graphite powder is priced from £ 1,900 / tonne (Lonza KS 75) to £ 5,800 / tonne (Lonza SFG 6) [59].

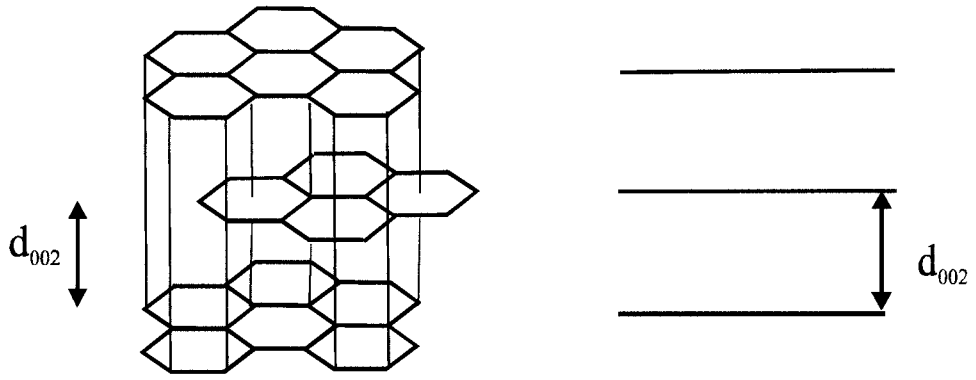

Figure 1.6 - ABAB hexagonal graphite structure

Many graphite intercalation compounds (GICs) have been formed, including compounds with lithium [52], sodium, potassium [53], rubidium and caesium [54].The diffusion coefficient for Na has been calculated at 10^{-11} $cm^2 s^{-1}$ [55] which is 3 orders of magnitude lower than the highest reported for lithium [56]. The expected reversible limit for electrochemical sodium intercalation is NaC_{12}. K, Rb and Cs have been chemically intercalated to limiting stoichiometries of MC_8. By direct reaction, at elevated pressure, LiC_2 and LiC_3 lithium intercalation compounds have been synthesised. However, resistance measurements indicated that these compounds were not stable with respect to LiC_6 and Li at temperatures above ~ 20 K [57]. LiC_6 may be expected to be the most concentrated lithium-GIC that can be formed electrochemically at room temperature and

pressure (RTP) - corresponding to a maximum insertion capacity of 372 mAh g^{-1}. Unlike graphite LiC_6 has an AAAA stacking order with respect to the graphite layers [58], Fig. 1.7.

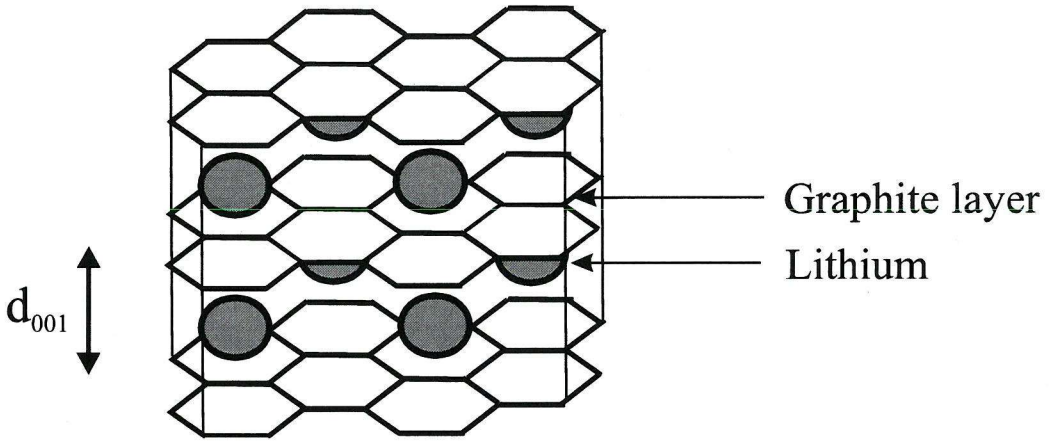

Figure 1.7 - structure of LiC_6

ii) Coke - a layered form of carbon which shows some buckling of the layers and turbostratic disorder (i.e. successive layers are not oriented relative to one another) [60], Fig. 1.8.

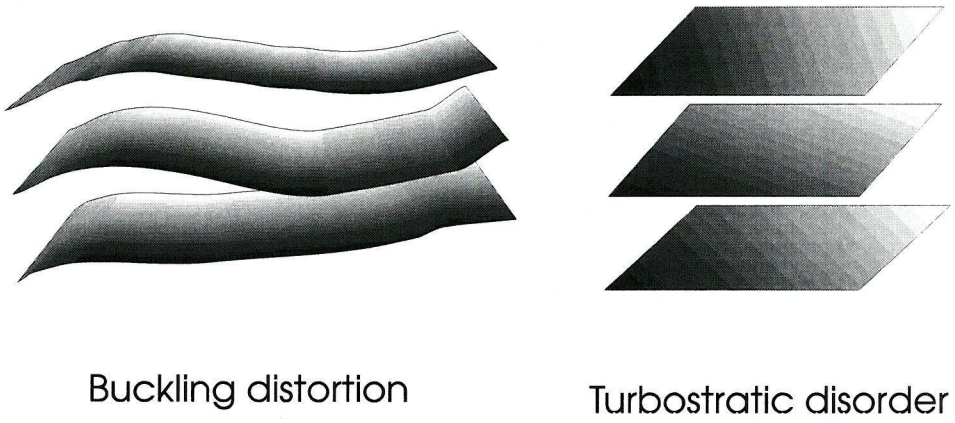

Figure 1.8 - types of layer disorder found in cokes

The disorder in coke creates insertion sites of different energies. Lithium ions have been found to fill the sites according to the local site energy regardless of their position. This suppresses the formation of crystalline structures (for example LiC_6), thus giving rise to a range insertion capacities that are dependent on the degree of disorder in the coke [61].

Cokes are harder than graphites and have found application in brake linings, clutch facings and grinding wheels [62]. Large quantities of coke are used in the refining

and hardening of metals [63]. They are available as inexpensive powders: ~ £ 1,300 / tonne (Lonza FC 250) [59].

iii) Buckminsterfullerene, C_{60} - a face-centred cubic structure, with respect to the C_{60} molecules [64]. Direct reactions of the alkali metal vapours have produced compounds of the form M_6C_{60} (M = K, Rb, Cs). Lithium has been electrochemically intercalated to give a series of compounds of the form Li_xC_{60} with $x \leq 11.5$ [65], corresponding to a maximum theoretical capacity of 428 mAh g^{-1}. The equilibrium insertion potential is found to drop with lithium intercalation from $Li_{<0.5}C_{60}$ ~ 2.4 V, $Li_{0.5-2}C_{60}$ ~ 1.9 V, $Li_{2-3}C_{60}$ ~ 1.6 V, $Li_{3-10}C_{60}$ ~ 0.8 V to $Li_{10-11.5}C_{60}$ ~ 0.3 V vs. Li/Li^+.

At present the use of fullerenes as electrode materials is not economically viable (1995 prices[66] of C_{60}, £ 230/ 0.5 g, C_{76} £ 825/ 0.005 g).

iv) Carbon blacks - particles of 10 - 300 nm diameter, consisting of four to six graphene layer microcrystals [67] (Fig. 1.9). Many families of carbon blacks exist (for example furnace blacks, channel blacks, lamp blacks and acetylene blacks), exhibiting a range of porosities, surface areas and conductivities.

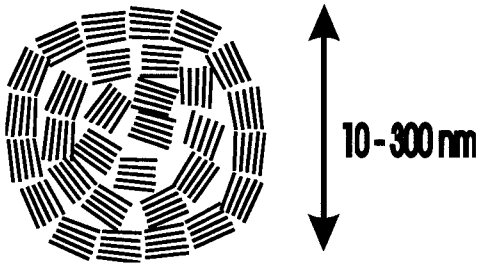

Figure 1.9 - carbon black particle

Electrochemical intercalation of lithium [68 - 70] and sodium [71] into several carbon blacks has been demonstrated.

Carbon blacks are widely used in inks, paints and to increase the conductivity of rubbers and plastics [72] . These markets for carbon blacks are well established, which is reflected in the prices, £ 1,550 / tonne (Monarch 120) to £ 13,560 / tonne (Black Pearls 2000) [73].

v) Pyrolysed organic compounds - a great variation of composition and structure depending on the pyrolysis temperature and precursor material. At low (< 900 °C) pyrolysis temperatures an impure form of carbon with a buckled, turbostratically disordered layer structure is generally produced. As the pyrolysis temperature is increased the concentration of impurities is found to decrease. At temperatures above 900 °C the layers begin to organise themselves (that is the amount of buckled layers decreases), above 2000 °C the layers begin to acquire registered hexagonal order [60].

A few studies have focused on the effects of starting materials containing nitrogen [74], sulphur [75], boron [76], silicon [77] and phosphorus [60]. Pyrolysed carbohydrates (wood, starch and sugar [78]) have also been examined. It has been shown that it is possible to prepare electrode materials with a range of chemical compositions by pyrolysis of appropriate compounds .

The cost of such electrodes is very dependent on the type of precursors, pyrolysis regime and scale of the process.

vi) Fibres may be produced with an oriented graphitic structure by heat-treatment of a suitable carbon precursor (for example pitch [79], poly (acrylonitrile) [80] or pyrolysed benzene [81]). The graphene layers of an axially aligned fibre may be oriented radially or concentrically, exposing an entirely 'edge' or 'basal' surface respectively, Fig. 1.10. However, the surface of electrodes constructed from graphite powders will be comprised of edge and basal faces. The basal planes of graphite may be expected to present a much greater barrier to intercalation of lithium than the edge planes. Thus, it may be predicted than electrodes constructed from edge-type fibres could be charged and discharged at higher rates than similar graphite-powder electrodes [82, 83]. Entangled fibres may also be expected to give rise to more robust electrodes than powders.

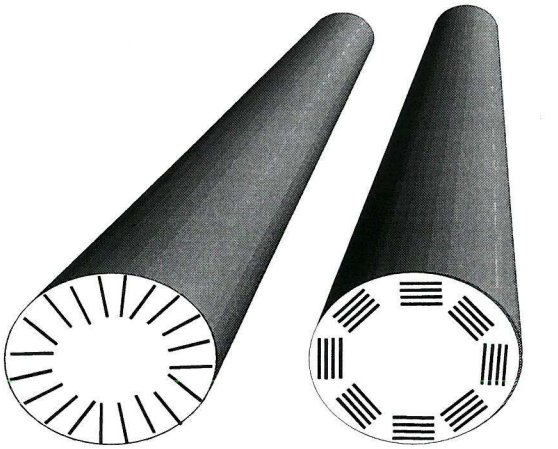

Radial orientation Concentric orientation

Figure 1.10 - axially aligned carbon fibres

Chapter 2

Experimental Techniques

2.1 Solvent

A range of solvent systems have been considered for use in lithium cells. Typically they contain two components, one of which may have a high dielectric constant, to encourage ionic dissociation of the salt, and hence improve conductivity. This component will also tend to have a high melting point, for example ethylene carbonate (EC), propylene carbonate (PC) [1], tetramethylene sulfone [2] and N,N-dimethylacetamide [3]. The other component may have a low viscosity, to improve the wetting of the rough electrode surfaces, and a low freezing point - for example diethyl carbonate (DEC), dimethylcarbonate [4] and diethyl ether [5]. It is desirable that the solvent is chemically and electrochemically stable with respect to both electrodes regardless of the degree of discharge of the cell. It is also important that the solvent does not dissolve or plasticise the cell casing or electrode binder.

Five solvent components were considered in the course of this work; PC (GPR grade, BDH Chemicals Ltd), EC (99 % Fluka), 12-crown-4 (1, 4, 7, 10-tetraoxacyclododecane, 98%Aldrich), triethylene glycol dimethyl ether (triglyme, 99 % Aldrich) and DEC (>99.5 % Fluka or 99 % Aldrich), as shown in Fig. 2.1.

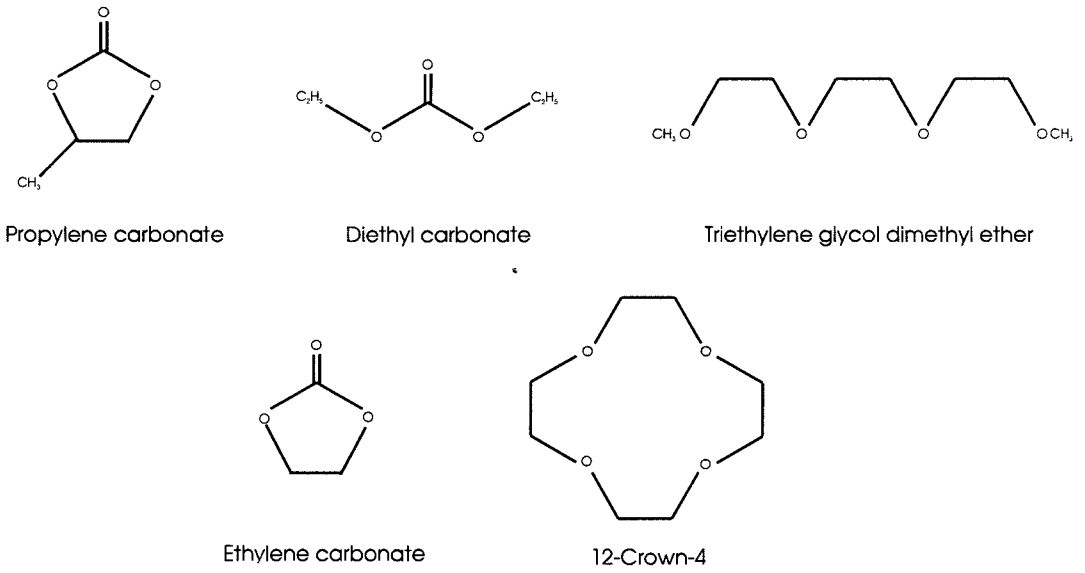

Figure 2.1

It has been noted that impurities, in the solvent, can greatly affect the performance of the negative electrode [6 - 9]. Thus it was decided to quantify and, if possible, reduce the level of impurities.

2.1.1 Water Determination

PC samples were analysed by the Karl-Fischer method of water determination [10, 11]; in which Karl-Fischer reagent (Aldrich) is titrated against a water-containing sample. Karl-Fischer reagent was introduced to the titration vessel, which contained the sample under a dry argon atmosphere, through a Suba-Seal ™. A sharp change in the solution resistance indicated the end-point of the titration. In practice it was found that the Karl-Fischer titrant only gave clear, reproducible resistance changes with distilled solvents.

A second method of water determination, in PC, DEC and EC/ DEC was performed quantitatively by using FTIR; using a Nicolet 510P Spectrometer with a demountable cell, of 10 mm pathlength, with calcium fluoride windows. The area under the $\nu_2 + \nu_3$ combination band at 5265 - 5350 cm^{-1} was found to be proportional to the amount of water added to the sample. Thus, by linear regression, it was possible to estimate the original water concentration in the solvent. This method was found to be more convenient and more widely applicable than the Karl-Fischer technique.

2.1.2 Propylene Glycol Determination

The method of determining propylene glycol in PC was based on the iodide/ periodate method [12]: a 30 mM aqueous sodium metaperiodate (99 %, Avocado Research Chemicals Ltd.) solution was added to the test solution in methanol in the dark and left for three minutes to react, according to Eqn. 2.1:

$$IO_4^- + CH_3.CH(OH).CH_2(OH) \rightarrow IO_3^- + CH_3CHO + CH_2O + H_2O \qquad \textbf{Equation 2.1}$$

To the resulting solution a pH 6.8 phosphate buffer (sodium phosphate dibasic (99 %, Fisons) 20 mM, potassium phosphate monobasic (99 %, Fisons) 40 mM) and an excess of potassium iodide (99 %, BDH Chemicals Ltd) was added. The solution was cooled in

a water/ice bath, to reduce the rate of further reactions of the iodine, formed according to Eqn. 2.2:

$$IO_4^- + 2I^- + H_2O \rightarrow IO_3^- + I_2 + 2OH^- \qquad \textbf{Equation 2.2}$$

The amount of iodine resulting from the iodide/ iodate reaction was then determined by titration with sodium thiosulphate (photographic grade, Hogg Laboratory Supplies). However, the amount of titre required was found to be time dependent. Thus, measurements were taken at regular time intervals, and extrapolated back to the initial time. Standardisation with several prepared samples of propylene glycol (99 %, BDH Chemicals Ltd) was required as the thiosulphate ion is unstable in aqueous solutions[13].

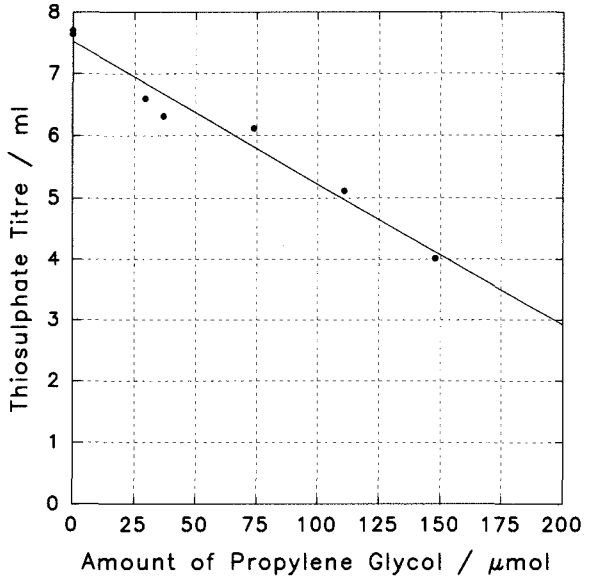

Figure 2.2 - Standardisation of thiosulphate solution against set amounts of propylene glycol.

2.1.3 Miscellaneous Impurities

The solvents used in this study were expected to contain many trace impurities [14], including propylene glycol, allyl alcohol and propylene epoxide. These impurities absorb light in the near UV. Hence, as a qualitative guide to the solvent purity UV spectra were recorded, using a Philips PU8730 spectrometer, with a 10 mm pathlength, quartz cell.

2.1.4 Solvent Purification

PC was purified by fractional distillation at 10 Pa, 40 - 43 ^{O}C. Middle fractions were used, in which the absorption band at 250 nm, due to impurities (chap. 2.1.3) reached a minimum. $A_{250\,nm} = 0.7$ as supplied, but $A_{250\,nm} < 0.05$ after distillation.

EC was purified by recrystallisation under reduced pressure.

DEC (> 99.5 %, Fluka) was used as supplied, except when it was to be used in the 'coffee-bag' cells (chap. 2.4.4), for which it was decanted from 4 Å molecular sieves. Aldrich DEC (99 %) was fractionally distilled under 101 kPa of dry argon.

2.2 Electrolyte Salts

In a Li-ion battery the electrolyte salt is required to impart high conductivity to the electrolyte and provide a reservoir of Li^+. An additional requirement is that the salt does not decompose at either the negative or positive electrodes of the battery. To these ends several anhydrous lithium salts with large, monovalent anions (e.g. BF_4^-, PF_6^- and ClO_4^-) have been suggested [15, 16].

Initially, lithium hexafluoroarsenate ($LiAsF_6$, electrochemical grade, Lithco) was used in this work. $LiAsF_6$ was heated in a drying tube for 24 hours, under reduced pressure at 90 °C, to remove water and other volatile impurities. The mass loss, after 24 hours, was found to be < 0.02 %.

During the course of this research, it became apparent that $LiAsF_6$ was too toxic to be used in commercial applications [17]. Therefore, the less harmful lithium trifluoromethanesulfonate (lithium triflate, $LiCF_3SO_3$, 97 % Aldrich) was used as an alternative. $LiCF_3SO_3$ was dried under reduced pressure, at 80 - 90 °C for 24 hours followed by 24 hours at 120 - 130 °C. A liquid nitrogen cold-trap was used, between the vacuum pump and drying tube, to reduce the partial pressure of water and thus increase the extent of drying. The two-stage drying processes was found to cause less discolouring of the salt than drying at 120 °C alone. The discolouring was attributed to decomposition of the salt, possibly by hydrolysis of the triflate anion.

2.3 Working Electrode

In the course of this work a range of working electrodes were examined. All of the electrodes were dried, under reduced pressure, for 2 - 4 hours prior to use. Composite electrodes, oriented pyrolytic carbon (OPC) and graphite sheet were dried at 150 - 200 ^{o}C. Other electrodes were dried at room temperature.

The OPC could be easily cleaved to expose reflective basal faces, however these had a scale-like morphology and required polishing with alumina powder to become flat on a micron scale. Similarly edge-face wafers were polished to a given thickness from 3 - 4 mm thick slices cut from the mother block.

Graphite monolithic electrodes were cut from a 100 μm thick sheet of pressed graphite (Alfa) and polished to a given thickness with increasingly fine grades of alumina powder.

Copper (Aldrich), silver (Agar), nickel (BDH Chemicals Ltd) and aluminium (AWCO) electrodes were cut to size from wires or foils, but were otherwise untreated before use.

Glassy carbon electrodes were made by sealing a glassy carbon rod (0.08 cm^2 cross-sectional area) into a glass tube with paraffin wax. Electrical contact was made to a copper contact wire with a Wood's metal joint. The carbon was polished with silicon carbide paper.

Composite electrodes were made by binding the active material (generally graphite powder) and conductivity additives onto a 15 - 25 μm thick copper backing foil (Aldrich).

The electrode binders were applied as solutions: either as 2 - 6 w/o ethylene propylene copolymer (EPM, Exxon) in cyclohexane or 5 - 10 w/o polyvinyldiene fluoride (PVDF, Aldrich) in 1-methyl-2-pyrrilodinone (NMP, Aldrich). For each solution, the exact concentration of binder was determined immediately prior to use, as they were found to vary over a period of days. The binder solutions were mixed with the other electrode components to form slurries, which were pasted onto the backing foil. Subsequently the solvents were allowed to evaporate, to leave materials, from which electrodes were cut. The electrodes were found to have carbon loadings of 4 - 20 mg cm^{-2}.

2.4 Cell Design

Several designs of cell were used through the course of this work. The cells were assembled in an argon-filled glove box (< 5 ppm water).

2.4.1 Three-electrode pear-shaped flask cell

This type of cell (Fig 2.3) was used predominantly for studying monolithic working electrodes, which were held in the electrolyte by means of a crocodile clip. It offered the following advantages:

i) *in-situ* visual observation of the working electrode and electrolyte.

ii) relatively facile cell assembly.

iii) small volumes (~2 ml) of electrolyte were required.

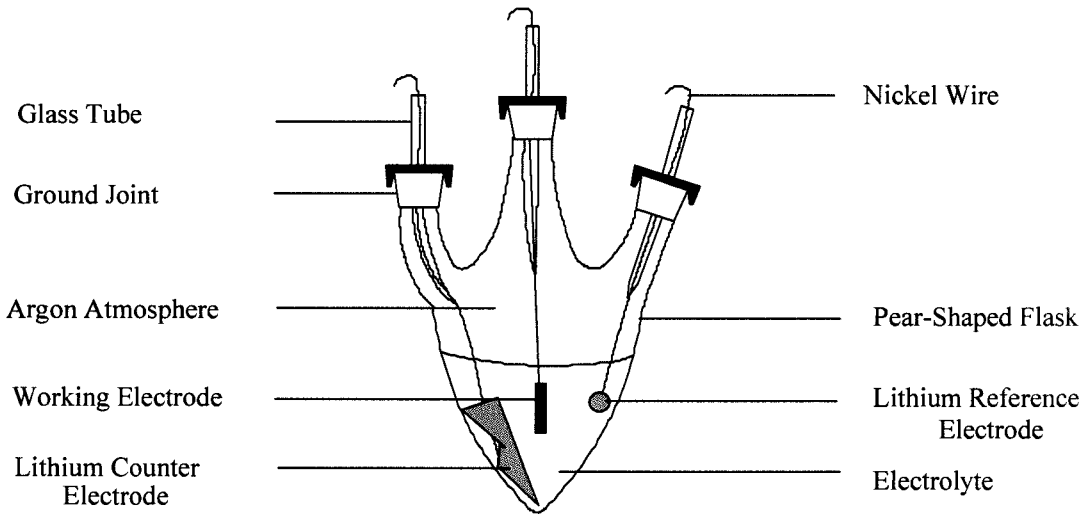

Figure 2.3 - Three-necked pear-shaped flask cell

The reference electrode was made by *in-situ* plating of lithium from the counter electrode onto a nickel wire (Fig. 2.3).

2.4.2 Basic pressure cells

A 'stack pressure', of 600 ± 100 kPa, was applied to the cell 'stack' (lithium foil, separator and working electrode - Fig. 2.4), via a spring pressing on a 10 mm diameter

nickel disk. Disposable PTFE 'O'-rings were used to seal the cell compartment, which held ~1 ml of electrolyte.

The nickel current-collectors and disk were polished prior to cell assembly.

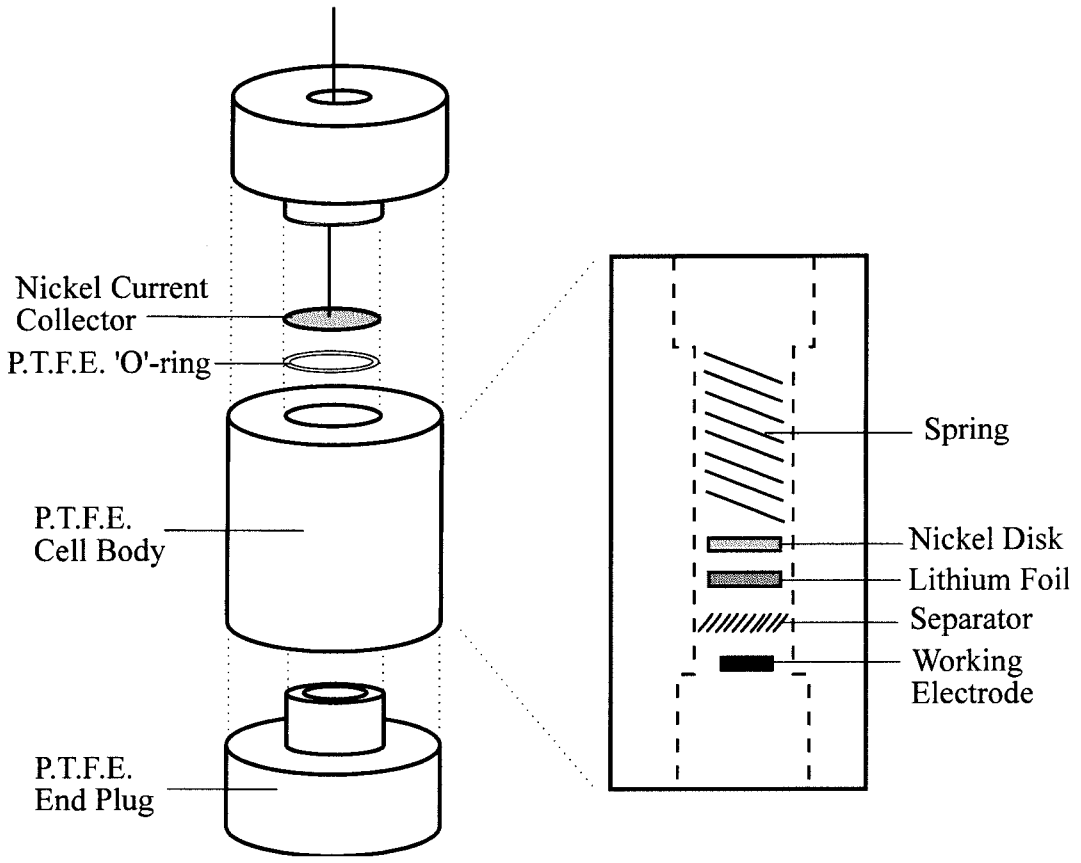

Figure 2.4 - Basic pressure cell (working electrode current collector omitted for clarity).

2.4.3 Brittle-electrode pressure cells

It was found that the nickel current-collectors deformed on assembly of the basic pressure cell (Chap 2.1.2). Therefore, for the examination of brittle working electrodes (notably graphite sheets), the basic pressure cell was used, but with the working electrode current-collector replaced with a 1 mm thick copper disk.

As with the basic pressure cell, the current-collectors and nickel disk were polished prior to use.

2.4.4 'Coffee-bag' cells

For X-ray diffraction studies (chap 2.5.5) a thin-layer cell was required. To this end, cell components were vacuum-sealed into an polyester/ aluminium/ polyethylene [26]

laminated foil (Lamofoil ™) pouch. A piece of glass filter-paper served the dual purpose of separator and electrolyte reservoir.

Electrical contact was made to the electrodes via nickel foils sealed through the edge of the bag (Fig. 2.5).

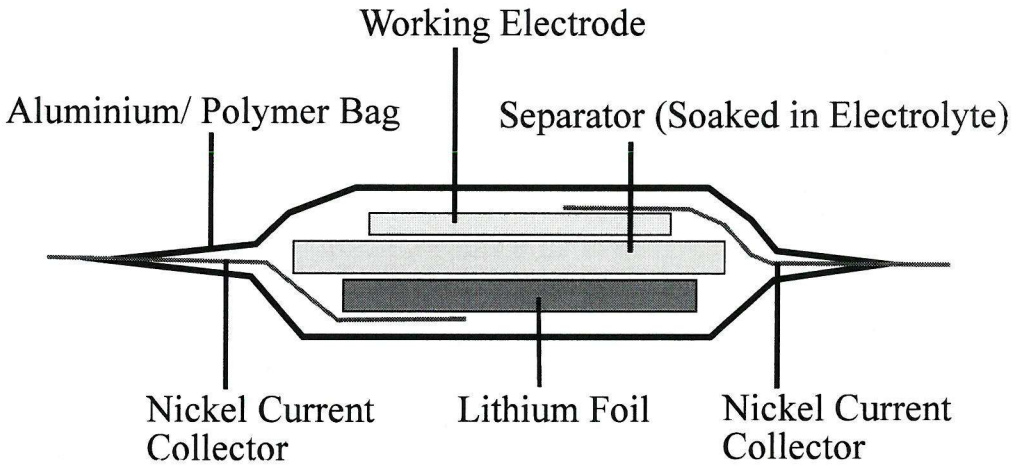

Figure 2.5 - 'Coffee-bag' cell

2.5 Equipment

2.5.1 Cyclic voltammetry

Two systems were used for cyclic voltammetry. The first system employed a purpose-built analogue scan unit to provide the voltage sweep for the purpose-built potentiostat. The potentiostat output was recorded by a Lloyd Instruments PL3 plotter. The second system used a microcomputer, via a 12-bit CIO-DAS08-AOL analogue and digital I/O board, to provide the voltage sweep and to record the potentiostat output. The potentiostat used in this system was also purpose-built.

The first system had a scan range of 1 mV s^{-1} to 1 V s^{-1}, and current-follower sensitivity range of 1 V μA^{-1} to 10^{-3} V μA^{-1}. The second system was designed for scanning more slowly, with a scan range of < 2 μV s^{-1} to 20 mV s^{-1} and current-follower sensitivity range of 50 V μA^{-1} to 5 x 10^{-3} V μA^{-1}.

2.5.2 Coulometric titration

A microcomputer was used, via a 12-bit PCL-812 analogue and digital I/O board, to control and to record the output of up to four purpose-built galvanostats (Fig. 2.6).

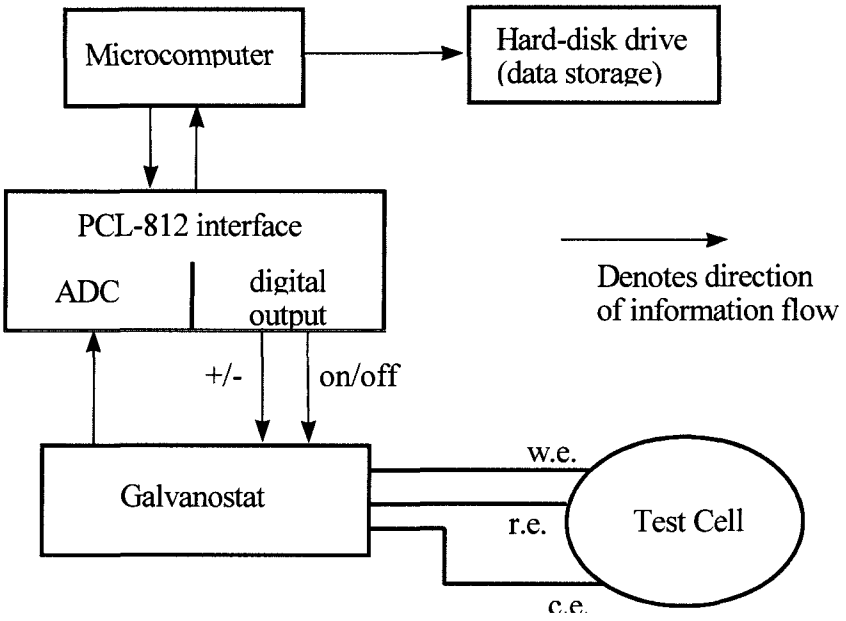

Figure 2.6 - Schematic representation of coulometric titration equipment

The PCL-812 may be considered to consist of two independent units, the analogue to digital converter (ADC) and digital output. The ADC was used to convert the galvanostat output to a digital signal which was recorded by the microcomputer. The recorded data was systematically copied onto the hard drive. The current direction (+/-) and interruption (on/off) were controlled via the digital output (appendix A).

Several programs were written to enable different titration regimes (e.g. appendix B) to be applied to the test cells.

The simple coulometric titration regime consisted of the application of a given current until the potential difference between working and reference electrodes reached a pre-set limit. Upon reaching this limit the current direction was reversed until the next limit was reached. In this manner the cell was cycled a given number of times between voltage limits.

Pulsed coulometric titration utilised a current which was systematically applied and interrupted by means of a computer-controlled relay within the galvanostat for pre-set periods of time. The titrations proceeded in a similar way to the simple coulometric titration except that only the final voltage readings of each current-off period were compared with the cycling limits. Hence, during the current-on periods the cell voltage would be expected to regularly exceed the cycling limits.

2.5.3 Voltage transient measurement

Voltage transients were produced during simple coulometric titrations by the application of a current pulse. The current pulse was either an interruption of the titration current or ± 1 μA current added to the titration current, created using a modified galvanostat. In the latter case the voltage transient was amplified, by means of a purpose-built fixed-gain (x 100) amplifier, before being measured (Fig. 2.7). In both cases the voltage transient was converted via a different channel of the ADC to the voltage profile of the coulometric titration. However, for the shortest measurements it was necessary to capture the voltage transient using a digital storage oscilloscope (Gould OS4000) before recording it with the microcomputer.

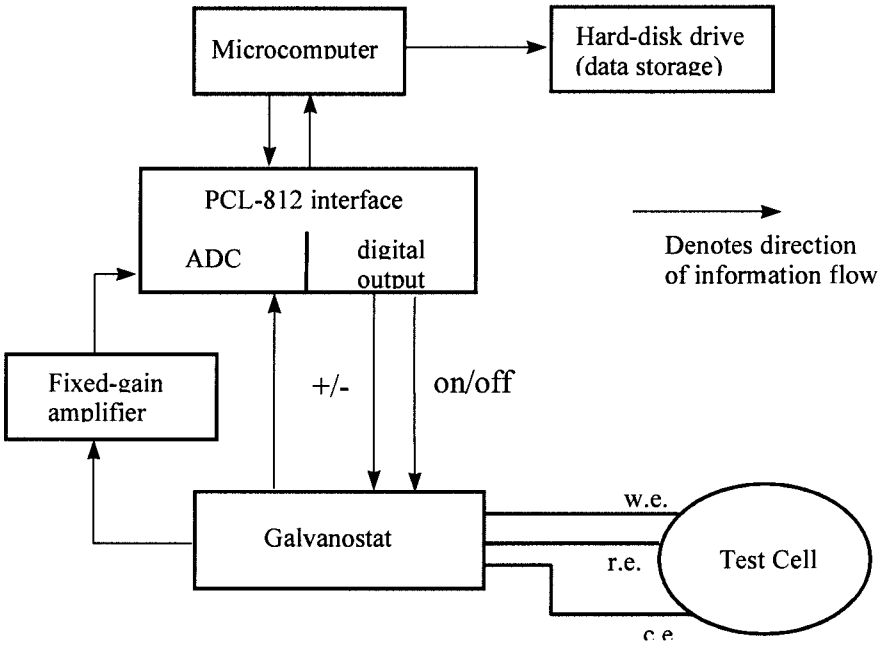

Figure 2.7 - Schematic representation of equipment for voltage transient measurement

2.5.4 Powder X-ray diffraction

To make the XRD measurements X-rays of a precise wavelength (CuKα) were selected with a monochromator and formed into a beam by means of a set of slits. The apparatus was arranged such that the beam was incident upon the sample (Fig. 2.8). X-rays diffracted by the sample were detected by a moving beam detector. The position of the detector and intensity of the diffracted X-rays were recorded by a microcomputer.

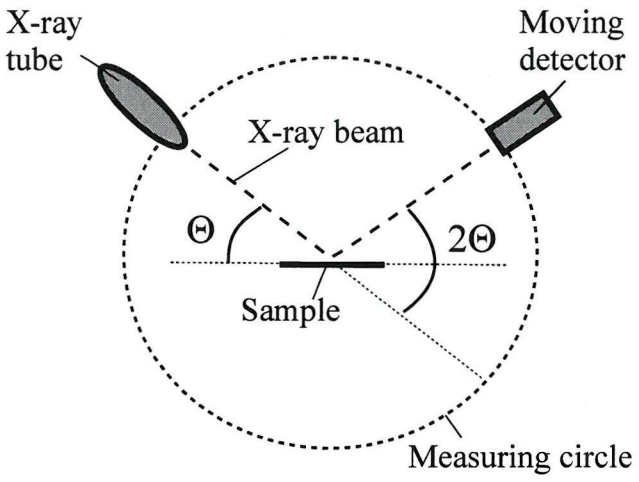

Figure 2.8 - Schematic representation of powder XRD equipment

The sample powder was pressed lightly into a shallow (< 3 mm deep) aluminium dish and the surface levelled-off with a microscope slide. The dish was placed in a holder which was magnetically clamped into the sample chamber of a Siemens diffrakometer D5000. The sample holder was rotated during measurement of the diffractogram, in order to decrease any effects of preferential orientation in the sample

2.5.5 *In-situ* X-ray diffraction

To record *in-situ* diffractograms of test electrodes during coulometric titrations 'coffee-bag' cells described previously (chap 2.4.4) were clamped between thin sheets of beryllium in a cell holder (Fig. 2.9). The beryllium sheets were used to maintain a 'stack pressure' in the cell in order to ensure that gaseous solvent decomposition products did not cause the cell to deform. Previously, it had been found that in cells which were cycled without beryllium sheets deformation of the cells had led to a large decrease in the maximum insertion charge and also to apparent shifts in the positions of the diffraction peaks.

The cell holder rotated the cell between two positions separated by 140^{o} at a rate of $\sim 3^{o}\ s^{-1}$. The sample was rotated to reduce the effect of preferred orientation in the electrode and polymer laminate bag.

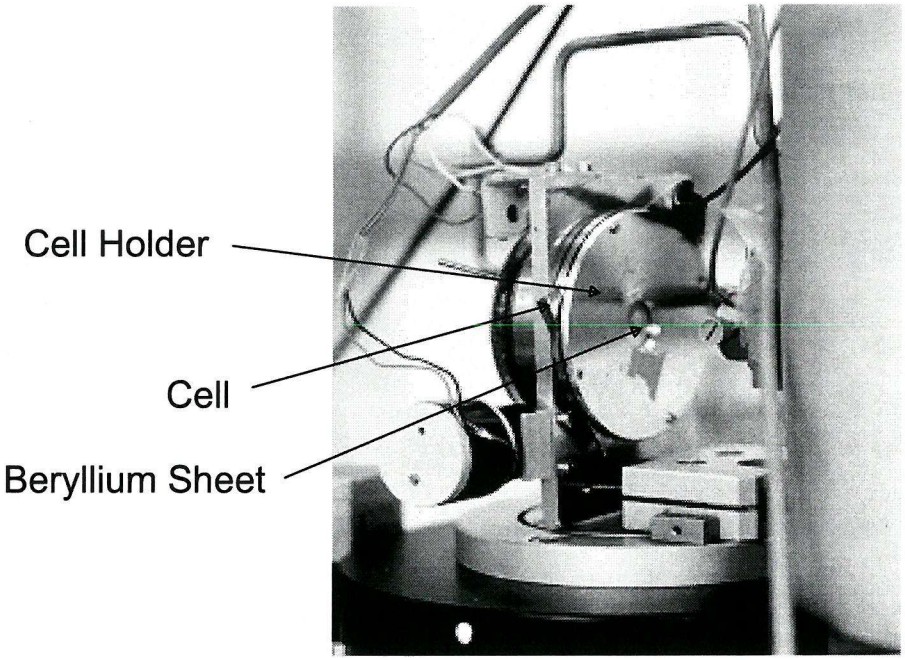

Figure 2.9 - Cell holder for X-ray diffraction

A STOE powder diffractometer (CuKα radiation) was used with a position sensitive detector (PSD) to make XRD measurements as concurrent electrochemical measurements were made with a MacPile II™ cycling system. The cycling system was electrically connected to the cell as shown in Fig. 2.10.

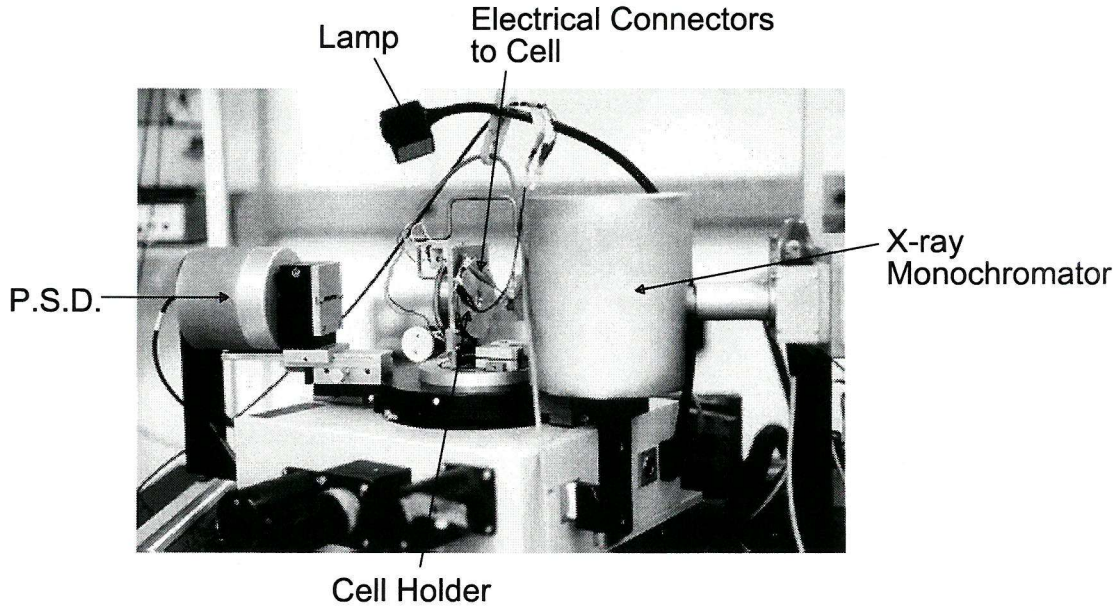

Figure 2.10 - *In-situ* X-ray diffraction equipment

The PSD covered 7° in 2Θ and was used in a fixed position. The use of a PSD enabled a larger proportion of the diffracted X-rays to be measured than would have been possible with a moving detector covering the same range. Consequently, consecutive diffractograms, of a given signal to noise level, could be measured more rapidly with the PSD system than would have been possible with a moving detector one.

2.5.6 AC impedance

AC impedance is one of the most common methods of non-destructive characterisation of the electrode/ electrolyte interface [18 - 20]. In this technique a small sinusoidal alternating voltage added to a bias voltage is applied between the working and reference electrodes of a test cell. The resulting current contains a component at the same frequency as the alternating voltage, although not necessarily of the same phase. In order to determine an AC impedance spectrum it is necessary to compare the relative amplitude and phase of the alternating voltage and current.

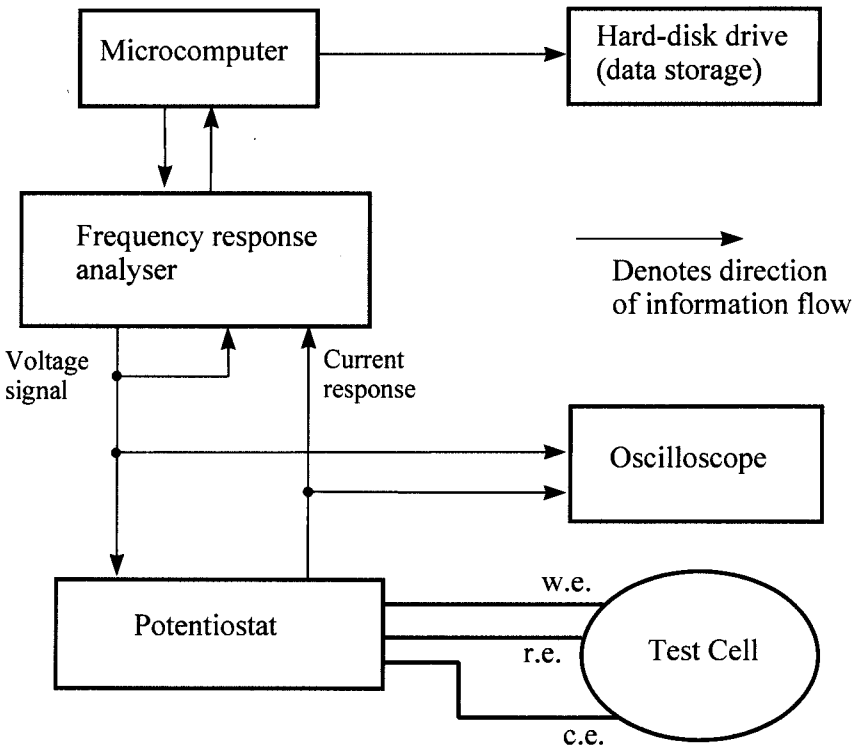

Figure 2.11 - Schematic representation of equipment for AC impedance measurements

A 1250 Solatron frequency response analyser (FRA) was used to generate appropriate voltage profiles. These were applied to the test cell by a purpose-built

potentiostat. The FRA compared the current response of the cell, converted by the potentiostat to a voltage signal, with the applied voltage. A microcomputer, which was running in-house software, recorded the impedance values from the FRA.

An oscilloscope (Gould Advance) was used for fault diagnosis (Fig. 2.11).

2.6 Standard Calculations

The following section is a summary of routine calculations and definitions of experimental parameters. A more detailed discussion of some more involved calculations is given in later chapters.

2.6.1 Cyclic voltammetry

The cycling efficiency, ζ, of a reaction may be defined as:

$$\zeta = \frac{q_{anod}}{q_{cath}} \times 100\ \% \qquad \textbf{Equation 2.3}$$

Where q_{anod} and q_{cath} are the anodic and cathodic charge passed. In order to compare voltammetric data it is useful to define anodic and cathodic charges per unit area of electrode, Q_{anod} and Q_{cath}, respectively. In general the charge passed per unit area is given by Eqn. 2.4, where j is the current density (i.e. j = i/A).

$$Q = \int j\,dt \qquad \textbf{Equation 2.4}$$

As the magnitude of scan rate, $|v|$ was a constant for a given scan, the charge per unit area was often calculated using Eqn. 2.5 and Eqn. 2.6.

$$Q_{anod} = -\frac{1}{|v|.A}\int i\,dV \qquad i<0 \qquad \textbf{Equation 2.5}$$

$$Q_{cath} = \frac{1}{|v|.A}\int i\,dV \qquad i>0 \qquad \textbf{Equation 2.6}$$

2.6.2 Coulometric titration

The cycling efficiency of a coulometric titration is defined according to Eqn. 2.3. However, for comparison of coulometric titrations of carbon electrodes against lithium it was necessary to determine charge passed per unit mass of electrode test material, Q rather than charge passed per unit area of electrode, Q:

$$Q = \frac{|i.t|}{m_{test}} \qquad \textbf{Equation 2.7}$$

where m_{test} is the mass of electrode test material.

Coulometric titration data is often displayed as a plot of electrode potential or cell voltage V against Q. However, it has been found that plotting dx/dV with respect to V can be of value in emphasising subtle changes of gradient in the V vs. Q curve [21]. x is the maximum theoretical amount of electrochemically inserted lithium such that the test material would have stoichiometry Li_xC_6.

2.6.3 X-ray diffraction

The X-ray intensity was recorded with respect to the angle between incident and reflected beams, 2Θ. A plot of X-ray intensity, from a crystalline sample, with respect to 2Θ typically revealed several peaks. The peaks originated through constructive interference of X-rays reflected from various crystal planes with miller indices hkl [22]. It may be shown that the lattice spacing d_{hkl} for a series of planes may be found from the glancing angle Θ_{hkl}, by the Bragg Equation (Eqn. 2.8).

$$n\lambda = 2d_{hkl}\sin\Theta_{hkl} \qquad \textbf{Equation 2.8 - Bragg equation}$$

where n is the harmonic index of the peak (generally n=1) and λ is the wavelength of the radiation ($\lambda(CuK_\alpha) = 1.54056$ Å).

Another dimension that may be extracted from XRD data is the average crystallite thickness in a given direction, t_{hkl}. This may be obtained by the Scherrer equation [23](Eqn. 2.9)

$$t_{hkl} = \frac{0.9\lambda}{\beta \cos\Theta_{hkl}}$$

$$\beta = \sqrt{B_{hkl}^2 - b^2}$$

Equation 2.9 - Scherrer equation

where B_{hkl} is the full-width half-maximum (FWHM) value of the hkl peak and b the equivalent instrumental broadening. However, more involved calculations of crystallite size have been undertaken [24].

2.7 Experimental Errors

In any comparative study it is essential to quantify experimental errors. In the following chapter, unless otherwise stated, it will be assumed that all parameters may be treated as if they had Gaussian distributions. For convenience, an estimated error in a quantity may be assumed to encompass 95 % of the distribution. Thus, an estimated error may be treated as if it were equal to twice the standard deviation, σ, of the distribution. Errors may therefore be treated by standard statistical methods, for example, for the two independent quantities a and b and there respective standard deviations σ_a and σ_b it follows that if,

$$y = k_a a + k_b b \qquad \textbf{Equation 2.10}$$

then

$$2\sigma_y = 2\sqrt{(k_a\sigma_a)^2 + (k_b\sigma_b)^2} \qquad \textbf{Equation 2.11}$$

Similarly if,

$$y = ka.b \qquad \textbf{Equation 2.12}$$

then

$$2\sigma_y = 2ka.b\sqrt{\left(\frac{\sigma_a}{a}\right)^2 + \left(\frac{\sigma_b}{b}\right)^2} \qquad \textbf{Equation 2.13}$$

2.7.1 Pulsed galvanostatic cycling

Many electrodes were tested by using a pulsed coulometric titration. The charge passed per unit mass of test material, Q, during any half-cycle of the titration is given by Eqn. 2.14:

$$Q = i\frac{t_{tot}t_1}{t_2+t_1}.\frac{1}{m_{test}} \qquad \textbf{Equation 2.14}$$

where t_{tot} is the total time for the half-cycle, t_1 is the current on duration, t_2 is the current off duration and m_{test} is the mass of the test material. Initially, m_{test} was calculated from the electrode area, A, average mass per unit area of the backing material, ρ_{area}, and the proportion material on the backing foil which is test material (i.e. not binder), P_{test}, by Eqn. 2.15:

$$m_{test} = P_{test}(m_{total} - A\rho_{area}) \qquad \textbf{Equation 2.15}$$

where m_{total} is the total mass of the electrode.

The errors involved in each measurement may be considered as:

i) P_{test}, is dependent on the accuracy to which the original binder/ test material paste was made and the homogeneity of the paste. An average value of P_{test} was 0.90 with an estimated magnitude of error of 0.01. To minimise the error in P_{test} binder stock solutions were calibrated at regular intervals to allow for solvent evaporation.

ii) ρ_{area} was determined by weighing and measuring the area of pieces of backing foil by the methods outlined for the electrodes. Sample pieces of backing foil had typical areas of ~10 cm^2 and mass ~220 mg. Thus, ρ_{area} had typical values of 22 mg cm^{-2} with errors of 0.5 mg cm^{-2}. Most of the error apparently arose from variations in the backing foil thickness, rather than the measurements.

iii) m_{total} was measured by using a Mettler AE 163 electronic balance, which was calibrated at regular intervals using standard masses. m_{total} had a typical value of 10 mg with an estimated magnitude of error of 30 μg.

iv) A was calculated from the length and width of the electrode which were measured by using a micrometer. Similar errors in A were found when using an optical microscope with graduated eyepiece, travelling microscope or vernier callipers. Of these techniques the former was found to be the most convenient. Values of A were typically of the order of 0.35 cm^2 with an estimated error of 0.03 cm^2.

v) t_1 and t_2 were dependent on the timing of voltage signals to the galvanostats and the speed of response of relays within the galvanostats. Typical values of t_1 and t_2 were greater than 100 s with estimated errors of 10 ms.

vi) t_{tot} was the time taken for the potential to reach a certain limit during the titration. Thus the precision with which t_{tot} could be measured was $t_1 + t_2$. As the accuracy in measuring t_{tot} may be taken as being similar to that for t_1 and t_2, t_{tot} may be considered an accurate but imprecise measurement. A typical value for t_{tot} was 8×10^4 s with an error of the order of 1×10^3 s.

vii) i was set by adjusting the galvanostat whilst measuring the output with an ammeter. Initially the accuracy of i was dependent on the accuracy of the ammeter. Subsequently error from long term drift in the current settings were found to be minimal by passing current through a known resistor for up to 24 h and logging voltage. i typically had values of 100 - 200 μA with errors of 0.3 μA.

The magnitudes of the errors outlined above have been summarised in Table 2.1

Table 2.1 - Typical errors in selected experimental parameters

Parameter	Magnitude of error
P_{test}	1.1 %
ρ_{area}	2.2 %
m_{total}	0.3 %
A	9 %
t_1, t_2	0.01 %
t_{tot}	1.2 %
i	0.3 %

It can be clearly seen that the largest source of error in Q was that from determination of the A. However, it should be noted that, the value of m_{test} was typically of the order of 2 mg which is roughly five times smaller than m_{total}. By combining the errors in Eqn. 2.15 according to Eqn. 2.11 and Eqn. 2.13, it may be shown that, by using the typical values of P_{test}, ρ_{area}, m_{total} and A given above, the value of m_{test} is 2.1 mg with an error of 0.7 mg (33 %). Hence, the final error in Q may be estimated at 33 %. Thus, it was considered necessary to repeat experiments based on these calculations several times and calculate an average value of Q.

An alternative approach to reducing errors was adopted for later titrations. In this approach the current was initially set based on a rough calculation of m_{test} by the method

outlined above. However, after the titration was completed the electrode was removed from the test cell and washed with copious de-ionised water to remove lithium. The test material and binder was then carefully removed from the backing foil. The mass of the backing foil, m_{foil}, was measured and the value of m_{test} recalculated using Eqn. 2.16

$$m_{test} = P_{test}(m_{total} - m_{foil}) \qquad \textbf{Equation 2.16}$$

The error in m_{foil} was comparable to that of m_{total}, i.e. 30 μg. This leads to an error in m_{test} of 45 μg (2.2 %). Thus the total error in Q is 2.5 %.

Shorter current pulses and relaxations (lower values of t_1 and t_2) for a given cycling rate were employed in some titrations to reduce the error in determining t_{tot}. Typically the error was reduced to 250 s (for $t_{tot} \sim 8 \times 10^4$ s), which reduced the error in Q to 2.2 %.

The cycling efficiency, ζ, of a given cycle is the ratio of charge passed on extraction to charge passed on insertion (Eqn. 2.3). Thus, ζ can be given by Eqn. 2.17:

$$\zeta = \frac{t_{tot,X}}{t_{tot,I}} \qquad \textbf{Equation 2.17}$$

where $t_{tot,X}$ and $t_{tot,I}$ are the total times of extraction and insertion respectively. It may be noted from Eqn. 2.17 that the method for determining m_{test} did not affect the error in ζ. The error in ζ was dependent on the number of current pulses required for insertion and extraction, as noted above. Thus, the error in ζ varied from 1.7 % to 0.4 % as $t_1 + t_2$ was decreased from 1000 s to 250 s ($t_{tot} \sim 8 \times 10^4$ s).

Values of dx/dV were calculated using in-house software (appendix C). To calculate dx/ dV the software selected the set of voltage points immediately prior to each current pulse for a given titration. The software then applied a simple routine, which is summarised in Fig. 2.12, to calculate values of dx/ dV. δV is a predetermined discriminator parameter.

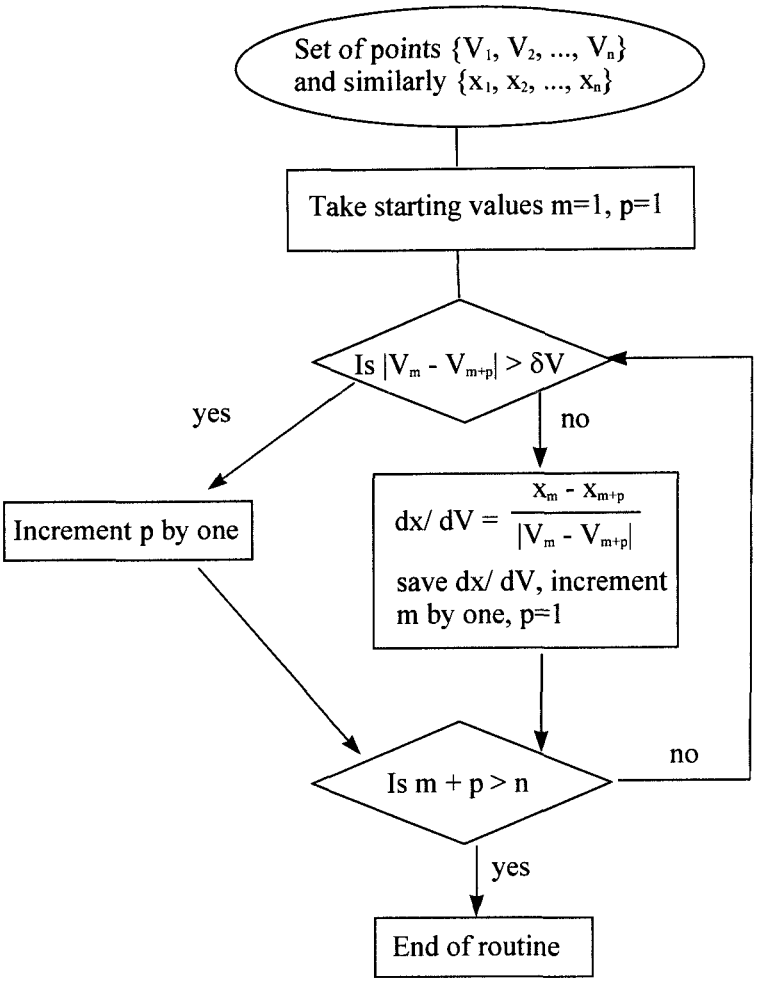

Figure 2.12 - Schematic representation of process to calculate values of dx/ dV from titration data

x is given by dividing the inserted charge by the charge required to form LiC_6, 372 mAh g^{-1} (chap. 1.2.2). Therefore, $x_m - x_{m+1}$ is given by Eqn. 2.18, where t_1 is in hours, i in μA and m_{test} in mg.

$$(x_m - x_{m+1}) = \frac{i.t_1}{372.m_{test}} \qquad \textbf{Equation 2.18}$$

Typical values of $x_m - x_{m+1}$ were 0.01 - 0.05, depending on the value of $t_1 + t_2$. The error in $x_m - x_{m+1}$ may be estimated, from the errors in i, t_1 and m_{test}, at 33 % to 2.2 % depending on the error in m_{test}.

When conducting a pulsed coulometric titration the computer recorded potential differences across each active channel of the ADC in turn, using in-house software (appendix B). Each recorded V was an average of many measured potential differences. By taking an average of a large number of readings it was possible to improve the

relative accuracy of V to better than resolution of the ADC (2.5 mV). This may be shown by using Eqn. 2.19 [25].

$$V_{true} = \underline{V} \pm t\left(\frac{s}{\sqrt{n}}\right) \qquad \textbf{Equation 2.19}$$

Where V_{true} is the true value of V, $\underline{V}$ is the average of n readings of voltage with a standard deviation s of the sample. t is a parameter which is dependent on the number of degrees of freedom in the distribution and on the confidence interval; for n >> 50 and 95 % confidence interval t = 1.96.

Typically a data point was recorded after sampling the galvanostat for 6 s at a sampling rate 2000 samples s^{-1}, giving n = 1.2 x 10^4 . 10 mV of random noise was associated with the sampled signal (s = 5 mV). Therefore, the error in V from random signal noise was 0.09 mV. Hence, the relative error in consecutive values of V may be taken as 0.13 mV. It should be noted, however, that the absolute error in V also included voltage offset terms from the ADC and galvanostat and may be estimated at 3 mV.

From the errors in x_m - x_{m+1} and V_m - V_{m+1} it is possible to estimate the error in dx/ dV for a given value of δV. Assuming the error in x_m - x_{m+1} was 2.2 %, and δV = 3 mV the error in dx/ dV was 4.9 %.

2.7.2 Cyclic voltammetry

Q, the charge per unit area of electrode was calculated from the cyclic voltammograms using Eqn. 2.4 for the computer-recorded data and Eqn. 2.5 and Eqn. 2.6 for the plotter-recorded data. The electrode area A had a typical value of 0.50 cm^2 with an estimated error of 0.05 cm^2. The integral of j with respect to t was approximated by Eqn. 2.20, in the microcomputer-controlled system.

$$\sum_n \frac{(i_{n+1} + i_n)}{2A} . (t_{n+1} - t_n) \approx \int j\,dt \qquad \textbf{Equation 2.20}$$

where i_n and t_n are the nth readings of current and time respectively.

The estimated systematic error in i_n was 0.2 % of the full current scale (f.s.). The random error in i_n was also estimated to be 0.2 % of the f.s. Therefore the systematic error in (i_{n+1} + i_n) was 0.4 % of the f.s., and the random error 0.3 % of the f.s. Similarly,

for a typical summation over 100 points, the random error would be 10 times less than the systematic error.

It may be assumed that the error in $(t_{n+1} - t_n)$ was negligible compared to the error in the other parameters.

For a typical scan f.s. may be 10 mA for $|\nu| = 20$ mV s^{-1}, A = 0.50 cm^{-2}, and an anodic current flow over the scan range 0.4 V $\rightarrow$ -0.2 V $\rightarrow$ 0 V. Therefore the voltage range to be summed over would be 0.8 V, giving a total of 320 data points (at 2.5 mV intervals), and a 40 s time range. Typically, Q may be 40 mC cm^{-2}, therefore the average current (over the integration range) would be 500 μA with an error of 20 μA. The error in Q would therefore be 4.3 mC cm^{-2} (11 %). It may also be noted that by a careful choice of the voltage integration region and appropriate choice of f.s. the error in Q may be significantly reduced.

When considering the errors in the plotted cyclic voltammograms it is necessary to note that i and V were not independent variables and so Eqn. 2.13 cannot be used. However, the cyclic voltammogram plots were calibrated with several values of i and V which were measured using a digital multimeter with a known resistor as the test cell. Therefore it may be expected that the dominant error in the integration of i with respect to V (Eqn. 2.5 and Eqn. 2.6) was due to the error in measuring the area under the curve. Typically the error in the integral may be estimated at 8 %.

If $|\nu|$ may be considered to have an error of less than 2 %, then the total error in Q would be 13 %.

As may be seen in Eqn. 2.3 the electrode area A is not required to determine the cycling efficiency ζ. A typical error in ζ for the computer-recorder voltammogram would be 8 % if the systematic error in i was in the same direction for the forward and reverse scans. Again, it may be noted that by an appropriate choice of the integration range and f.s. the error may be significantly reduced.

The error in ζ for the plotted voltammogram would be 11 %.

2.8 Transient Calculations

Voltage transients were obtained from electrochemical cells as outlined in chap 2.5.3. A typical electrode response to a current pulse is shown schematically in Fig. 2.13.

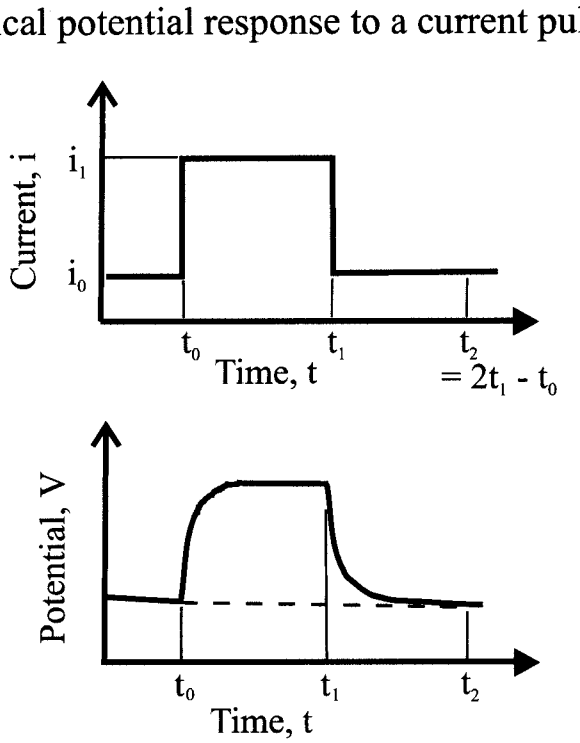

Figure 2.13- Schematic representation of a potential response to a current pulse

In order to analyse the potential response to the current pulse it was necessary to subtract the 'background' potential profile. A first-order approximation to the expected background profile was used, as shown schematically in Fig. 2.13 by the dotted line joining the potentials at t_0 and t_2. It may be noted that if the entire potential response from t_0 to t_2 was considered, only the potential gradient would have to be removed as time-independent potential offsets would not be expected to contribute to the transformed terms (at non-zero frequencies). However, the methods employed in this work used only half of the potential transient, from t_0 to t_1, on the assumption that the potential transient from t_1 to t_2 was symmetrically related to that from t_0 to t_1. This approximation may readily be shown to be valid for ideal capacitors and resistors, and would be expected to be valid for most real reversible systems.

To justify the use of a first-order 'background' curve, a typical transient from an electrochemical cell (graphite powder working electrode, lithium counter electrode) was

examined, Fig. 2.14. The transient was divided into two curves from t_0 - t_1 and t_1 - t_2 which were translated by -t_0 and -t_1 along the time-axis respectively, so that they both originated at t = 0. If the subtraction of a first-order 'background' curve would leave the two transients related under reflection in a plane parallel to the time-axis (after translation) then the system may be described by Eqn. 2.21;

$$V_0(t) - \alpha t = A - [V_1(t) - \alpha t] \qquad \textbf{Equation 2.21}$$

where V_0 and V_1 are the potential of the cell at a time t + t_0 and t + t_1 respectively, α is the gradient of the 'background' potential curve and A is a potential offset term. Eqn. 2.21 may be rearranged to give Eqn 2.22:

$$\frac{V_0(t) + V_1(t)}{2} = \frac{A}{2} + \alpha t \qquad \textbf{Equation 2.22}$$

Thus, the mid-points of the two translated curves should fall along a first-order curve, with gradient α, when arranged against time. This may be seen to agree well with a typical experimental transient, Fig 2.15.

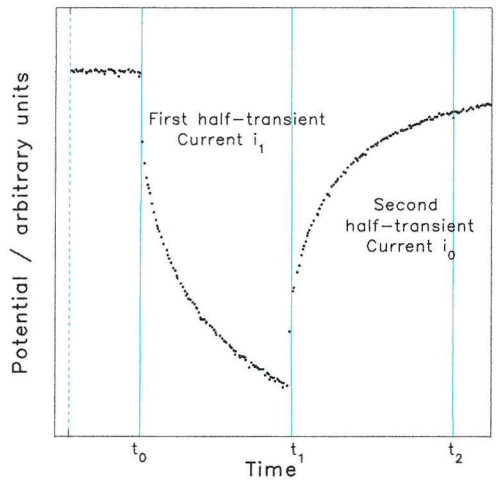

Figure 2.14 - Potential transient resulting from a current pulse in a Li/graphite cell

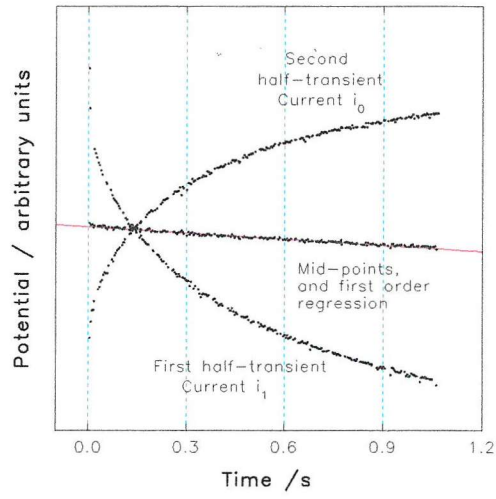

Figure 2.15 - Comparison of transient halves from Fig. 2.14

2.8.1 FT impedance

Fourier analysis models repeating patterns by the superimposition of many sine and cosine functions of appropriate amplitudes and frequencies. This process is shown pictorially in Fig 2.16 for a current pulse and Fig. 2.17 for the consequent voltage transient.

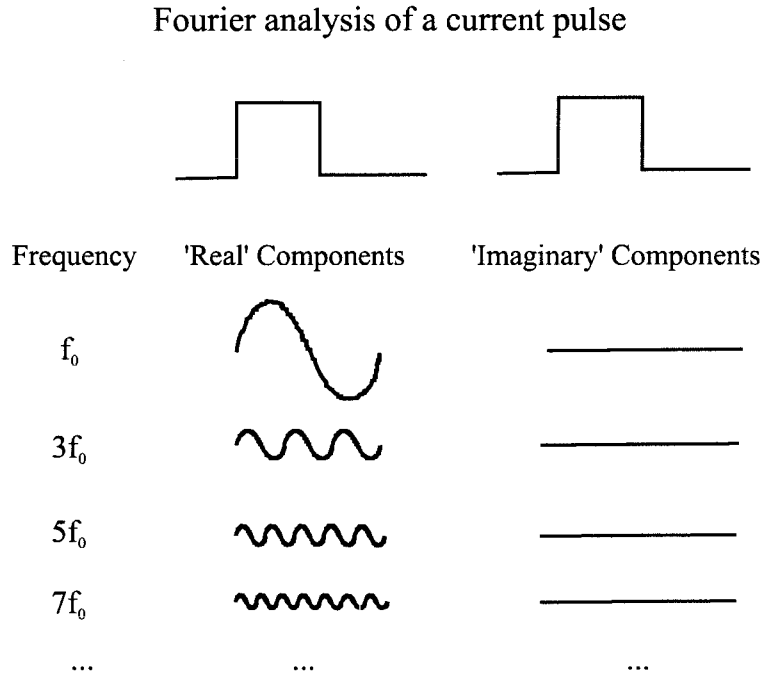

Figure 2.16 - Pictorial representation of Fourier deconvolution of a current pulse

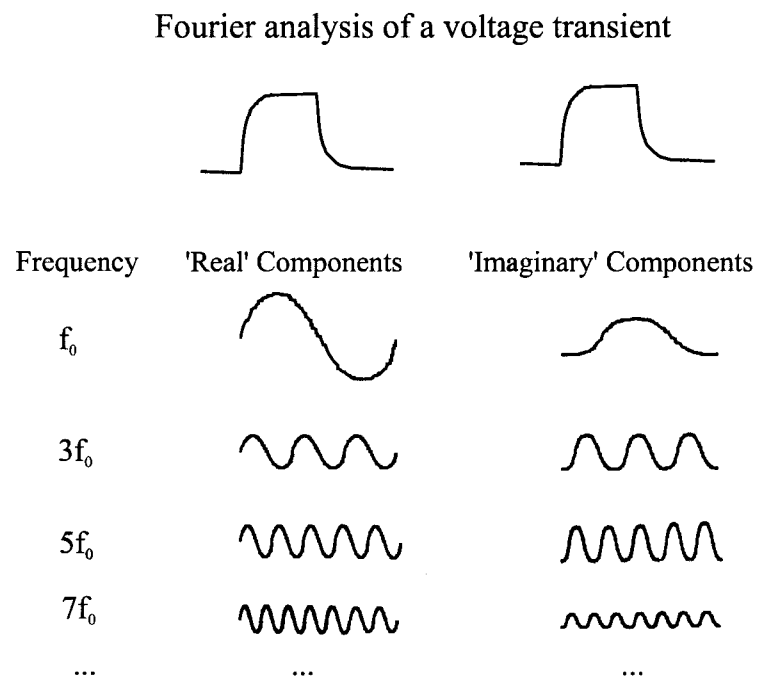

Figure 2.17 - Pictorial representation of a Fourier deconvolution of a voltage transient

The alternating currents represented by sine functions have been termed real and those by cosine functions imaginary, by analogy with AC impedance - taking the onset of the current pulse as t = 0.

Mathematically, a current, i(t), as shown Fig. 2.13 may be expressed by Eqn 2.23 (taking $t_0 = 0$).

$$i(t) = \frac{i_0 + i_1}{2} + \frac{i_1 - i_0}{\pi}\left(\sin\omega_0 t + \tfrac{1}{3}\sin 3\omega_0 t + \ldots\right) \qquad \textbf{Equation 2.23}$$

where $\omega_0 = 2\pi f_0$ and $f_0 = 1/t_2$.

It may be seen from Eqn. 2.23 (and Fig. 2.16) that the current pulse is comprised entirely of 'real' components at angular frequencies, $\omega = (2n + 1)\omega_0$ where n = 0, 1, 2, ... Therefore, the voltage profile may be expected to consist of real $V'(\omega).\sin(\omega t)$ and imaginary $V''(\omega).\cos(\omega t)$ components which may be obtained from the baseline-corrected voltage transients by integration with sine and cosine functions over an appropriate range of frequencies using Eqn. 2.24.

$$\int_0^{\frac{2\pi}{\omega_0}} \sin(n\omega_0 t).\sin(m\omega_0 t)\,dt = \begin{cases} 0 & n \neq m \\ \dfrac{\pi}{\omega_0} & n = m \end{cases} \qquad \textbf{Equation 2.24}$$

and similarly for the cosine functions.

V'(w) and V''(w) are related to the current terms by Eqns. 2.25 and 2.26, respectively.

$$V'(\omega) = i(\omega).Z'(\omega) \qquad \textbf{Equation 2.25}$$

$$V''(\omega) = i(\omega).Z''(\omega) \qquad \textbf{Equation 2.26}$$

where $i(\omega) = (i_1 - i_0).\omega_0/(\omega.\pi)$, Z'(w) is the resistance and Z''(w) is the reactance. Hence Z' and Z'' may be obtained from the voltage transient. However, this method only gives impedance values at a limited number of frequencies, determined by $t_2 - t_0$ and the maximum data sampling frequency. It was also noted that equal weighting was given to all points in the voltage transient even when calculating the highest frequency components. It has already been shown that the two halves of the voltage transient are symmetrical related,

and stated that only one half (from t_0 to t_1) is used in the Fourier analysis. As the second half of the voltage transient has been assumed it was decided that a valid Fourier analysis could be performed by considering reduced lengths of the original half-transient. Therefore, a second method of analysis was performed (appendix D) by considering only the fundamental component of a series of transients of decreasing length, as opposed to the original method which considered fitting components of increasing frequency to a transient of fixed length. A comparison of impedance data produced by the two techniques from the same voltage transient obtained from a real electrochemical cell (graphite working electrode/ lithium counter electrode) is shown in Fig. 2.18.

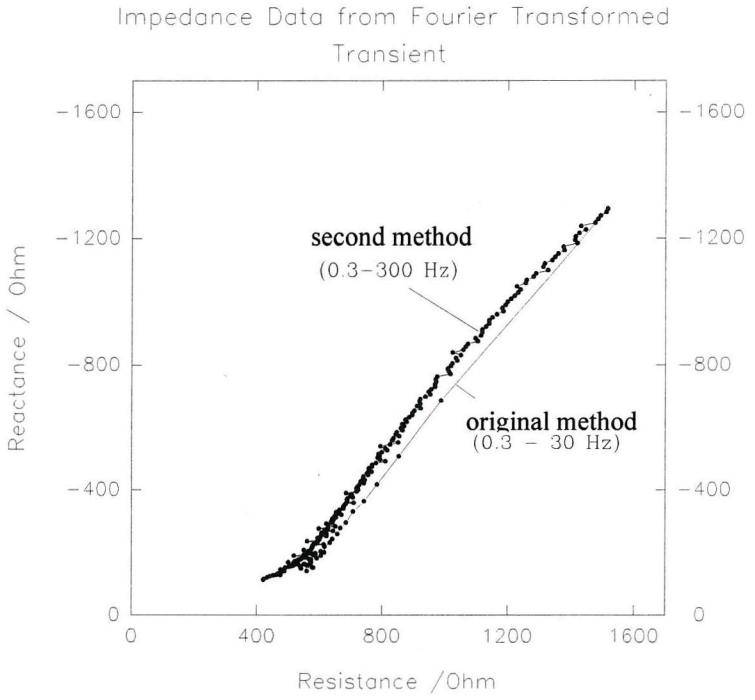

Figure 2.18 - Impedance data produced by transforming the same transient data with different FT methods

As would be expected the two techniques gave similar values of impedance for a given frequency and the second method gave many more data points over an extended range. The slight difference in the shape and position of the curves arose from the incorrect assumption that the baseline gradient was independent of the transient length. For any circuit with parallel capacitive elements the second method would be expected to give values of reactance at high frequencies that were too negative. However by comparison of impedance plots obtained by the two methods the validity of the second method may be examined in any given cell.

2.8.2 Artefacts and errors

Clearly FT impedance would be expected to be prone to many of the same artefacts as AC impedance [27]. These have been summarised along with potential sources of error, their effects and how they may be detected in Table 2.2. The term 'ideal' equivalent circuit refers to a circuit constructed from well-characterised electronic components.

Table 2.2 - Summary of sources of error in FT impedance and possible means of detection

Source of error/ artefact	Effect	possible means of detection
slow galvanostat response	negative pseudo-inductance	'ideal' equivalent circuits
stray instrument capacitance	extra capacitance terms	'ideal' equivalent circuits
saturation of amplifier, galvanostat or ADC	various distortions of the impedance profile	'clipping' of transient
incorrect baseline slope (see Fig. 2.19)	increase or decrease in capacitance terms	'ideal' equivalent circuits, less of a problem with the second analysis method
incorrect baseline offset	positive of negative resistance offset	as for baseline slope, also reanalysis of the data
voltage noise	noise in Z' and to a lesser extent Z"	noise in the transient appears in impedance data from the second method
inaccurate timing of t_0	high frequency distortion	reanalysis of the same pulse, repeated pulses or higher frequency data sampling
non-linear electrochemical response	low frequency distortion (non-ideal R_{ct})	pulses at lower i, comparison with AC impedance data

Fig. 2.19 shows the effect of an inappropriate baseline slope (zeroth order in place of first order baseline). As expected the error becomes more marked at lower frequencies ($Z''(\text{capacitor}) = -1/\omega C$). The transient used to obtain the data for Fig. 2.19 was obtained from an electrochemical cell (graphite powder/ lithium). However, as indicated in Table 2.2 many artefacts and errors may be detected by using 'ideal' equivalence circuits.

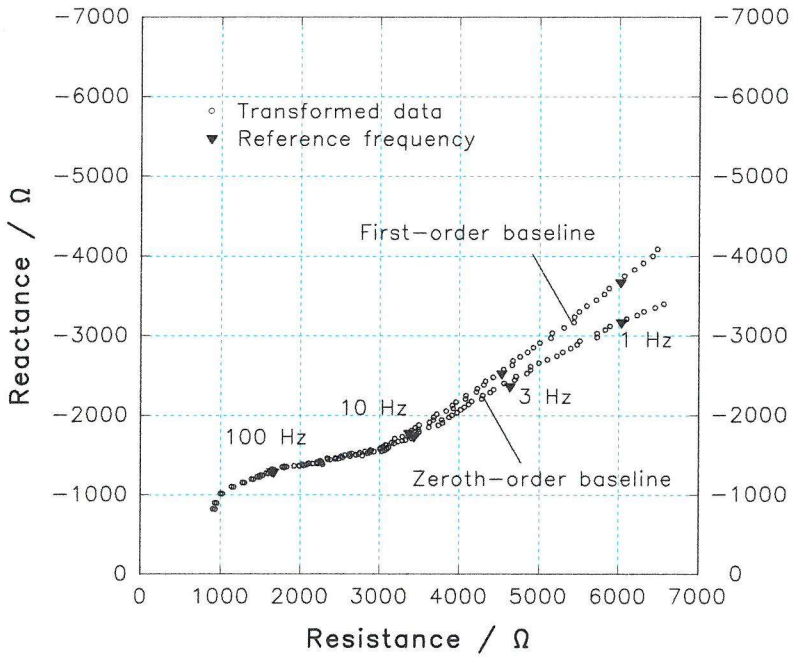

Figure 2.19 - Comparison of impedance data produced by transforming a potential transient using different baseline approximations

The data obtained from 'ideal' circuits may be compared with theoretical models or experimental AC impedance data. Fig. 2.20 shows a comparison of FT impedance (method 2) data with an AC impedance response and theoretical curve for the same circuit (Fig. 2.21 - 100 kΩ resistor in parallel with a 0.47 μF non-electrolytic capacitor). It is clear that the techniques are in good agreement at low frequencies (< 3 Hz). However, at high frequencies the FT impedance data diverges slightly from both the theoretical and AC impedance values. A similar divergence was found when other transients obtained from the same circuit were transformed. This would indicate that inaccurate measurement of t_0 was unlikely to have contributed to the high-frequency distortion of the FT impedance data.

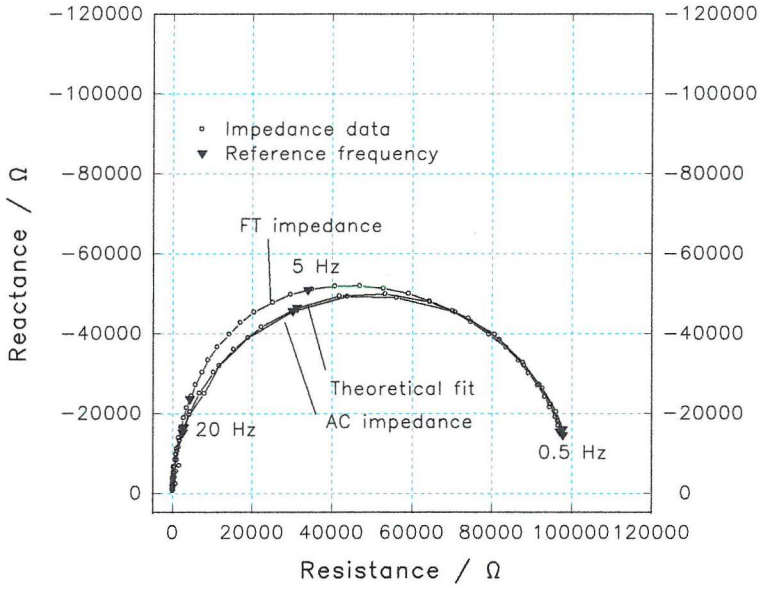

Figure 2.20 - Comparison of theoretical, FT and AC impedance data for the circuit shown in Fig. 2.21

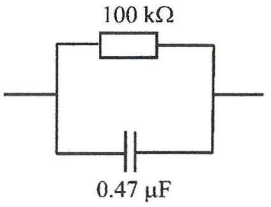

Figure 2.21 - Test circuit

To examine the possibility that divergence was due to a slow galvanostat response a second 'ideal' circuit, consisting of a single 100 kΩ resistor, was examined. The transformed data (Fig. 2.22) showed almost ideal behaviour, indicating that the galvanostat was unlikely to have caused the previous distortion (Fig. 2.20).

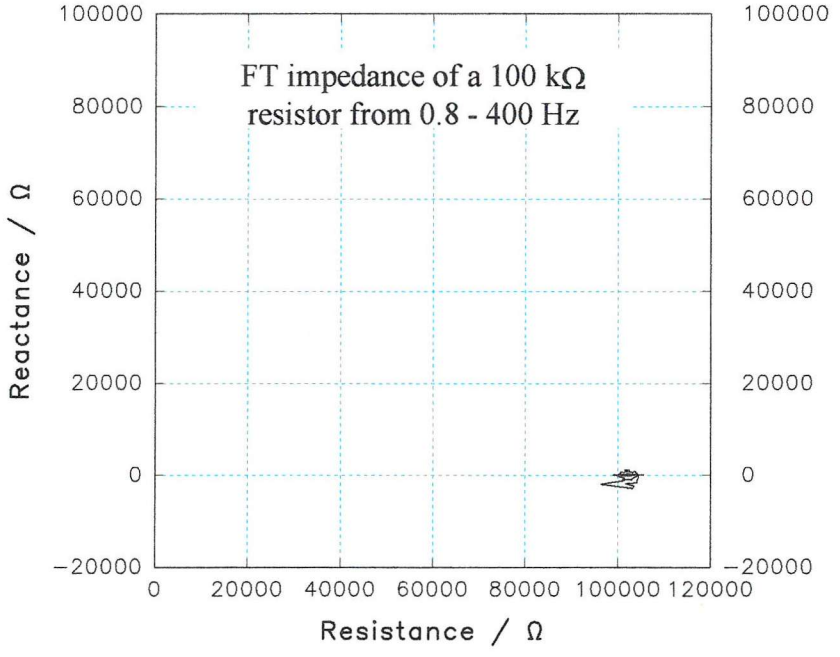

Figure 2.22 - FT impedance of a 100 kΩ resistor

It appears that the most likely source of high-frequency distortion would be the baseline assumption used in the second FT method - it may also be noted that for a pure RC circuit the baseline is given by Eqn. 2.27 which only approximates to first order when the transient length t_1 is much larger than the product of resistance and capacitance:

$$baseline\,V(t) = V_0 + \frac{(i_1 - i_0)R}{2}\left(1 - e^{\frac{-t - t_1}{RC}}\right) \qquad \textbf{Equation 2.27}$$

where i_0, i_1 and t_1 are as shown in Fig. 2.13 and $V_0 = V(t_0)$.

2.8.3 Laplace transforms

Laplace transformation of transients has been used to extract impedance parameters from biological systems [28] and lithium metal/ polymer electrolyte cells [29]. Laplace analysis may be used to convert data from a real-time to frequency domain, according to the following general equation:

$$F(s) = \int_{t=0}^{\infty} f(t).e^{-st}\,dt \qquad \textbf{Equation 2.28}$$

Eqn. 2.29 may be used to obtain impedance values, Z(s), from the Laplace transformed current and voltage profiles, i(s) and V(s) respectively.

$$Z(s) = \frac{V(s)}{i(s)} \qquad \textbf{Equation 2.29}$$

However, Eqn. 2.29 leaves the real and imaginary impedance terms unseparated. The Z(s) term may be analysed by fitting explicit, pre-determined functions. In this manner a good fit was found between AC impedance and a theoretical impedance curve simulated from parameters obtained by Laplace transformation of a current transient, for the circuit shown in Fig. 2.25.

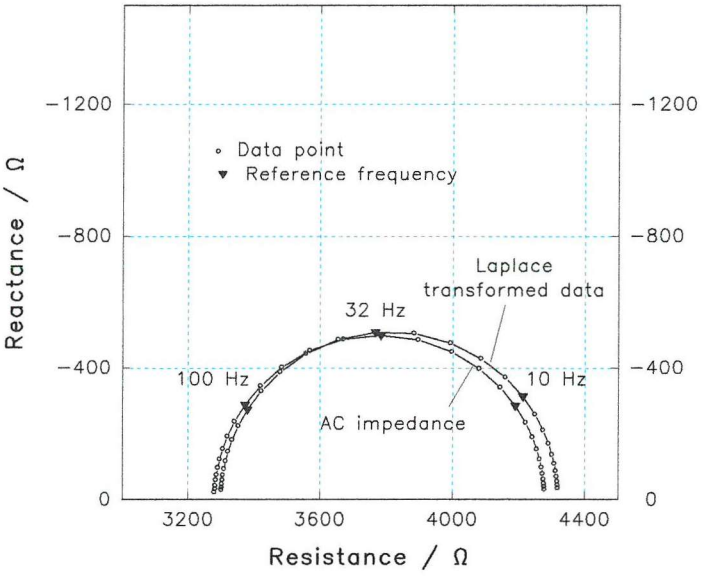

Figure 2.23- Comparison of AC impedance and simulation from parameters obtained by Laplace transformation, from 1 Hz - 1 kHz for the circuit shown in Fig. 2.24

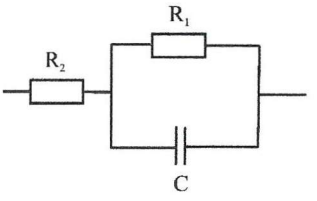

Figure 2.24 - Test circuit

For the circuit shown in Fig. 2.24 the Laplace impedance Z(s) had the form shown in Eqn. 2.30:

$$Z(s) = R_2 + \left(sC + \frac{1}{R_1} \right)^{-1}$$ **Equation 2.30**

Although, such a technique may be of value in instances where a suitable equivalent circuit can be proposed *a priori*, it was found to be difficult to unambiguously fit curves to Z(s) for electrochemical cells.

Chapter 3

Results & Discussion - Monolithic Electrodes

For the purpose of the following sections a monolith is defined as a single object consisting primarily of only one compound. The electrodes examined in the following chapter were monolithic prior to cycling.

The following electrodes - with the exception of lithium metal [1] - have not been considered for commercial application. The interest in their study arose from the anticipation that by using monolithic electrodes, in preference to composite electrodes (chap. 4), a clearer understanding of cycling behaviour of individual electrode materials could be obtained. It was expected that any insights into the performance of individual electrode materials would be beneficial in optimising composite electrode systems.

3.1 Lithium Metal

As expressed previously lithium metal has many properties which are desirable in a negative electrode material (chap. 1): the standard electrode potential of lithium metal is more negative and the charge capacities per unit volume and mass are greater than for any alternative electrode material considered for use in lithium batteries.

The following studies were carried out to examine the compatibility of substrate materials and solvents with lithium metal and to evaluate the performance of lithium metal as a the negative electrode in secondary cells, for comparison with carbon-based electrodes.

3.1.1 Substrate

Three-electrode cells were constructed, each with a lithium reference electrode, a lithium counter electrode and a metal working electrode. The electrolyte was 1 M $LiAsF_6$ in PC. Cyclic voltammetry was used to examine the effect of substrate on lithium plating/stripping. Copper, silver, aluminium and nickel working electrodes were studied.

Fig. 3.1, shows a cyclic voltammogram, at 20 mV s^{-1}, of a copper working electrode. The cell was cycled five times from +1 V → -0.2 V → 1 V vs. Li/Li^+.

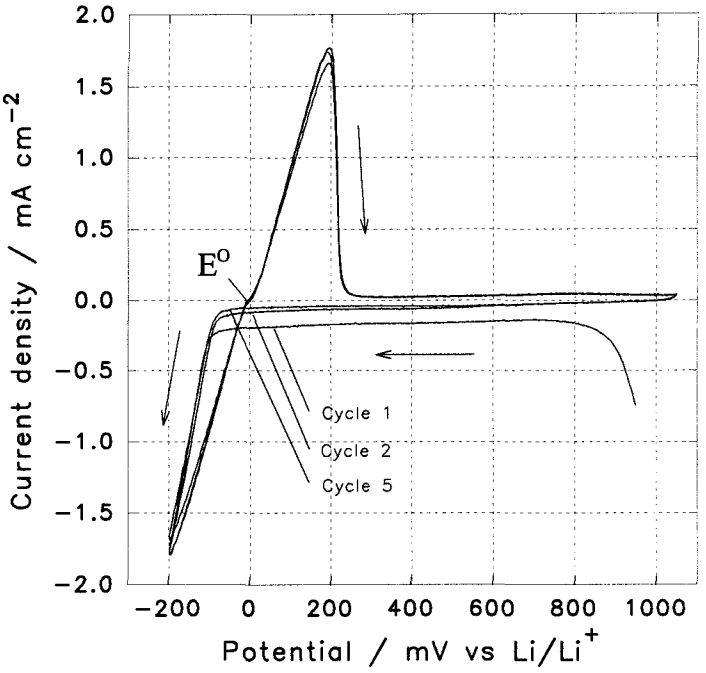

Figure 3.1 - Cyclic voltammogram of lithium on copper at 20 mV s-1

Several features of the cyclic voltammogram (Fig. 3.1) may be noted:

i) the cycling efficiency, ζ, as defined in Eqn. 2.3, of the first cycle was lower than that of subsequent cycles.

ii) the cell cycled reproducibly from the second to fifth cycles, with ζ = 73 %.

iii) there was an overpotential to lithium plating, η_{plate}, of about 60 mV, as defined by Eqn. 3.1.

$$\eta_{plate} = \Delta E_{max} \qquad \textbf{Equation 3.1}$$

$$where\ \Delta E(i) = E(i, \frac{dE}{dt} > 0) - E(i, \frac{dE}{dt} < 0) \quad , i < 0$$

For comparison, cyclic voltammograms of nickel, silver and aluminium electrodes were recorded using the same experimental parameters as above.

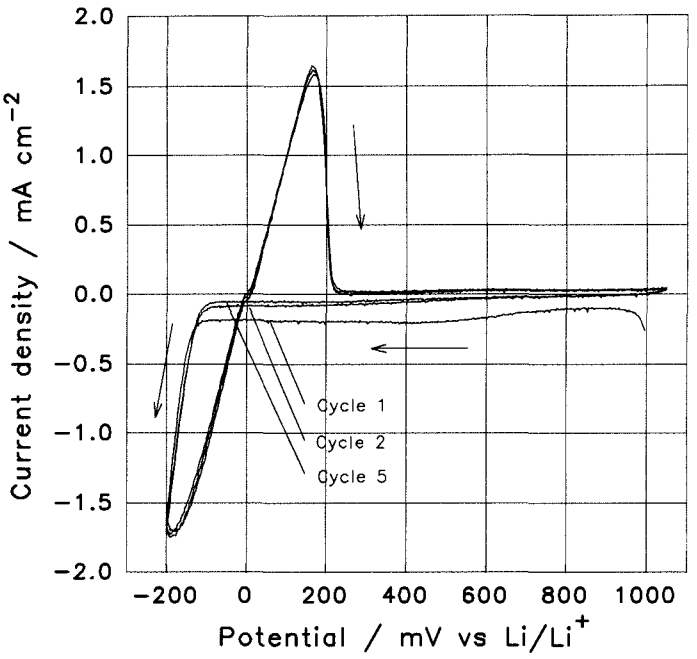

Figure 3.2 - Cyclic voltammogram of lithium on nickel at 20 mV s^{-1}

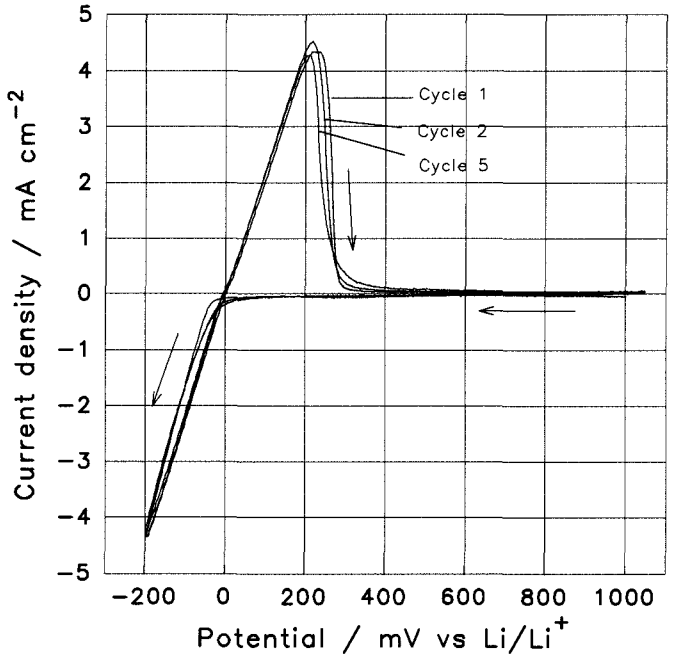

Figure 3.3 - Cyclic voltammogram of lithium on silver at 20 mV s^{-1}

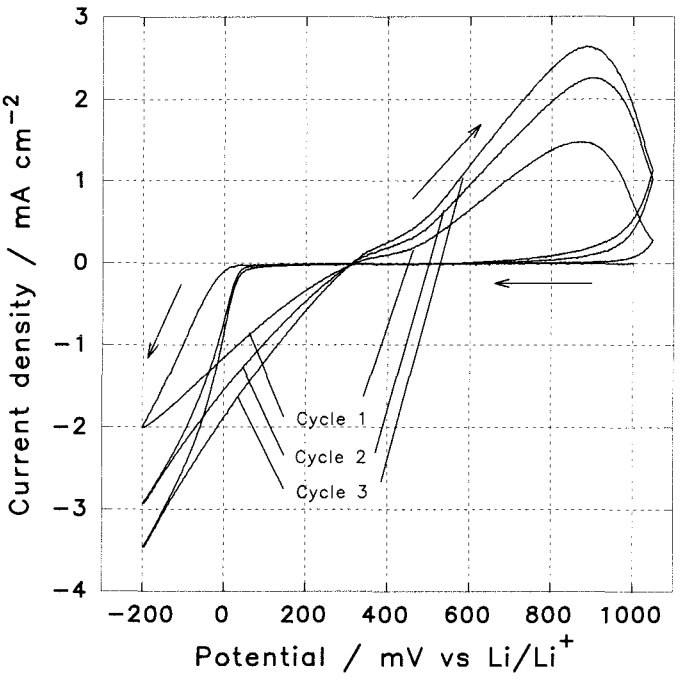

Figure 3.4 - Cyclic voltammogram of lithium on aluminium at 20 mV s^{-1}

Using Eqns. 2.3 and 3.1, η_{plate} and ζ were calculated, for the second cycle of each of the electrodes, (Table 3.1). The potentials at which there was no net current flow in the lithium plated electrodes, E^O, are also given.

Table 3.1 - Voltammetric parameters of selected metals.

Material	η_{plate} / mV	E^O / mV vs. Li/Li$^+$	ζ %
Copper	60	-5	73 ± 6
Nickel	95	0	67 ± 5
Silver	15	-5	89 ± 7
Aluminium	260	+315	89 ± 7

From the values of E^O it is apparent that the anodic reaction of 'lithium-plated' aluminium was different to those of copper, nickel and silver electrodes. The values of E^O for 'lithium-plated' copper, silver and nickel were within 5 mV of the Li/Li$^+$ equilibrium potential. Thus it may be assumed that the anodic reaction in these cases was: $Li \rightarrow Li^+ + e^-$, whereas it is unlikely that the same reaction accurately described the situation for 'lithiated' aluminium.

It is well known that lithium can form alloys with aluminium [2], which exhibit an equilibrium potential positive to that of the plated metal [3]. The value of E^O for aluminium (Table 3.1) implies that the 'lithiated' aluminium would more accurately be described as a lithium-aluminium alloy than as lithium-plated aluminium. Therefore, the lithium-aluminium anodic reactions would have been of the form: $Li_xAl \rightarrow Al + xLi^+ + xe^-$. The value of E^o (+315 mV vs. Li/Li^+) is close to the accepted average value for the LiAl phase (+360 mV vs. Li/Li^+ [4]). η_{plate} for aluminium is the overpotential for nucleation of a lithium-aluminium phase.

The maximum cathodic current increased for the first five cycles of the aluminium electrode (Fig. 3.4 - fourth and fifth cycles not shown, for clarity). However, the other metals showed reproducible behaviour after the second cycle. In the aluminium cell, the increase in cathodic current may have resulted from an increase in the electrode surface area, through surface cracking, as observed by Maskell and Owen [3]. Such surface cracking can occur as a result of volume changes on alloying/ dealloying and would not be expected under simple plating/ stripping conditions

Silver showed slightly different cycling behaviour to copper or nickel in that it exhibited a lower value of η_{plate} and a higher cycling efficiency. It should also be noted that the anodic peak shape changed slightly with cycle number. On the fifth cycle an appreciable anodic current flowed at potentials significantly above that of the stripping peak. This would be expected if the lithium was being removed from more than one type of site. From the value of E^O it was inferred that some of the lithium was plated on the surface, therefore it may be anticipated that some lithium was either on a different type of surface site or that it was alloyed with the silver. The latter hypothesis is credible as a series of lithium-silver phases have been formed at elevated temperatures [5, 6] ($AgLi_{0-0.87}$, $AgLi_{1-1.27}$, $AgLi_{1.74-2.7}$, $AgLi_{3.2-12}$, $Ag_{0.005-0}Li$) and it has been suggested that lithium-silver alloys can be formed electrochemically at room temperature [7].

Lithium was not expected to alloy markedly with nickel at room temperature as the maximum solubility of nickel in lithium at 200 °C is 0.0060 w/o, and at 600 °C is 0.066 w/o [8] (cf. silver in lithium 7.5 w/o). In contrast, the maximum solubility of lithium in copper at 179 °C is 2.7 w/o [9] (cf. lithium in silver 6 w/o) and it has been suggested that lithium-copper alloys can be formed electrochemically from aqueous solution [10]. However, the voltammetric parameters for nickel and copper (Table 3.1)

were similar as were the anodic peak shapes. This suggests that there was little alloying of the lithium with either metal, under the cycling conditions applied. Hence, in order to study lithium plating/ stripping nickel flags were used and it was decided to construct current-carrying cell parts from nickel or copper.

3.1.2 Charge loss

As stated previously the first cycle efficiency of the copper electrodes was lower than that of subsequent cycles. From Fig. 3.1 it is apparent that an appreciably larger amount of charge was passed on the first cathodic sweep from 1000 mV to 0 mV vs Li/Li^+ than on subsequent sweeps over the same region. A similar phenomenon may be observed for nickel (Fig. 3.2). It may also be noted that the values of ζ for lithium on nickel and copper were much below 100 % on every cycle. Low values of ζ have been found for a number of different solvents [11], salts [12] and impurities [13]. A low value of ζ indicates irreversible or 'charge loss' processes. The 'charge loss' processes generally associated with plating and stripping lithium metal are considered to be film forming parasitic reactions [14 - 18] and electrical isolation of dendritic lithium deposits [19, 20].

In an attempt to examine the extent of each process a series of cyclic voltammograms were recorded for lithium plating and stripping on a nickel flag electrode from a 1 M $LiAsF_6$/ PC solution.

The cell was initial subjected to three 'conditioning cycles' from 1 V $\rightarrow$ -250 mV $\rightarrow$ 1 V vs Li/Li^+. The electrode was then cycled from the open circuit voltage $\rightarrow$ -390 mV $\rightarrow$ 0 mV vs Li/Li^+ at a rate of 20 mV s^{-1}, held at open-circuit for a set period of time t_{oc} , and then cycled from 0 mV to 1 V vs Li/Li^+ at 20 mV s^{-1}. t_{oc} was increased from 0 to 180 s for successive scans.

Q_{cath} was found to vary little on successive cycles (Table 3.2), as may be expected from the previous uninterrupted voltammograms (Fig. 3.2), but the cycling efficiency was found to decrease as t_{oc} increased from 0 to 180 s. Hence, it may be concluded that some 'charge loss' process was occurring continuously, for at least 180 s after the lithium was deposited.

Table 3. 2 - Cycling efficiency dependence on open-circuit duration

t_{oc} /s	Q_{cath} / mC cm^{-2}	ζ / %
0	230 ± 30	58 ± 6
60	230 ± 30	49 ± 5
180	230 ± 30	35 ± 4

A further series of voltammograms were recorded for similar cells cycled between 1 V and -200 mV vs Li/Li$^+$ at scan rates, ν, varying from 10 mV s^{-1} to 100 mV s^{-1}. In these cells it was found that ζ increased slightly as ν increased from 10 mV s^{-1} to 50 mV s^{-1} (Table 3.3). However, ζ for the scan at 100 mV s^{-1} was found to be lower than that at 50 mV s^{-1}. It was also observed that after repeated cycling many disconnected particles, presumably of lithium, were present in the electrolyte.

Table 3.3 - Cycling efficiency dependence on scan rate

ν / mV s^{-1}	ζ / %
10	53 ± 6
20	54 ± 6
50	62 ± 6
100	60 ± 6

The trend towards lower cycling efficiencies at slower scan rates may be expected from the 'continuous' charge loss process suggested by the previous results. However, it should be noted that over the range of scan rates ζ remains well below 100 %. This may be accounted for by assuming the disconnection of plated lithium to be an 'inherent' charge loss process, that is independent of scan rate (at least over the range studied).

3.1.3 Solvent purity

It was noted during the course of this work that the cycling efficiency for lithium on nickel varied markedly for cells cycled under similar conditions. One cause of this variation may have been the differing levels of impurities in the electrolyte. For

example, samples of PC (Aldrich, as supplied) taken from two containers were found to have 370 ± 40 ppm and 510 ± 40 ppm glycols. However distilled PC had < 40 ppm glycols. Similarly the level of water in a 1 M $LiAsF_6$ in PC electrolyte was found to be 750 ppm, but that in PC was 20 ppm. Therefore it may be assumed that the level of water in the electrolyte was critically dependent on the drying regime and storage conditions of the salt. The UV/ Vis absorption spectra was found to vary with the concentration of undetermined impurities.

The highest cycling efficiencies of > 90 % (ν = 100 mV s^{-1}) were found in impure solvents (PC used as supplied). Similar results have been observed by Aurbach and Zaban [21] in electrolytes with relatively large concentrations of intentionally added 'impurities'. However, in order to accurately compare systems it was deemed necessary to use solvents with a constant level of impurities. Hence, in all further work, unless otherwise noted, the electrolytes were rigorously purified (chap 2.1.4). It may also be noted that the high cycling efficiency observed in some impure solvents is lost after extensive cycling.

3.2 Glassy Carbon

The extent and nature of film formation on carbon electrodes has been little studied [22, 23]. In order to make a preliminary study of film formation glassy carbon was chosen as a model substrate. Glassy carbon offered several advantages over more practical composite electrodes (chap 4), such as a low insertion capacity for lithium and a well-defined surface that was amenable to polishing.

The glassy carbon electrode was held at 0.50 V vs a lithium reference electrode in a 1 M $LiAsF_6$/ PC electrolyte. Impedance spectra were recorded at roughly 200 s intervals, over a frequency range of 2 Hz to 65 kHz with a 10 mV oscillator level (Fig. 3.5).

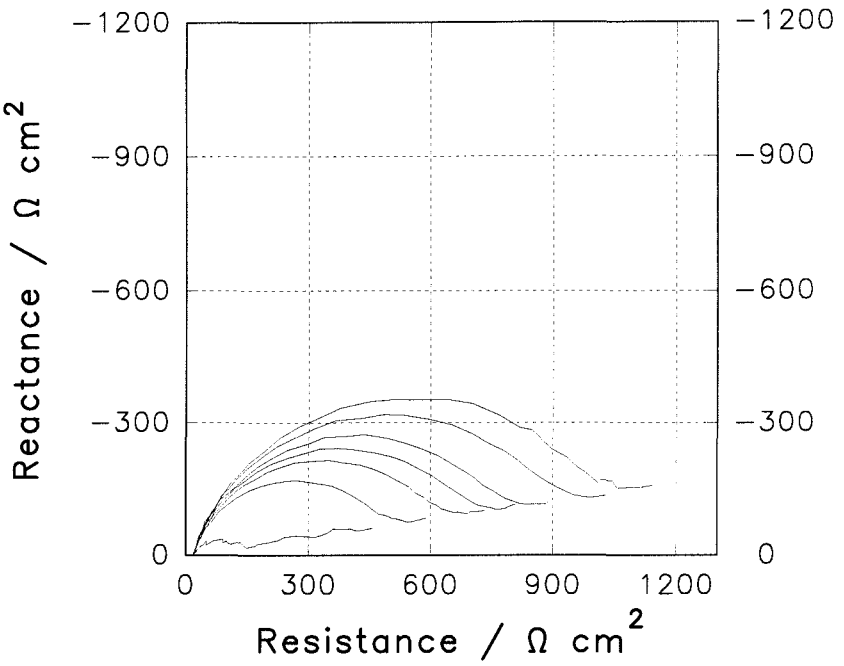

Figure 3.5 - Impedance spectra of glassy carbon at 0.5 V vs Li/ Li^+

The impedance spectra may be interpreted in terms of semi-depressed semi-circles, resulting from charge transfer and film resistances (R_{ct}, R_f) in parallel with double-layer and film capacitances respectively (C_{dl}, C_f). The semi-circles are offset from the origin by the uncompensated solution resistance (R_u). The low frequency (high impedance) feature may be modeled with a constant phase element (Z_{CPE}). These components are shown in equivalent circuit I [24] in Fig. 3.6.

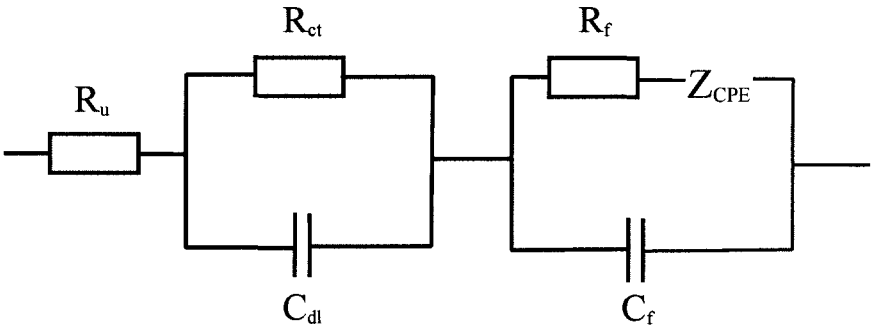

Figure 3.6 - Equivalent circuit I, for a film-coated glassy carbon electrode

By fitting the data using this circuit, it may be seen that R_u remains constant at 20 Ω cm^2. However, the time constants for the two parallel RC sub-circuits were too similar to obtain meaningful values of both R_{ct} and R_f. Therefore, a simpler equivalent circuit

(Fig. 3.7 - circuit II) was suggested to model the data, in which R_{ct} and R_f were replaced by a single interfacial resistance R_i and C_{dl} and C_f by a single interfacial capacitance C_i.

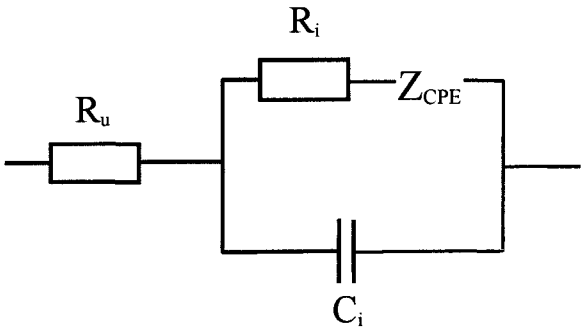

Figure 3.7- Equivalent circuit II, for film-coated glassy carbon electrode

However, simulations based on equivalent circuit II were found to fit the data poorly. In order to simulate the experimental data more closely it was found necessary to use a model which could give depressed semi-circles by using less-ideal components. This was achieved by replacing the CPE with a Warburg impedance element (Z_W) and the interfacial capacitor, C_i with a CPE with $n > 0.5$ (Fig. 3.8 - circuit III). Similar circuits have been required for many real systems [25].

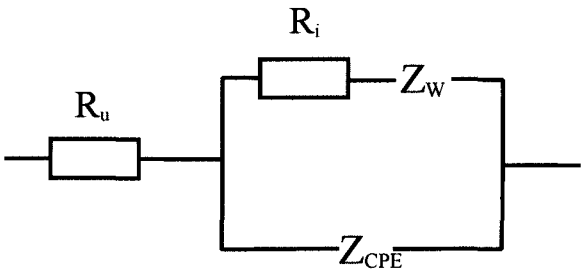

Figure 3.8 - Equivalent circuit III, for a film-coated glassy carbon electrode

The merit of this equivalent circuit may be seen by a typical plot of the simulated and experimental impedance data (Fig. 3.9).

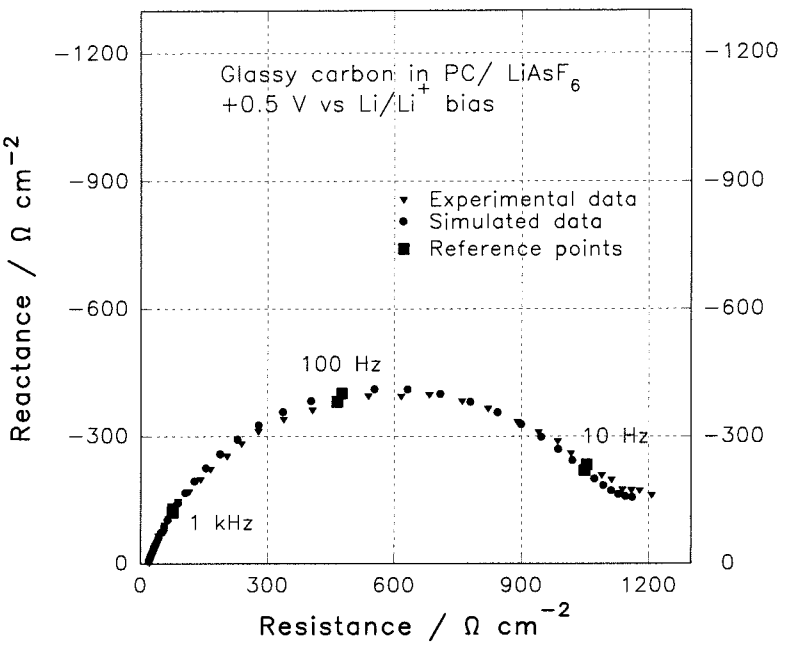

Figure 3.9 - Fit of impedance data to experimental data

By using a simulation based on equivalent circuit III to model the experimental data it was possible to obtain values of the circuit components. As before, R_u was found to be virtually independent of time, however R_i and the CPE prefactor, Yo, were found to have some time-dependence (Fig. 3.10).

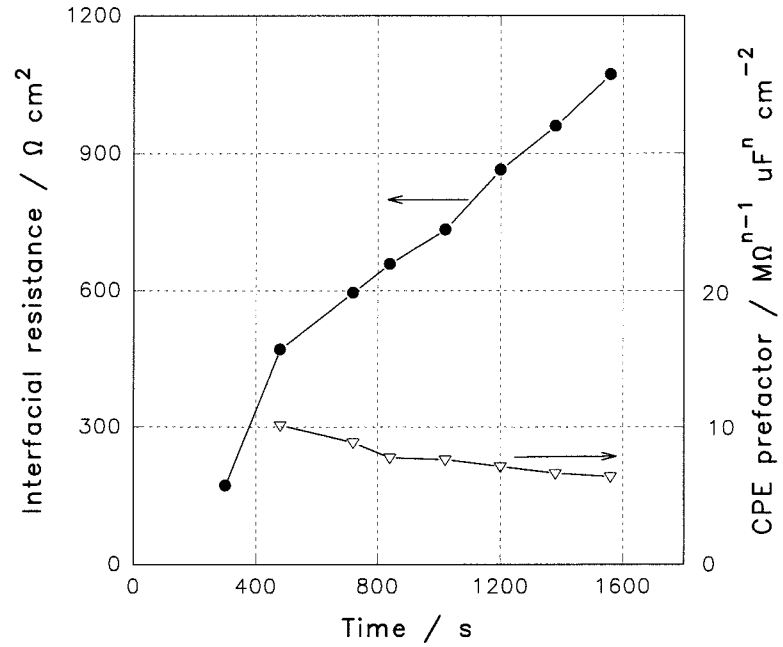

Figure 3.10 - Time dependence of interfacial resistance and CPE prefactor (PC/$LiAsF_6$ electrolyte)

Y_o was expressed in terms of $M\Omega^{n-1}\ \mu F^n\ cm^{-2}$, in preference to $M\Omega^{-1}\ s^n\ cm^{-2}$, to emphasise that if the CPE exponent, n, was varied from zero to one Y_o would change from being an area conductance to area capacitance term. For the simulated data n remained relatively constant at 0.79 ± 0.01, thus Y_o had a largely capacitive character. This may be expected as the CPE of equivalent circuit III (Fig. 3.8) was used to replace the interfacial capacitance of equivalent circuit II (Fig. 3.7).

The increase in R_i may be understood in terms of a resistive film growing on the surface of the glassy carbon electrode. This may be similar to the 'continuous' charge loss process associated with plated lithium.

The CPE prefactor decreased with time, but to a lesser extent than the increase in R_i - Y_o roughly halved, but R_i increased fivefold from 300 s to 1600 s. The film may have a capacitance per unit area comparable to that of the double layer. This would be so if the film were thin. For example, if the film dielectric permittivity, $\varepsilon = 10$ and the capacitance per unit area was ~ 5 $\mu F\ cm^{-2}$ then the film thickness, d would be ~ 50 Å (Eqn. 3.2). Such a film would be similar to the solid electrolyte interface model for films on lithium [22, 27] and graphite [28].

$$\frac{C}{A} = \frac{\varepsilon . \varepsilon_0}{d} \qquad \textbf{Equation 3.2}$$

A similar set of impedance measurements was made on a cell with a 1 M $LiCF_3SO_3$/ EC/ DEC electrolyte (Fig. 3.11). It may be noted that in this electrolyte the interfacial resistance increased very little after 400 s, in contrast to the previous striking increase. Also, the magnitude of R_i is less than that for the PC/$LiAsF_6$ electrolyte at t > 400 s.

Although the magnitude of Y_o cannot be compared directly with values obtained previously as the CPE exponent is significantly lower (n = 0.70 ± 0.01 compared to 0.79 ± 0.01), it can be seen that the relative change in Y_o is smaller in the EC/DEC electrolyte. From these observations it appears that on glassy carbon at 0.5 V vs Li/Li^+ a passivating film may form in the EC/DEC/$LiCF_3SO_3$ electrolyte within 400 s, but in the PC/$LiAsF_6$ electrolyte a continuous film-forming reaction proceeds for at least 1600 s.

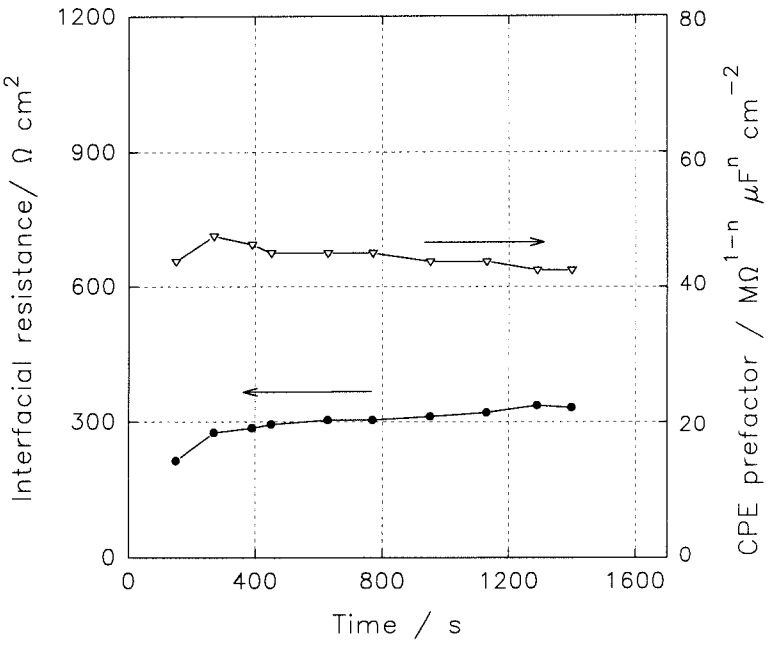

Figure 3.11 - Time dependence of interfacial resistance and CPE prefactor (EC/DEC/$LiCF_3SO_3$ electrolyte)

To determine whether the differences in the impedance profiles in the glassy carbon cells could be attributed specifically to the salt or solvent components of the electrolyte a further cell with a PC/$LiCF_3SO_3$ electrolyte was examined, Fig 3.12:

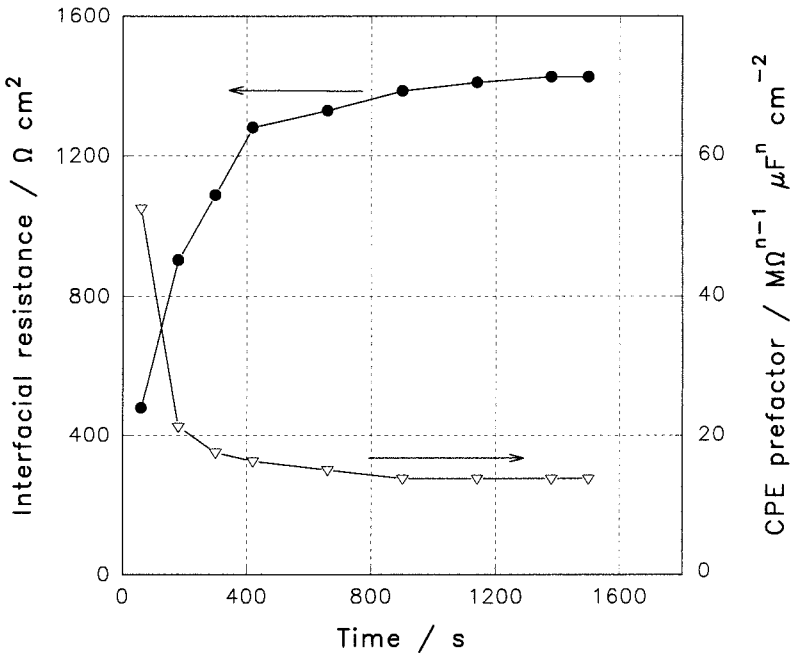

Figure 3.12 - Time dependence of interfacial resistance and CPE prefactor (PC/$LiCF_3SO_3$ electrolyte)

From Figs 3.10 - 3.12 it may be observed that the rate of resistance increase with time, at t > 400 s, was considerably lower in the cells containing $LiCF_3SO_3$ then those containing $LiAsF_6$. However, the cells containing PC had higher resistances and lower CPE prefactors than the EC/ DEC cell. Therefore, it seems likely that the rate of formation and constitution of films formed on glassy carbon were determined by both the salt and the solvent in the systems studied above. This is consistant with other, recent observations [28].

3.3 Oriented Pyrolytic Carbon (OPC)

A sample of soft pyrolytic carbon (David Hart Ltd., interlayer spacing 3.435 Å, FWHM 0.70° ,L_c ~ 130 Å) was used to examine solvent compatibility with the faces of an oriented material with a moderate lithium insertion capacity.

The original OPC sample had distinct, macroscopic (> 10 mm) edge and basal surfaces. Wafer electrodes were prepared from the block as described previously (Chap 2.3). As the wafers were approximately 130 μm thick with sides of ~ 4.5 mm the ratio of the exposed basal:edge surface areas in the two types of wafer were 100:12 and 6:100. The wafers were designated according to the predominant surface orientation.

The two types of electrodes were examined by cyclic voltammetry in 1 M $LiCF_3SO_3$/ PC at 30 μV s^{-1}, over the scan range 1.50 V→ 0.02 V → 1.80 V → 1.50 V vs. Li/Li^+ (Fig. 3.13).

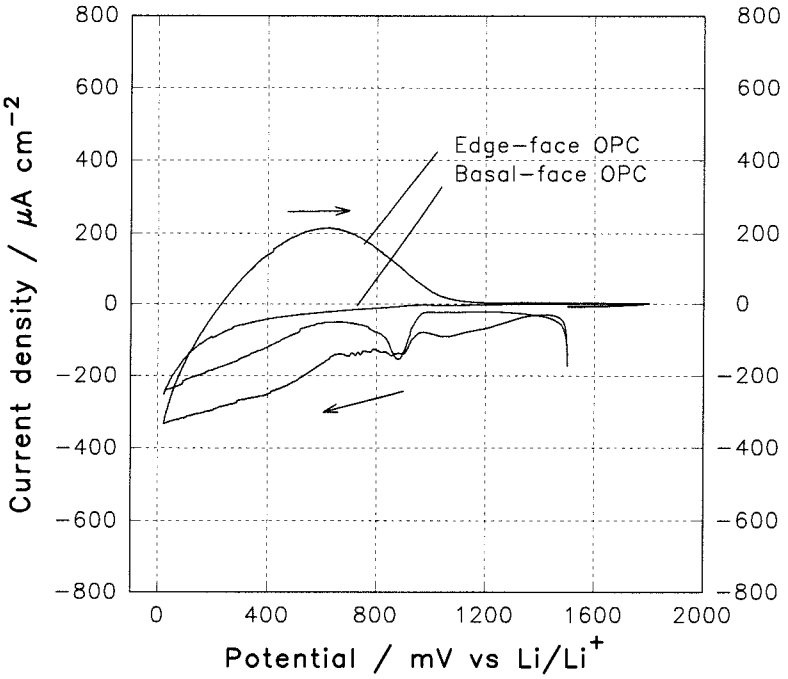

Figure 3.13 - Cyclic voltammograms of edge and basal-face OPC in PC-based electrolyte

The cyclic voltammogram shows a significant peak at 900 mV vs. Li/Li^+ on the first cathodic sweep, which is more pronounced for the basal-face than the edge-face electrode. There is also a broad cathodic feature and for the edge-face oriented OPC a broad anodic feature. The anodic peak is much more symmetrical than the 'sail-shape' stripping peaks of lithium from nickel.

ζ is low for both electrodes, at 43 % for the edge plane and < 1 % for the basal plane. One cause of these low values may be anticipated to be parasitic solvent-decomposition reactions from the previous observations on glassy carbon. In an attempt to verify this theory the electrodes were examined *ex situ* under an optical microscope after cycling (Figs. 3.14 - 3.16).

Figure 3.14 - Basal plane of OPC after cycling in PC-based electrolyte

The basal-face OPC electrode was extensively pitted after cycling (Fig. 3.14), whereas the edge-face electrode was split in several places along the line of the grain (Fig. 3.15).

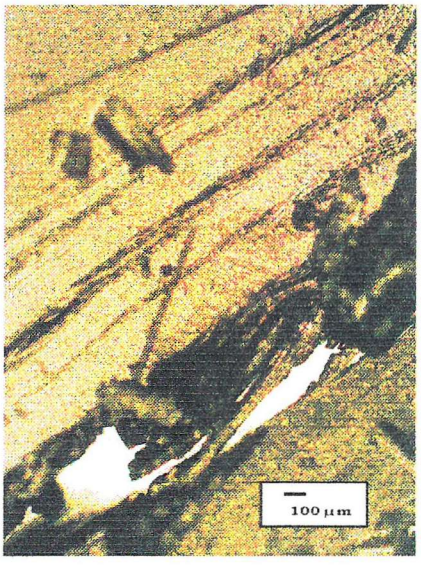

Figure 3.15 - Edge plane of OPC after cycling in PC-based electrolyte

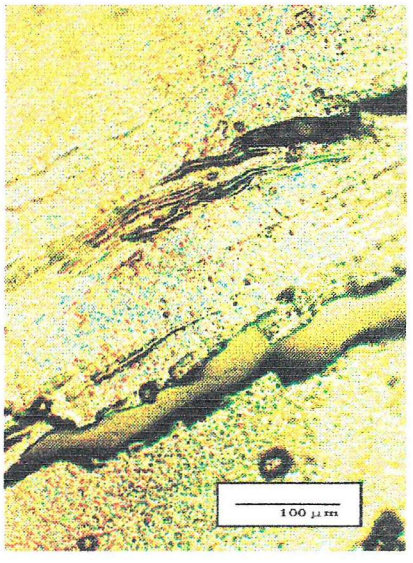

Figure 3.16 - as Fig. 3.15 but at higher magnification

At high magnification (Fig. 3.16) it was observed that the electrode surface was mottled in a variety of colours. However, the native OPC edge surface was black, the

electrolyte colourless and most plausible solvent decomposition products would have been colourless (lithium fluoride [29], lithium carbonate [30, 31] and lithium alkyl carbonates [29]). Therefore it seems probable that the colours arose from interference of light reflected from the front and back surfaces of thin films on the electrode.

For a film of thickness d constructive interference will occur at an angle Θ for light of a wavelength λ according to a form of Bragg's equation (Eqn 3.3) which has been modified to account for the refractive index of the film, m (derived from [32]).

$$n\lambda = 2d\sqrt{m^2 - \cos^2\Theta} \qquad \textbf{Equation 3.3}$$

As the electrodes were viewed with overhead illumination, Θ may be assumed to be ~90°. Therefore, the film thickness would be given by:

$$d = \frac{n\lambda}{2m} \qquad \textbf{Equation 3.4}$$

From this equation it may be seen that visible light of several different wavelengths may interfere constructively (with different values of n) if d is large. Therefore for a film that was thick, in comparison with the average wavelength of the incident white light, the reflected light would also appear to be white. It is clear then that for interference to give rise to observable coloured regions d would have to be approximately half the wavelength of visible light (i.e. ~ 300 nm) and be relatively constant across areas of the surface.

Gas evolution was often observed on lithium metal in contact with PC/ $LiAsF_6$ and propene has been identified by Arakawa and Yamaki [33] as a cathodic decomposition product of PC in contact with graphite. Gas evolution on or near the electrode surface may have caused the OPC layers to separate, giving rise to the pitting of the basal face and splitting of the edge face electrodes.

Two further electrodes were cycled under similar conditions in a 1 M $LiCF_3SO_3$/ EC/ DEC electrolyte (Fig. 3.17).

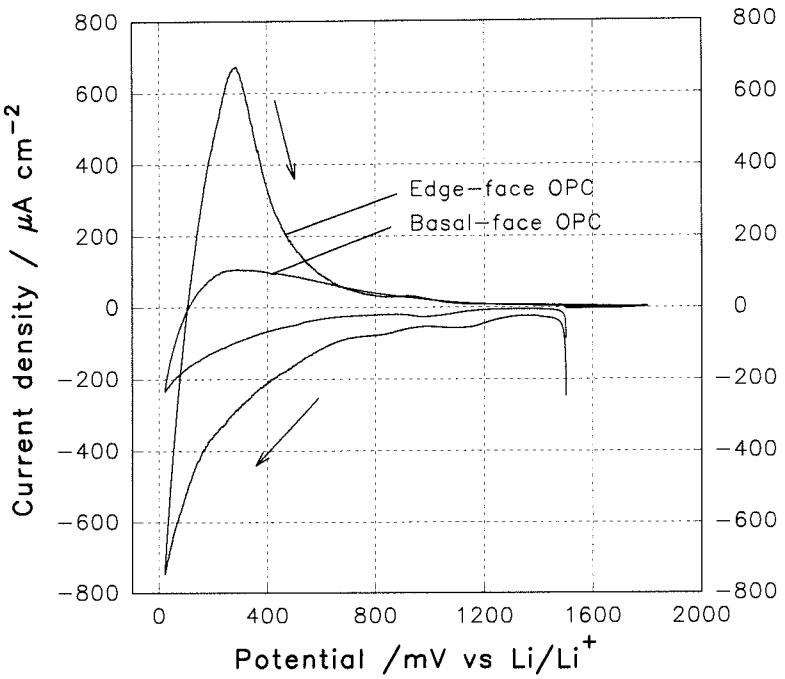

Figure 3.17 - Cyclic voltammograms of edge and basal-face OPC in EC/DEC electrolyte

ζ for both of these electrodes was 77 %, which is much greater than for the PC electrolyte. The peaks at around 900 mV vs. Li/ Li^+ in the EC/ DEC electrolyte are less pronounced than in PC. Also anodic peaks are apparent for both electrode orientations in the EC/ DEC electrolyte, with maxima at ~ 300 mV compared to ~ 600 mV for the PC. It may also be noted that the potential at which no net current flowed in the EC/ DEC electrolyte, was 100 mV for both electrodes.

In a given solvent at nearly all potentials < 1.2 V vs. Li/ Li^+ the magnitude of the current density was greater for the edge-face than the basal face electrode with two minor exceptions; the 0.9 V cathodic peak in PC and a part of the anodic feature > 0.65 V vs. Li/ Li^+ in EC/ DEC. That the current density is greater for edge-face than basal-face electrodes may be anticipated if it is assumed that the lithium intercalation/ deintercalation reactions give rise to a large proportion of the current at all potentials < 1.2 V vs. Li/ Li^+ and that either lithium diffusion, which is much greater in-plane than perpendicular to the planes [34], or intercalation, which is much faster into the edge-face than the basal face [35], is rate-limiting. The 900 mV cathodic peak in PC may be due to a solvent decomposition process which may have occurred to similar extents on both types of electrode.

Optical examination of the electrodes cycled in EC/ DEC revealed extensive surface colouring, but no splitting or pitting (Figs. 3.18- 3.20). If the colouring could be attributed to interference from thin surface films, as above, then it may be concluded that the films formed in EC/ DEC are more uniform than in PC from the larger coloured regions. However, it is also apparent that the thickness, or refractive index, of the films was not constant across the surface of the electrode.

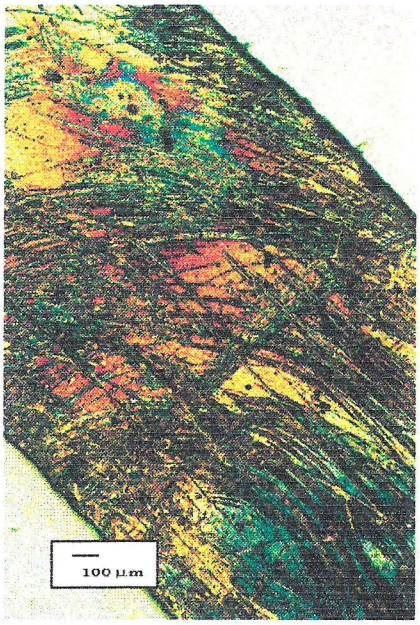

Figure 3.18 - Edge plane OPC after cycling in EC/DEC electrolyte

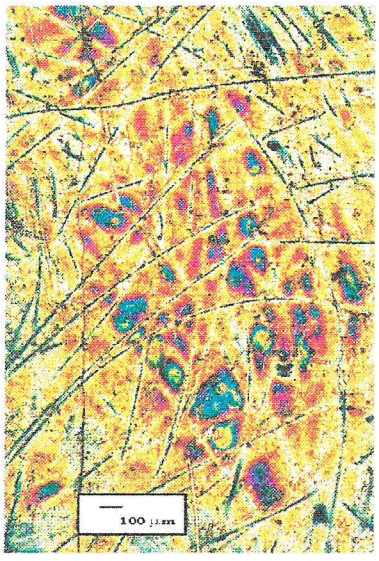

Figure 3.19 - Front face of basal OPC electrode after cycling in EC/DEC electrolyte

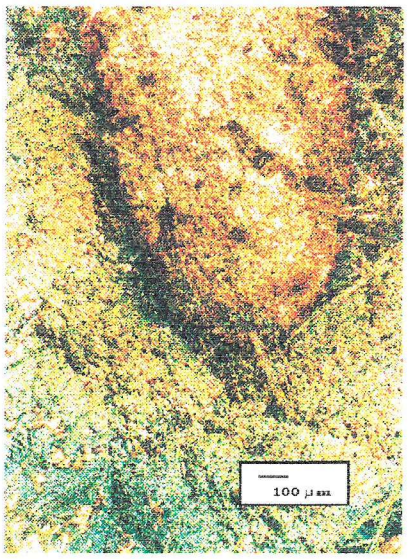

Figure 3.20 - Rear face of basal OPC electrode after cycling in EC/DEC electrolyte

From Fig. 3.20 it appears that a very thin layer of film may have formed on the surface of the basal plane electrode that was in contact with the current collector. It can also be seen that the dark lines that are visible on the front faces of the electrodes (Figs. 3.18 and 3.19) are absent from the rear face.

It was expected that aqueous washing would remove lithium compounds from the electrode surface, thus reducing the intensity of interference patterns resulting from any lithium-based films. In order to test this theory a piece of the edge plane OPC was washed with deionised water, dried carefully with paper towel and then re-examined under an optical microscope (Fig. 3.21).

Figure 3.21 - Cycled edge OPC electrode after washing with deionised water

It was found that this process removed both the coloured patches and the dark lines. Thus, it may be assumed that the dark lines were associated with the films and not with the underlying OPC surface. Thus it is credible that the dark lines were due to thin regions of film caused by contact of the glass wool separators with the electrode. Similar features were not apparent on the electrodes cycled in PC possibly because of the less uniform nature of the surface films and from the presence of gas bubbles.

3.4 Graphite

3.4.1 Rate dependence of insertion

To examine the insertion of lithium into graphite a 100 μm thick pressed graphite sheet (Alfa chemicals) was used as the working electrode, with a 1 M $LiCF_3SO_3$/ EC/ DEC electrolyte. Pulsed coulometric titration at a rate of C/21 was conducted until the relaxed potential was below 45 mV vs. Li/Li^+ (Fig. 3.22).

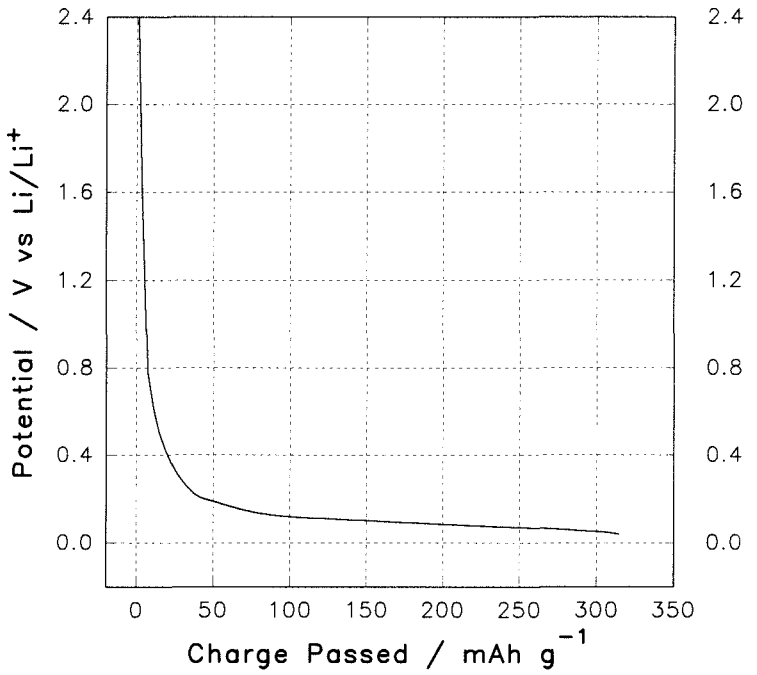

Figure 3.22 - Coulometric titration curve of lithium against graphite sheet

Dahn has reported [36] that lithium intercalation occurs at potentials below 0.52 V to form graphite intercalation compounds (Li-GICs). From Fig. 3.22 it is apparent that a much larger proportion of the total charge is passed in the potential range 520 - 45 mV than > 520 mV (95 % to 5 % respectively). There is also little evidence of solvent decomposition at ~ 900 mV, as noted previously for OPC in PC and to a lesser extent in EC/ DEC (chap 3.3).

To determine the extent of irreversible reactions the lithium was extracted, again by pulsed coulometric titration, until the relaxed potential exceeded 1.0 V vs. Li/Li^+.

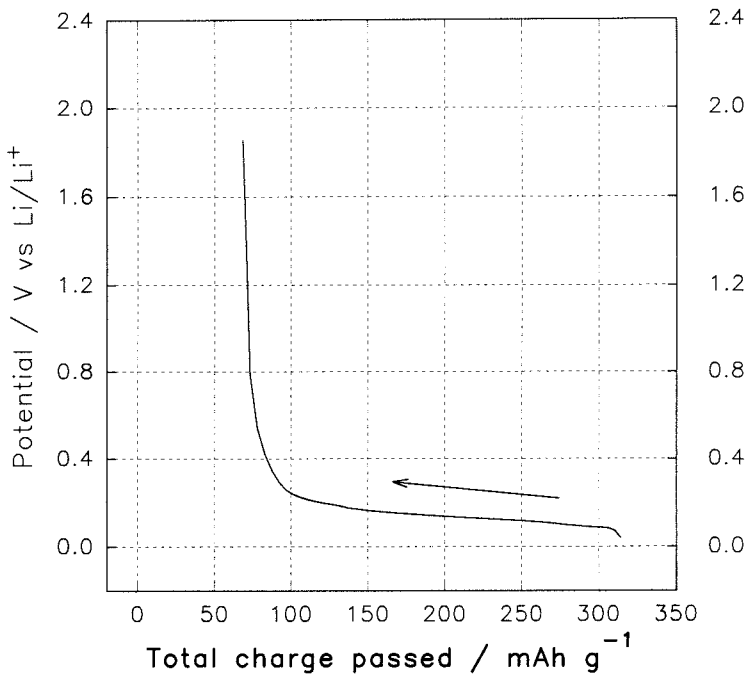

Figure 3.23 - Potential curve for lithium extraction from lithiated graphite sheet

The shape of the extraction curve is similar to that of the insertion curve (Figs. 3.23 and 3.22 respectively). However, there was an apparent 'charge loss' of 68 mAh g^{-1}, which is equivalent to an extraction efficiency of 78 %. In order to examine the possibility that the irreversible capacity arose from a incomplete lithium extraction it was decided to repeat the titration in many similar cells over a range of charge rates from C/3 to C/126.

Fig. 3.24 shows the insertion, extraction and irreversible charges plotted against inverse cycling rate for the first insertion/ extraction cycle. Fig. 3.25 shows equivalent data for the second cycle. The error bars have been calculated from the estimated errors in electrode mass, current and timing (Chap. 2.7). From the shape of the insertion and extraction curves in Figs. 3.24 and 3.25 it appears that there may be another source of error which has a more marked effect on the first cycle than the second.

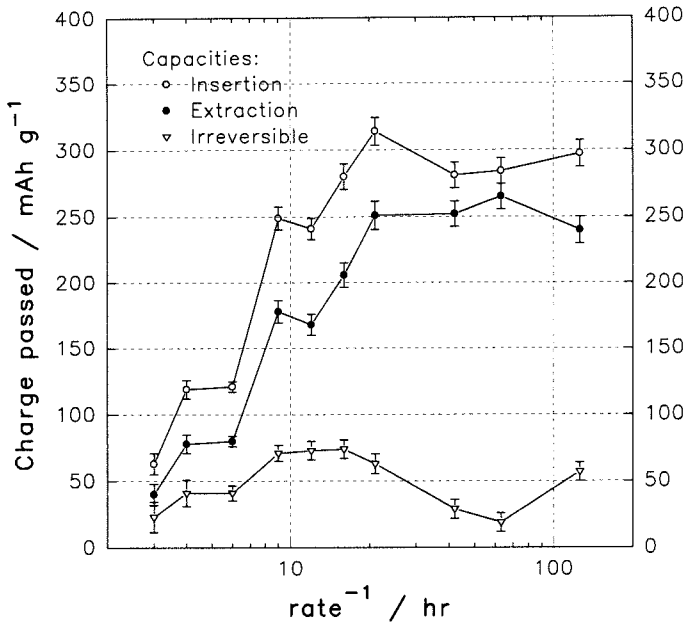

Figure 3.24 - first cycle charge dependence on cycling rate

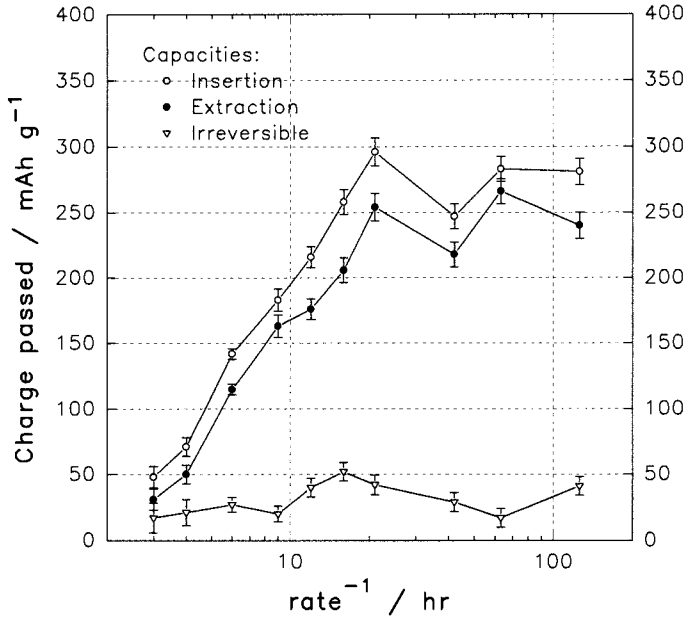

Figure 3.25 - second cycle charge dependence on cycling rate

From Figs. 3.24 and 3.25 it can be clearly seen that the insertion and extraction capacities increased to a maximum at about C/20, after which they remained almost constant.

A simple model that may be envisaged to account for the irreversible capacity arising from incomplete lithium extraction at short times employs semi-infinite linear

diffusion conditions [37]. This model leads to the expectation that the irreversible capacity would equal two-thirds of the inserted charge. This value is much greater than those obtained at the highest charging rates (30 - 35 %). Therefore, it may be concluded that either the semi-infinite boundary condition was invalid at these rates (C/6 to C/3) or that the lithium diffusion coefficient was not constant. There is some evidence to suggest that the latter may be correct [38], although estimates of the values of chemical diffusion coefficients for lithium in similar carbons vary by at least two orders of magnitude [39].

Qualitatively it may be expected that the contribution to irreversible capacity from incomplete lithium extraction would increase with inserted charge at high rates (semi-infinite boundary conditions). At low rates complete lithium extraction may be expected (thin-film boundary condition). It may also be expected that, because some lithium remains in the electrode after the first extraction at high charge rates, the second cycle insertion and irreversible capacities would be slightly lower than those of the first cycle.

As predicted there was found to be an increase in the irreversible capacity on the first cycle, to a limit of 75 mAh g^{-1} at ~ C/14. The irreversible capacity then decreased to 20 mAh g^{-1} at C/63. The second cycle insertion capacities at high rates (C/3 - C/16) were an average of 23 mAh g^{-1} lower than those of the first cycle, and the irreversible capacities 25 mAh g^{-1} lower. These values may be compared with 15 mAh g^{-1} and 6 mAh g^{-1} respectively at low rates (C/42 - C/126).

The irreversible capacity at C/126 was notably higher than those at C/21 and C/42. This may result from atmospheric components (notably water and oxygen) diffusing through the cell (or more likely the PTFE O-ring) and reacting irreversibly with the lithiated electrode. Such reactions may be expected to become more dominant at long times. The extent of irreversible capacity arising from inherent impurities in the electrolyte may be expected to be less than or equal to the smallest irreversible capacity measured on the first cycle, 17 mAh g^{-1}.

In summary, three types of irreversible capacity have been proposed:

i) incomplete lithium extraction, 0 - 75 mAh g^{-1}, maximum at intermediate rates

ii) inherent irreversible reaction with the solvent/ solvent impurities, ≤ 17 mAh g^{-1}.

iii) irreversible reaction with reactants that have diffused into the electrolyte, presumably negligible at low rates, increasing to ~ 40 mAh g^{-1} at C/126.

3.4.2 Interpretation of low potential insertion features

During intercalation Dahn [36] observed a series of plateaux in the potential profile which were interpreted in terms of the successive formation of two-phase systems.

Fig. 3.26 shows the low potential (<0.3 V vs. Li/Li^+) region of a pulsed coulometric titration at C/126. It may be seen that the potential profile may be separated into three plateau regions, denoted a, b and c. However, it has been shown that subtle changes in the gradient of titration curves are easier to resolve in a plot of dx/dV vs. V [40], Fig. 3.27. A sharp peaks in the dx/dV vs. V plot corresponds to a plateau in the V vs. Q plot.

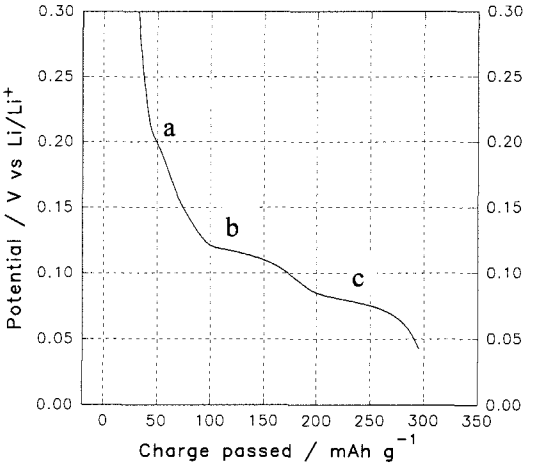

Figure 3.26 -lithium insertion profile at a rate of C/126 into a graphite monolith

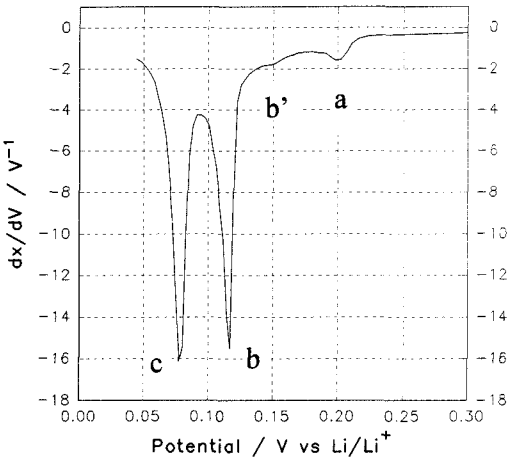

Figure 3.27- dx/dV vs. V for data shown in Fig. 3.26 (2.5 mV discriminator level)

The potentials of peaks a, b and c, as shown in Fig. 3.26, are 200, 119 and 79 mV vs. Li/Li^+ respectively. These values are close to the accepted values at low insertion rates (C/43 - C/800) for peaks 1, 4 and 5 in Table 3.4. In Fig. 3.26 there is a shoulder on peak b (denoted as b') at 150 mV which may correlate to peak 2

Table 3.4 - dx/dV peak positions

dx/dV peak positions / mV vs. Li/Li^+				
Graphite monolith (this work)	**NG-7 graphite powder [41]**	**PGCCL graphite monolith [42]**	**KS44 graphite powder [36]**	**Peak label**
200 (peak a)	203	210	205	1
150 (peak b')			150	2
		130	130	3
119 (peak b)	117	120	120	4
79 (peak c)	82	80	70	5

It may be concluded that at a rate of C/126 the graphite monolith showed insertion behaviour that was close to successive 'ideal' two phase. However, cycling rates lower than C/126 may produce a narrowing of the dx/dV peaks.

The phases which form during intercalation have been determined from XRD and coulometric titration measurements as in Table 3.5, where the stage number refers to number of carbon layers that separate successive intercalated lithium layers.

Table 3.5 - dx/dV peak potentials and phase assignment

Peak potential	**Phase assignment**	**Phase stoichiometry**	**Peak label**
203 - 210 mV	stage 4 and either stage 1' or stage 8	LiC_{24}[43], LiC_{36}[41] or LiC_{50}[36] $Li_{<0.04}C_6$[36] LiC_{72}[41]	1
150 mV	stage 3 and unknown phase	LiC_{18}[43], LiC_{27}[41] or LiC_{29}[36]	2
130 mV	stage 3 and stage 2L	LiC_{18}[43], LiC_{29}[36] or LiC_{27}[41] LiC_{18}[41, 42] or LiC_{24}[36]	3
117 - 120 mV	stage 2L and stage 2	LiC_{18}[41, 42] or LiC_{24}[36] LiC_{12}[36, 41 - 43]	4
70 - 82 mV	stage 2 and stage 1	LiC_{12}[36, 41 - 43] LiC_6[36, 41 - 43]	5

For dilute lithium phases calculation of the stoichiometry from the amount of charge passed is complicated by the unknown extent of 'charge loss' processes.

To investigate the rate dependence of phase formation in the graphite sheet, dx/dV vs. V plots were constructed for several similar cell over a range of rates, from C/4 to C/126 (Fig. 3.28).

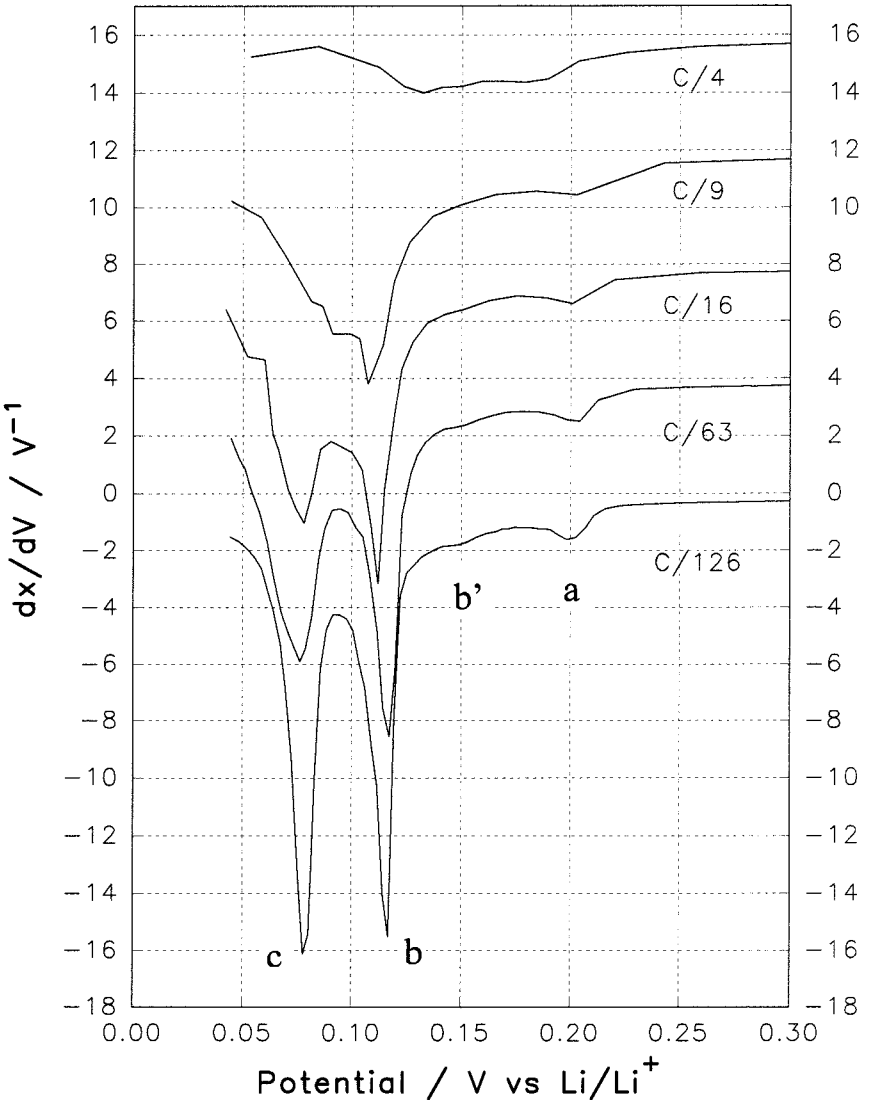

Figure 3.28 - dx/dV vs. V profiles for lithium insertion into graphite sheet at selected rates from C/4 to C/126. The traces have been offset from the x-axis by: C/126 no offset, C/63 +4 V^{-1} offset, C/16 +8 V^{-1} offset, C/9 +12 V^{-1} offset, C/4 +16 V^{-1} offset.

From Fig. 3.28 it is evident that peak b shifted to more negative potentials as the scan rate increased from C/126 to C/9. Peak c shifted little (< 5 mV) but broadened from C/126 to C/16. At C/21 (not shown) peaks b and b' could not be independently resolved.

At C/9 peaks b, b' and c could not be independently resolved. At the highest rate, C/4, only one broad peak was apparent in the dx/dV plot.

Non-equilibrium distributions of phases would be expected to form at the electrode surfaces when lithium is being inserted, during the current pulses. However, if the current relaxation times are too short it would be anticipated that a potential would be recorded for the non-equilibrated phases. A system under these conditions would not be expected to display ideal two-phase behaviour. Hence, the broadening and merging of peaks may be attributed to the incomplete equilibration of lithiated-graphite phases at the electrode surfaces. Following this hypothesis the broad feature at 100 mV vs. Li/Li^+ at C/9 may result from a mixture of stage 1, 2 and 2L phases (Table 3.5) or from a thermodynamically unstable non-stoichiometric phase.

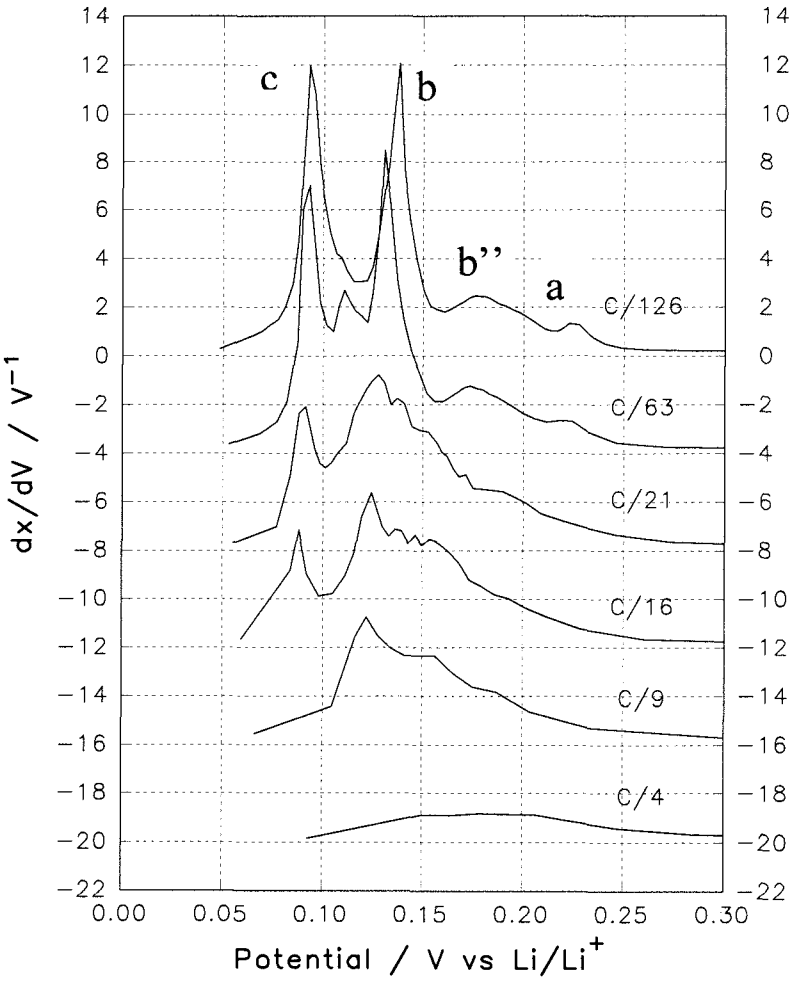

Figure 3.29 - dx/dV vs. V profiles for lithium extraction from graphite sheet electrodes at selected rates from C/4 to C/126. The traces have been offset from the x-axis by: C/126 no offset, C/63 -4 V^{-1} offset, C/21 -8 V^{-1} offset, C/16 -12 V^{-1} offset, C/9 -16 V^{-1} offset, C/4 -20 V^{-1} offset.

A similar broadening of the peaks is seen in the extraction (Fig. 3.29) as in the insertion (Fig. 3.28) as the charging rate in increased. However, peak b broadens more noticeably in the extraction than the insertion. The extraction charge associated with peak c decreased as the charge rate increased, but the peak position changed little.

It is also noteworthy that at low rates (less than C/21) the insertion and extraction capacities changed little, but the dx/dV plots showed distinct differences in the rate of formation of the Li-GIC phases at the electrode surface. This illustrates a difference between surface (dx/dV behaviour) and bulk (insertion/ extraction capacities) properties of the graphite.

Chapter 4

Results & Discussion - Powder Electrodes

4.1 Electrolyte

In the previous chapter it was observed that there was a varied behaviour of different aprotic electrolytes towards glassy carbon and OPC at low potentials (chaps. 3.2 and 3.3) and that high charge efficiencies were observed for lithium plating/ stripping in impure solvents (chap 3.1.3). It was decided to examine the insertion of lithium into graphite powder electrodes (90 w/o KS44, 10 w/o EPM) and coke powder electrodes (95 w/o ball-milled coke, 5 w/o EPM [11]) in a range of electrolytes. In general three-electrode pear-shaped flask cells were used.

4.1.1 Propylene carbonate

Although AC impedance measurements had been used previously to examine film growth on a glassy carbon electrode it was decided that FT impedance would present a less disruptive technique for examination of the graphite electrode/ electrolyte interface during coulometric titration, because the cell could remain connected to a single experimental setup rather than having to be moved between two (chap. 2.5.6).

Fig. 4.1 shows typical FT impedance data obtained during titration of lithium against graphite in a PC electrolyte. The data was modelled by equivalent circuit IV shown in Fig. 4.2: in which R was equal to the sum of film and solvent resistances and Z_{CPE} was derived from the double-layer capacitance and/ or diffusion processes by analogy with equivalent circuit I (Fig. 3.6). The capacitance of the film was not required in circuit IV due to the low frequencies examined

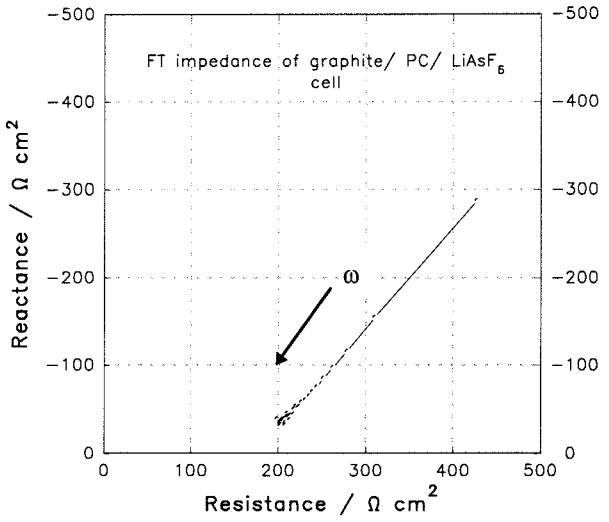

Figure 4.1 - Typical FT impedance plot for graphite powder/ 1 M $LiAsF_6$ in PC cell, from 300 mHz - 20 Hz

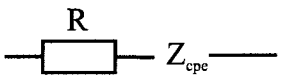

Figure 4.2 - Equivalent circuit IV used to model data shown in Fig. 4.1

Fig. 4.3 shows the potential profile of a graphite/ PC/ $LiAsF_6$ cell at a charging rate of C/5 (200 μA cm^{-2}) and Fig. 4.4 the corresponding variation of R and CPE prefactor.

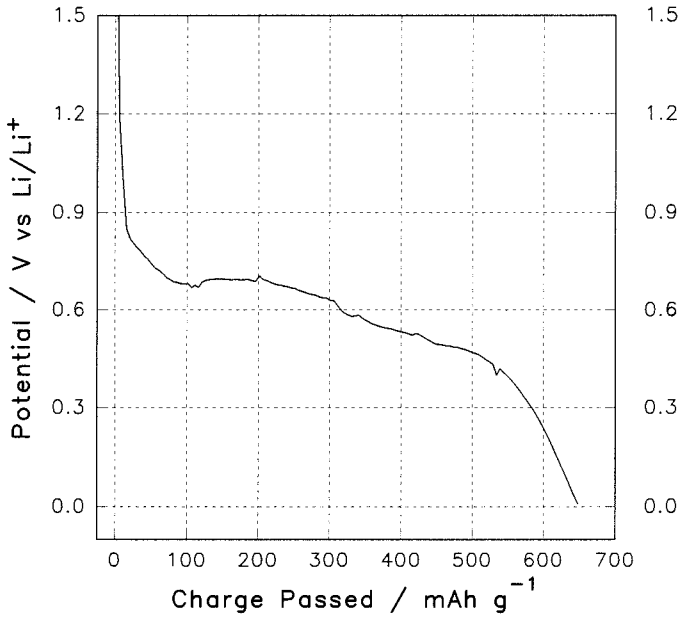

Figure 4.3 - Coulometric titration of lithium against graphite powder in PC/ $LiAsF_6$, C/5 rate

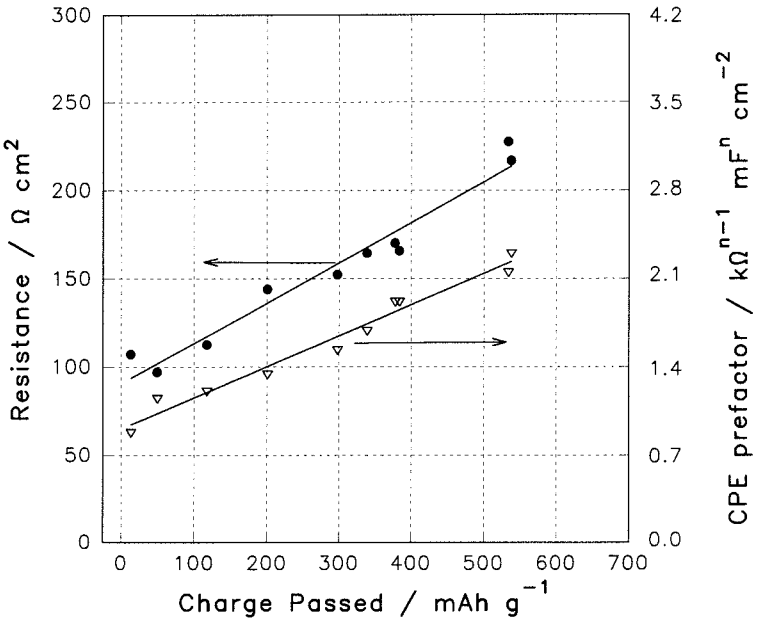

Figure 4.4 - Variation of R and CPE prefactor with charge for a graphite/ PC/ $LiAsF_6$ cell (lines as a guide to the eye)

As lithium insertion into graphite is not expected to occur to a measurable extent at potentials above 0.5 V (chap. 3.4) it may be assumed from Fig. 4.3 that less than 18 % (110 mAh g^{-1}) of the total charge passed corresponded to lithium insertion reactions. It was anticipated that solvent decomposition reactions, as observed previously on OPC (chap. 3.3), accounted for the remaining charge.

From Fig. 4.4 it may be seen that the resistance increased with charge passed ; this coincides with observations of glassy carbon in PC/ $LiAsF_6$ electrolyte (chap. 3.2), which were attributed to film growth. However, in contrast to the glassy carbon results, the magnitude of the CPE prefactor was found to increase with charge for the graphite powder electrode. The magnitude of the graphite CPE prefactor was approximately 100 times larger than the glassy carbon prefactor, R was approximately 5 times smaller and hence the film resistance would have been >5 times smaller. Also, the order of the CPE was lower (n = 0.67 initially, but then fell to 0.56 ± 0.04) for the graphite powder than glassy carbon (n = 0.79 ± 0.01). These differences may be attributed, in part, to the roughness of the graphite powder electrodes (lower n) and the consequent inequality of geometric and electrochemically active surface areas (lower R, higher CPE prefactor).

If the CPE is considered to represent blocking behaviour at a rough electrode the increase in prefactor magnitude and the decrease in n may be attributed to fragmentation of

the electrode, as observed for OPC (chap. 3.3), causing the electrochemically active surface area to increase with charge. It was predicted that if fragmentation of the graphite particles was occurring a hard carbon powder electrode would behave differently. In order to verify this conclusion it was decided to examine the effect of lithium insertion into a coke powder electrode from 1 M $LiAsF_6$/ PC.

Fig. 4.5 shows the coulometric titration curve and Fig. 4.6 the corresponding Nyquist plots of the FT impedance data for a coke powder electrode in PC/ $LiAsF_6$.

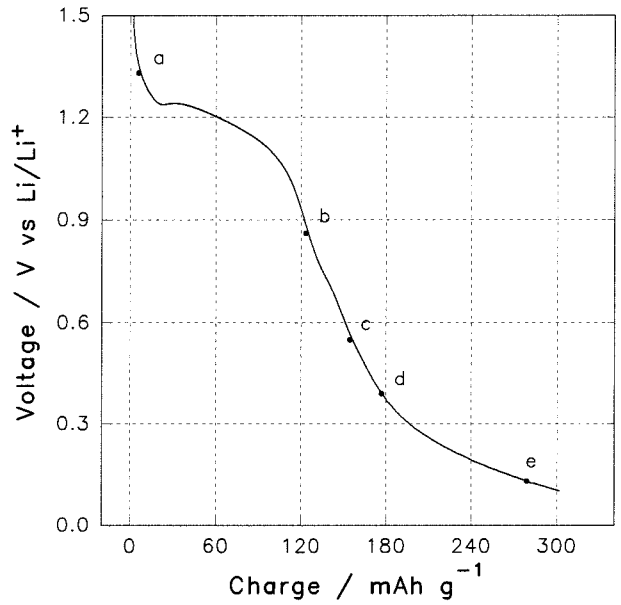

Figure 4.5- Coulometric titration of lithium against coke powder in PC/ $LiAsF_6$, C/5 rate. Letters denote points at which voltage transients were recorded.

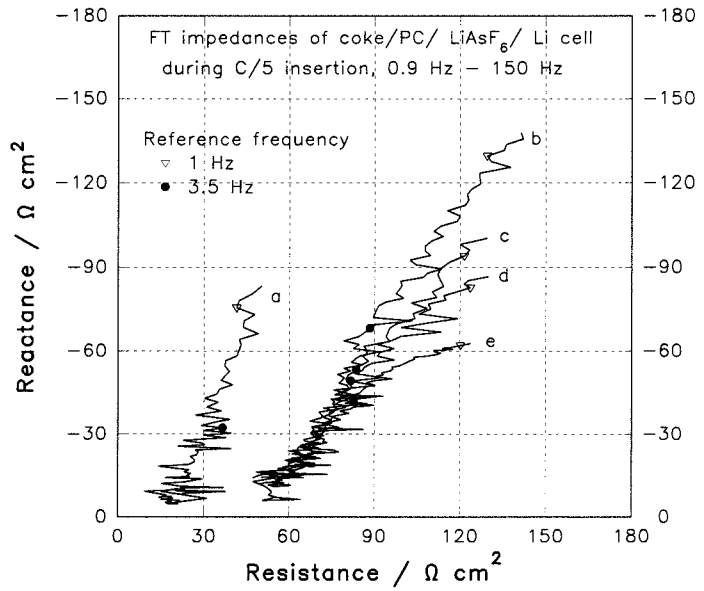

Figure 4.6 - Nyquist plots pertaining to transients acquired at the positions denoted in Fig. 4.5

Lithium insertion into coke has been found to commence at higher potentials (~ 1.2 V vs. Li/Li^+) than for graphite (~ 0.3 V vs. Li/Li^+) [2 -4]. From Fig. 4.5 it appears plausible that insertion accounted for a greater proportion of the charge in the coke cell (≤ 80 %) than the graphite one (< 18 %). It may also be noted by comparison of Figs. 4.5 and 4.3 that less charge per mass of carbon was passed in the coke cell.

Using equivalent circuit V shown in Fig. 4.7 to model the Nyquist plots shown in Fig. 4.6 it is apparent that R_1 did not noticeably increase beyond point b (Fig. 4.5).

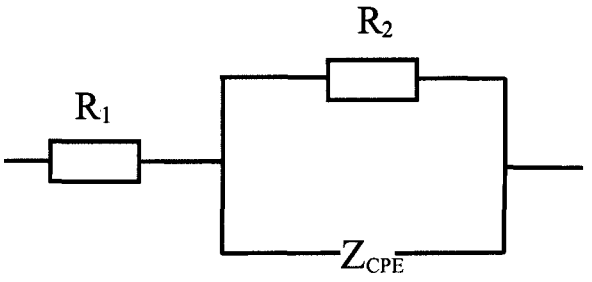

Figure 4.7 - Equivalent circuit V, used to model data shown in Fig. 4.6

It may be seen that equivalent circuit V is related to equivalent circuit I (Fig. 3.6), where $R_1 = R_u + R_f$, $R_2 = R_{ct}$ and Z_{CPE} is derived from C_{dl}. As R_1 is the sum of film and solution resistances it may be deduced that the resistance of the film ceased to increase beyond point b.

The CPE prefactor decreased from 2.9 $k\Omega^{n-1}$ mF^n cm^{-2} to 1.9 $k\Omega^{n-1}$ mF^n cm^{-2} between points a and b. This agrees with the behaviour previously associated with film-formation on glassy carbon but contrasts with the increase in CPE prefactor associated with fragmentation of the graphite powder electrode.

From points b to e, R_2 decreased indicating that a charge-transfer process, presumably intercalation, was proceeding more readily [5].

4.1.2 Propylene carbonate/ ethylene carbonate

A 1 M $LiAsF_6$ in 1:1 PC/ EC solution was used to examine the effects of EC on film-formation. Fig. 4.8 shows a coulometric titration curve for a graphite powder electrode in EC/ PC at a C/5 rate.

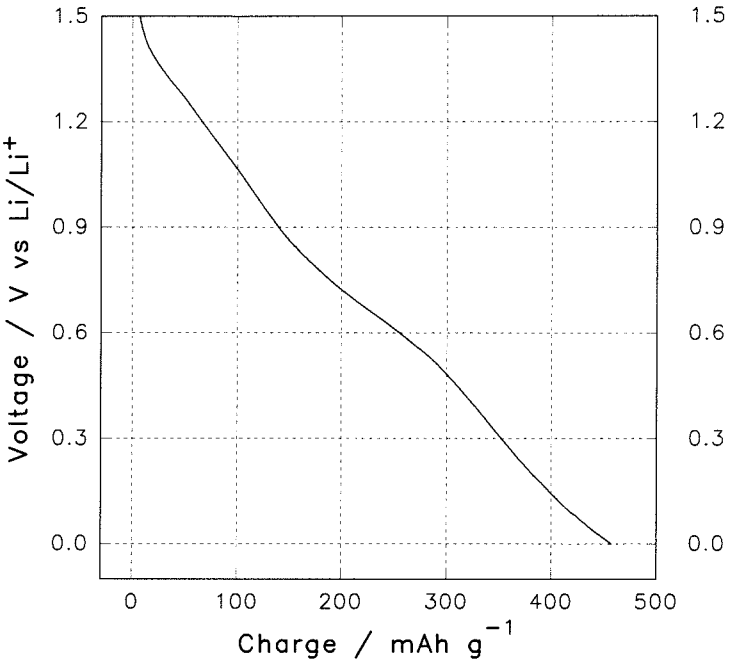

Figure 4.8 - Coulometric titration of lithium against graphite powder in a EC/ PC electrolyte, C/5 rate

When the titration was repeated with similar electrodes over a range of insertion rates from C/2 to C/20 the total charge passed was found to vary from 165 - 460 mAh g^{-1} and the proportion of the charge passed at < 0.5 V vs. Li/Li^+ varied from 33 - 50 % of the total charge. By comparison with the titration in a PC-only electrolyte on graphite powder electrode (above) it appears that the addition of EC limited but did not prevent the electrolyte decomposition reactions.

4.1.3 Propylene carbonate/ ethylene carbonate/ 12-crown-4

It has been reported that the use of 12-crown-4 as an additive in PC-based electrolytes can reduce the amount of solvent decomposition [6]. To study the action of 12-crown-4 an electrolyte consisting of 1 M 12-crown-4 in a 1 M $LiAsF_6$, 1:1 EC/ PC solution was used in a cell with a graphite powder electrode. The coulometric titration curve, with transient measurement points, is shown in Fig. 4.9. Fig. 4.10 shows Nyquist plots of the corresponding FT impedance data obtained from the transients.

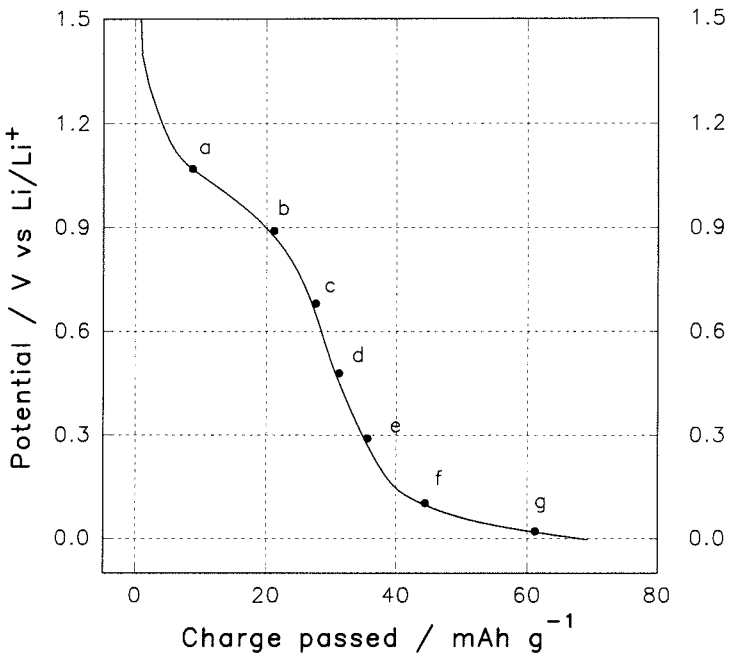

Figure 4.9 - Coulometric titration of lithium against graphite powder in a EC/ PC/ 12-crown-4 electrolyte, C/20 rate. The letters denote points at which voltage transients were recorded.

From Fig. 4.9 it can be seen that the amount of charge passed at a rate of C/20 is less for the cell containing 12-crown-4 (68 mAh g^{-1}) than without (chap. 4.1.2 - 250 mAh g^{-1}) and the proportion of the charge passed at potentials below 0.5 V vs. Li/Li^+ is higher (57 % compared to 33 %). Also the potential profile for the cell containing 12-crown-4 has a noticeable plateau in the lithium insertion region (chap. 3.4) which is absent from cells without crown ether.

Equivalent circuit V was necessary and sufficient to model the low frequency data shown in Fig. 4.10. However, part of an additional high frequency feature can be seen in some of the plots. As with the coke powder/ PC cell, resistor R_2 may be taken to represent a charge-transfer process. The kinetic facility of this process varied little from points e to g, i.e. when the potential was below 0.3 V.

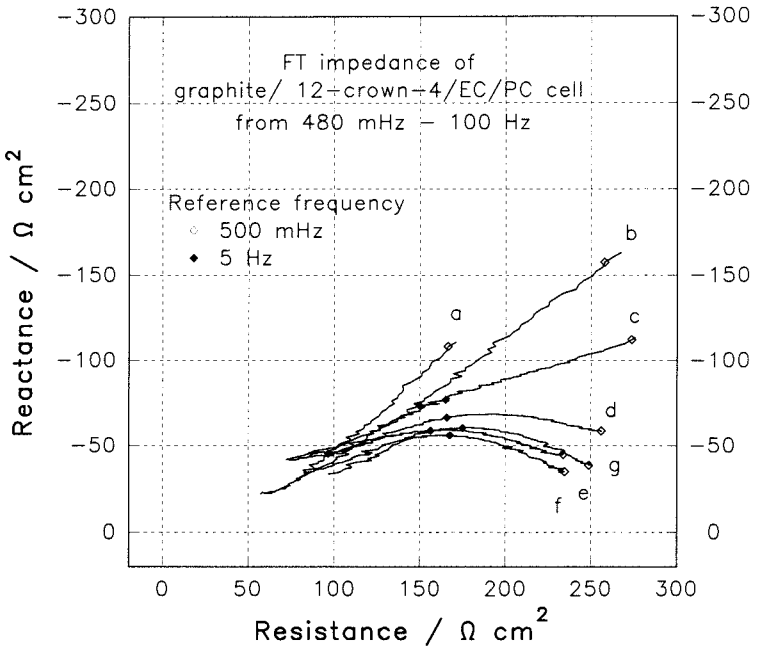

Figure 4.10 - Nyquist plots pertaining to transients acquired at the positions denoted in Fig. 4.9

12-crown-4 clearly reduced the amount of solvent decomposition on the graphite powder electrode whilst permitting a degree of insertion. It has been postulated that PC co-intercalates prior to decomposition [6, 7]. Lithium complexation to 12-crown-4 reduces the amount of PC that is co-intercalated and hence reduces the amount of solvent decomposition. However, it is also possible that PC decomposition occurs at the graphite surface without co-intercalation and that 12-crown-4 and to a lesser extent EC act to form a passivating layer on the graphite.

4.1.4 Triglyme

Although solvent decomposition may be reduced by the addition of 12-crown-4 , as shown above, it is unlikely to be exploited commercially due to its high toxicity and expense. In an attempt to find a cheaper, less harmful alternative an open chain isomer, triglyme, was used as a solvent. Fig. 4.11 shows the potential profile of a coulometric titration of lithium against graphite in 1 M $LiAsF_6$/ triglyme.

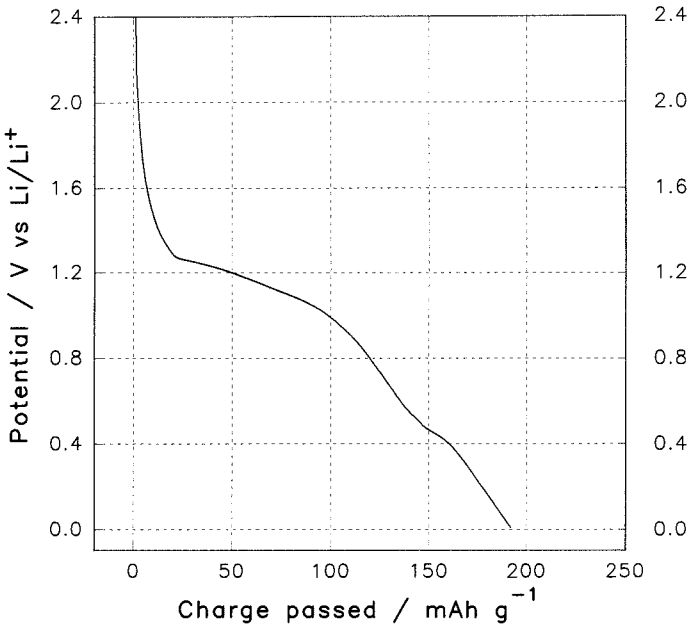

Figure 4.11 - Coulometric titration of lithium against graphite powder, 1 M $LiAsF_6$/ triglyme, C/5 rate

As may be seen from Fig. 4.11 the extent of lithium intercalation was low (charge passed at potentials < 0.5 V vs. Li/Li^+ was 26 %). However, the charge passed in solvent decomposition was less than for PC or PC/ EC electrolytes at the same insertion rate.

For the electrolytes used above (chap 4.1.1 to 4.1.4) the water concentrations were found, by the methods described in chap. 2.1.1, to be quite high; 780 ± 80 ppm. It may be supposed that some of the 'charge loss' is due to the reduction of water rather than reaction of the electrolyte *per se*. In subsequent electrolytes the water concentrations were < 150 ppm.

4.1.5 Ethylene carbonate/ diethyl carbonate

It has been noted that PC appears to be detrimental to lithium insertion into graphite powder electrodes. Also insertion into monolithic graphite appeared to progress readily from an EC/ DEC/ $LiCF_3SO_3$ electrolyte (chap. 3.4). Therefore it was decided to titrate lithium against a graphite powder electrode in a similar electrolyte, Fig. 4.12.

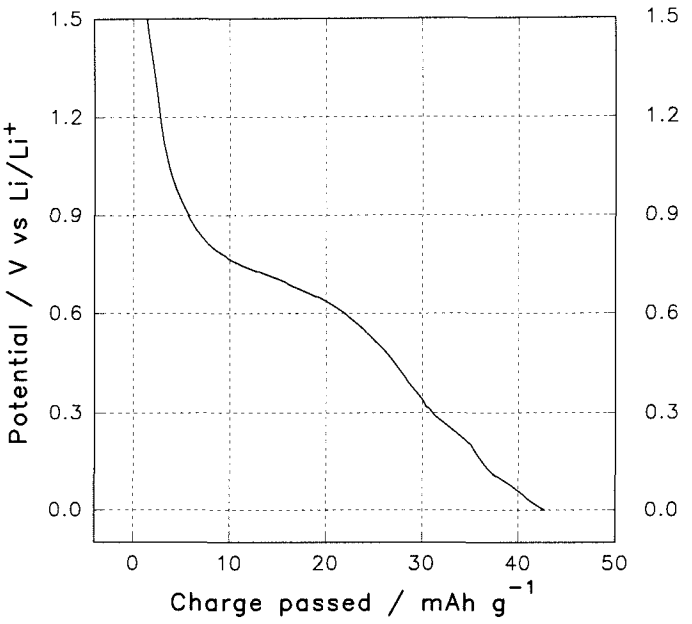

Figure 4.12 - Coulometric titration of lithium against graphite powder, 1 M $LiCF_3SO_3$/ EC/ DEC, C/10 rate

From Fig. 4.12 it may be seen that in the EC/ DEC electrolyte there is a similar amount of charge passed in solvent decomposition as in the PC/ EC/ 12-crown-4 (~ 25 mAh g^{-1} charge passed at potentials > 0.5 V vs. Li/Li^+). However, there is no insertion plateau observable in the EC/ DEC electrolyte.

4.2 Stack Pressure

Graphite powder electrodes showed little insertion (41 mAh g^{-1} below 0.5 V vs. Li/Li^+) when cycled at approximately atmospheric pressure (100 kPa), even when cycled at rates as low as C/80 in $LiAsF_6$/EC/PC/12-Crown-4 electrolyte, Fig. 4.13.

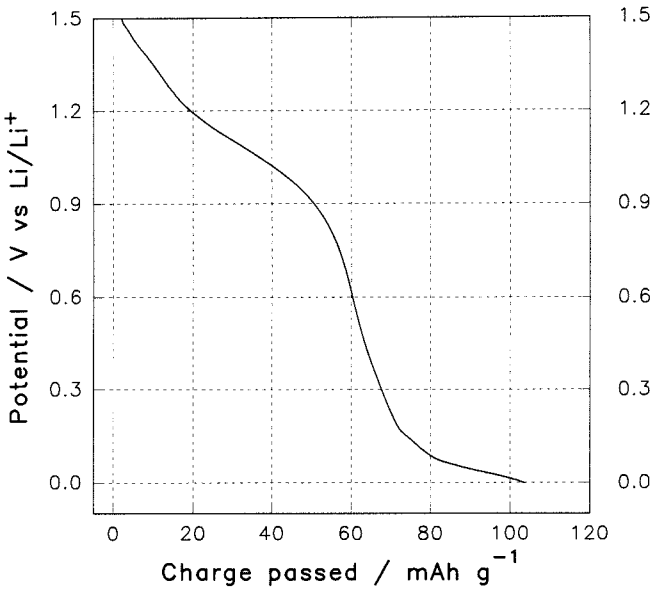

Figure 4.13 - Titration of lithium against graphite powder in EC/ PC/ 12-crown-4 at a rate of C/80 at atmospheric pressure

In a $LiCF_3SO_3$/ EC/ PC/ 12-crown-4 electrolyte under ~ 500 kPa of stack pressure the insertion profile showed an extended insertion region; Fig. 4.14. However, the difference in these profiles cannot be unequivocally attributed to the increase in stack pressure, because the salt and insertion rates differed.

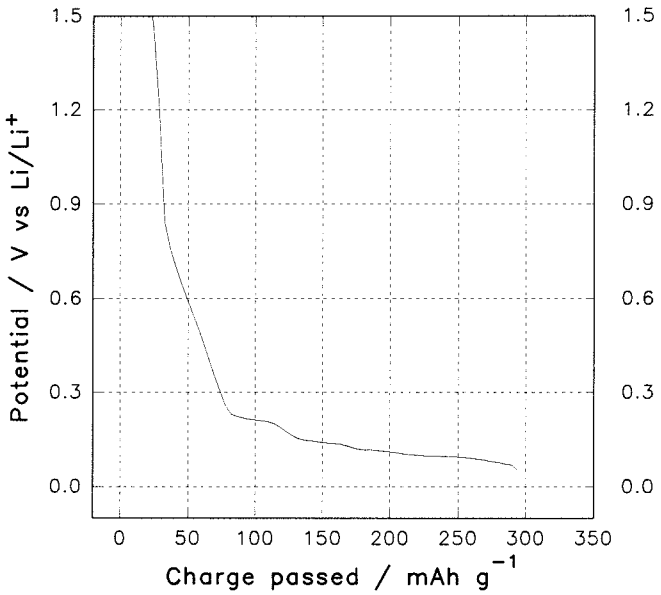

Figure 4.14 - Titration of lithium against graphite powder in EC/ PC/ 12-crown-4 at a rate of C/175 and ~ 500 kPa of stack pressure

A more accurate assessment of the effect of stack pressure can be made by comparison of lithium insertion into a graphite powder electrode in EC/ DEC/ $LiCF_3SO_3$ electrolyte at a rate of C/21, under two different stack pressures, Fig. 4.15

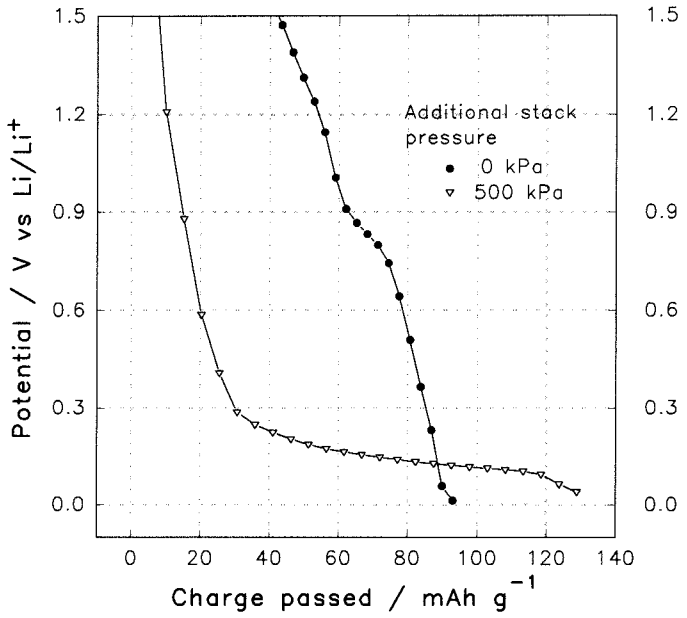

Figure 4.15 - Lithium titration curves for graphite powder electrodes in EC/ DEC/ $LiCF_3SO_3$ electrolyte at a rate of C/21 under atmospheric pressure and with 500 kPa of stack pressure.

It is clear from Fig. 4.15 that applying stack pressure can reduce the amount of charge used in solvent decomposition and increase the amount passed in insertion reactions. Thus it may be reasoned that the application of stack pressure kept the graphite particles in close contact so that less surface area was exposed for film-forming parasitic reactions. In addition, in the cell without stack pressure the formation of films may have led to the electrical isolation of many of the graphite particles, hence reducing the electrode insertion capacity.

It may be noted that although applying 500 kPa of stack pressure increased the graphite insertion capacity, a decrease in capacity due to Le Chatelier's principle would become non-negligible at much higher pressures (~ 1 GPa) [9].

4.3 Conductivity Additives

The lithium insertion profile into graphite powder electrodes from a suitable electrolyte, at low rates (< C/21), with stack pressure, resembled that of monolithic

graphite. However, the first cycle extraction efficiencies were much lower, even at very low rates; for example ~ 26 % at C/190 rate. Electrodes from which the lithium had been extracted, such that the OCV was ≥ 1.0 V vs. Li/Li^+, were found to evolve gas vigorously on the addition of distilled water. From this it was concluded that at least a part of the capacity loss was due to electrical isolation of lithiated graphite particles. It seems likely that as during extraction of lithium from the electrode, the lithiated particles contracted and became isolated by the formation of an insulating film, Fig. 4.16.

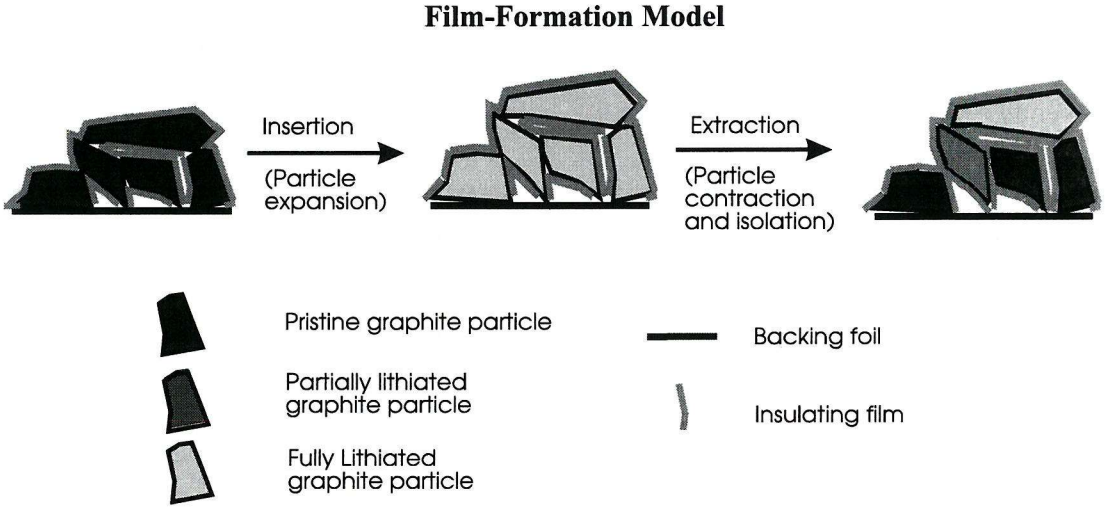

Figure 4.16 - Model to show the isolation of lithiated particles by insulating films on cycling of graphite powder electrodes

From the model depicted in Fig. 4.16 it is clear that the extraction efficiency would be greatly enhanced if the particles remained in good electrical contact with the backing foil at all stages of cycling.

4.3.1 Carbon black

It has been reported that various carbon blacks may be added to the electrode to improve particle-particle conductivity [10]. Electrodes were fabricated with 10 w/o of either carbon black or copper conductivity additives. The electrodes were evaluated by pulsed coulometric titration in EC/ DEC/ $LiCF_3SO_3$ electrolyte, with ~ 500 kPa of stack pressure at an overall rate of C/21, e.g. Fig. 4.17 for a Cabot Black Pearls 2000 electrode. Some of the titration parameters along with the conductivity additive surface areas have been summarised in Table 4.1:

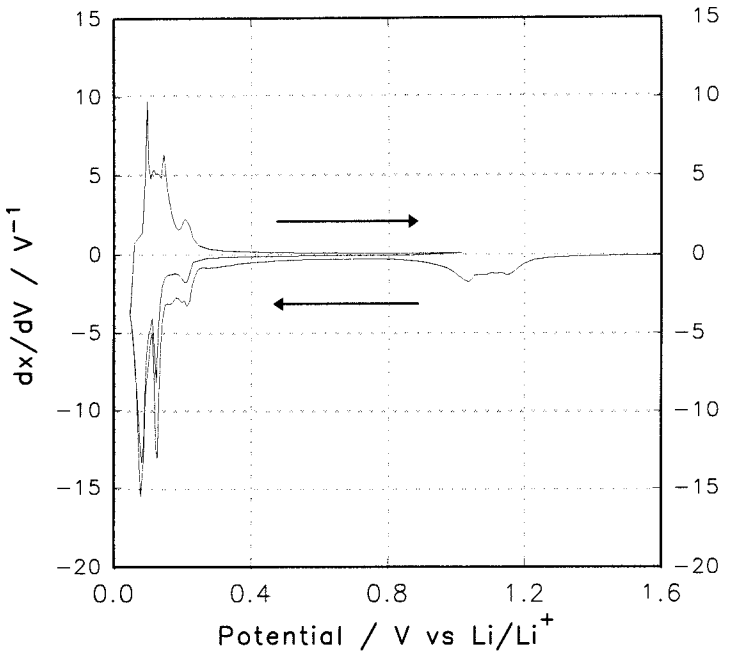

Figure 4.17 - dx/dV vs. V plot for the first 1½ cycles of an electrode with Cabot Black Pearls 2000, as a conductivity additive

Table 4.1 - Summary of titration parameters of electrodes containing 10 w/o of conductivity additives and their respective surface areas.

Conductivity additive	BET surface area (free powder) / $m^2 g^{-1}$	Charge passed on insertion / mAh g^{-1}	Extracted charge / mAh g^{-1}	Cycling efficiency / %
none	-	130 ± 25	60 ± 10	46 ± 1
Copper flake, Synchemica	~ 3 *	360 ± 60	235 ± 40	65 ± 1
Degussa lamp black	20 [11]	440 ± 80	255 ± 50	58 ± 1
Vulcan XC72, carbon black	252 [11]	430 ± 80	200 ± 40	47 ± 1
Acetylene black	> 80 [12]	460 ± 110	200 ± 45	43 ± 1
Cabot Black Pearls 2000, carbon black	1400 [11]	690 ± 160	220 ± 50	32 ± 1

* - estimate from particle size determination by optical microscopy

Each of the electrodes containing any conductivity additive gave the same extraction capacity (within experimental error) of ~220 mAh g^{-1}, which was significantly higher than that of electrodes containing no conductivity additive; ~ 60 mAh g^{-1}. Therefore, it may be assumed that 10 w/o of any of the conductivity additives examined constituted an excess. It may also be seen from Table 4.1 that the extraction efficiency decreased with increasing surface area of the conductivity additive. This may have been predicted from previous observations on solvent decomposition. It is also clear from the first insertion of the electrode prepared with Cabot Black Pearls 2000 carbon black (Fig. 4.17) that a significant amount of charge was passed between 1.3 and 0.8 V vs. Li/Li^+ which is well above the lithium insertion region (chap. 3.4). It may also be noted that there was a significant decrease in the insertion peak areas between the first and second insertions, this may be due to particle isolation (as in the film-formation model) or reaction of the low potential solvent decomposition reactions on the first insertion (possibly involving inserted lithium).

Although copper powder appeared to be the most promising conductivity additive, it was found that the irreversible capacity of copper-based electrodes increased with storage time, when they were stored in air, possibly due to oxidation of the copper powder. Therefore 10 w/o of lamp black was used as a conductivity additive in the following work. The cycling dependence of copper powder electrodes on storage conditions may be explored in subsequent work.

4.3.2 Rate dependence

Figs. 4.18 shows the rate dependence of charge insertion into graphite powder electrodes with (9 w/o EPM, 8:1 ratio of KS44 to lamp black) and without (10 w/o EPM, 90 w/o KS44) conductivity additive. Fig. 4.19 shows the corresponding charge extraction data.

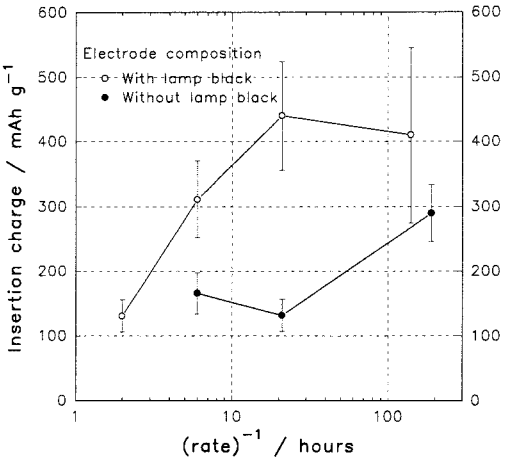

Figure 4.18 - Rate dependence of insertion into graphite powder electrodes

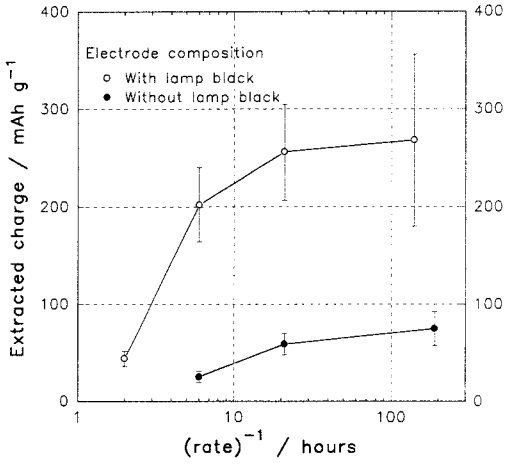

Figure 4.19 - Rate dependence of extraction from graphite powder electrodes

It seems apparent that for the electrode containing lamp black both the extraction and insertion charges reach limiting values at a cycling rate between C/6 and C/21. However, from the electrodes without conductivity additive a much lower cycling rate (≤ C/190) is required to reach the maximum charge limits.

It may also be noted that the maximum diffusion length in particles of KS44 graphite would be approximately five times shorter than those in the monolithic graphite electrodes; 20 μm and 100 μm respectively. Thus, if lithium diffusion in the graphite was the rate limiting process it would be expected that the maximum charge limit would be reached at roughly 25 times higher rates for the powder electrode than for the monolithic one, from Eqn. 4.1 [28].

$$\tau = \frac{l^2}{D} \qquad \textbf{Equation 4.1}$$

where τ is the time constant for diffusion, l the diffusion length and D the rate of diffusion.

As the onset of insertion-site limitation was observed to occur between the rates of C/16 and C/21 for the monolithic graphite the corresponding rates for a KS44 powder electrodes should be between 1.6C and 1.2C. However, as stated above the observed rates for the powder electrodes were much lower (between C/6 and C/21 for the electrode with conductivity additive). Hence, it may be assumed that either lithium diffusion in the graphite particles was not the rate determining process in these electrodes or that the use of Eqn. 4.1 is inappropriate. It is possible that phase nucleation, lithium diffusion through the

interfacial film, lithium transport in the electrolyte or electron conduction in the electrode could be rate limiting.

4.4 Binder Concentration

Ideally the binder should be a chemically and electrochemically unreactive material which holds all of the electrode material in good electrical contact with the backing foil. As the binder has no insertion capacity for lithium ions it follows that to optimise the overall electrode capacity the amount of binder must be minimised. To examine the insertion capacity dependence on binder concentration a range of electrodes were fabricated containing a ratio of 8:1 KS44 graphite to lamp black with 5 - 29 w/o EPM binder. The graphite loading of the electrodes was 8.5 +/- 1.1 mg cm^{-2}.

Figs. 4.20 and 4.21 show scanning electron microscopy images of electrodes with 5 w/o and 22 w/o EPM respectively. By comparison of the images it may be observed that the edges of the particles are less well-defined, and the corners less sharp in the 22 w/o EPM electrode, indicating that the EPM binder forms a relatively uniform coating over a large proportion of the surface of the carbon particles. It may also be noted that the smallest particles (< 1 μm diameter) tended to form aggregates.

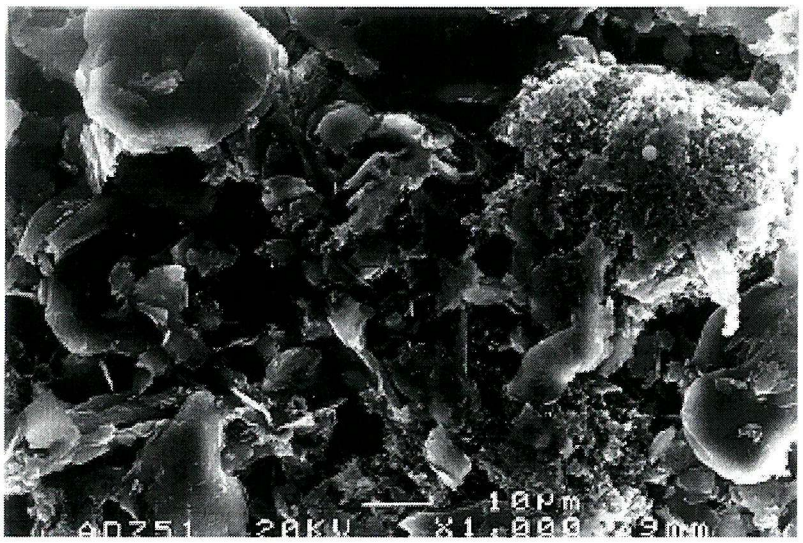

Figure 4.20 - Scanning electron microscopy image of a 5 w/o EPM electrode

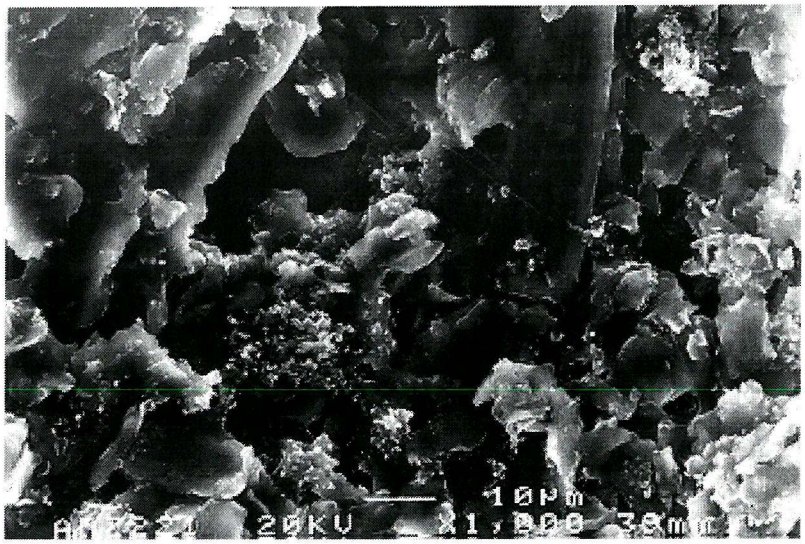

Figure 4.21 - Scanning electron microscopy image of a 22 w/o EPM electrode

Lithium was inserted into the electrodes by pulsed coulometric titration, at an overall rate of C/21, from $LiCF_3SO_3$/ EC/ DEC electrolyte. The amount of charge passed <0.4 V vs. Li/Li^+ was used as a measure of the extent of intercalation, based on the insertion profiles of monolithic graphite (chap. 3.4). Fig. 4.22 and Fig. 4.23 show the dependence of the extent of intercalation, as charge per unit mass of carbon and charge per unit mass of carbon and binder respectively, with binder concentration. (The error bars are as defined in chap. 2.7)

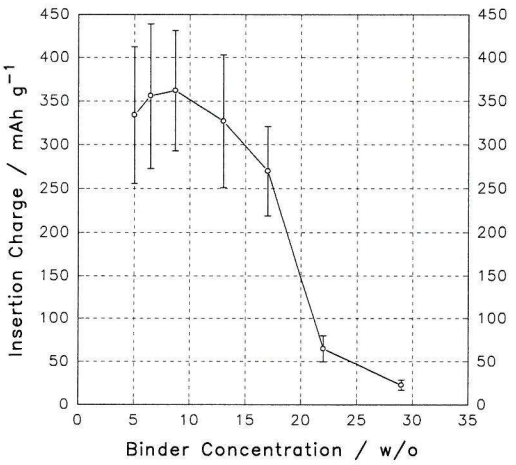

Figure 4.22 - Variation of insertion capacity (per mass of carbon) with binder concentration

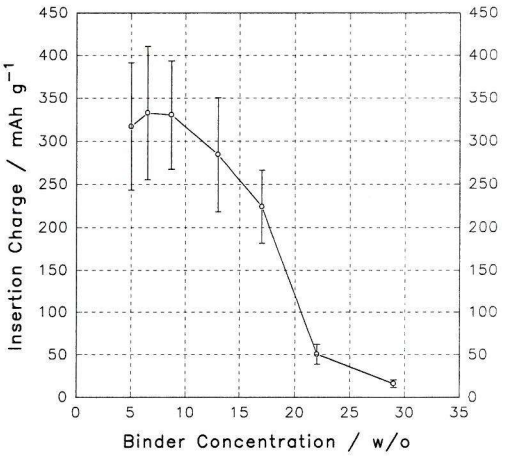

Figure 4.23- Variation of insertion capacity (per mass of carbon + binder) with binder concentration

It can be seen from Figs. 4.22 and 4.23 that, under these conditions, the optimum binder concentration was < 13 w/o (it has been reported that the optimum PTFE binder content is 3 w/o in pressed graphite electrodes [13]). However, at the lowest binder concentrations many cells failed through short-circuit as the graphite was only weakly bound to the backing foil. It may also be noted from Fig. 4.22 that the charge per unit mass of carbon decreased suddenly between 17 w/o and 22 w/o binder. To explore this behaviour in more detail plots of dx/dV vs. V were constructed for representative cells over a range of binder concentrations, Fig. 4.24.

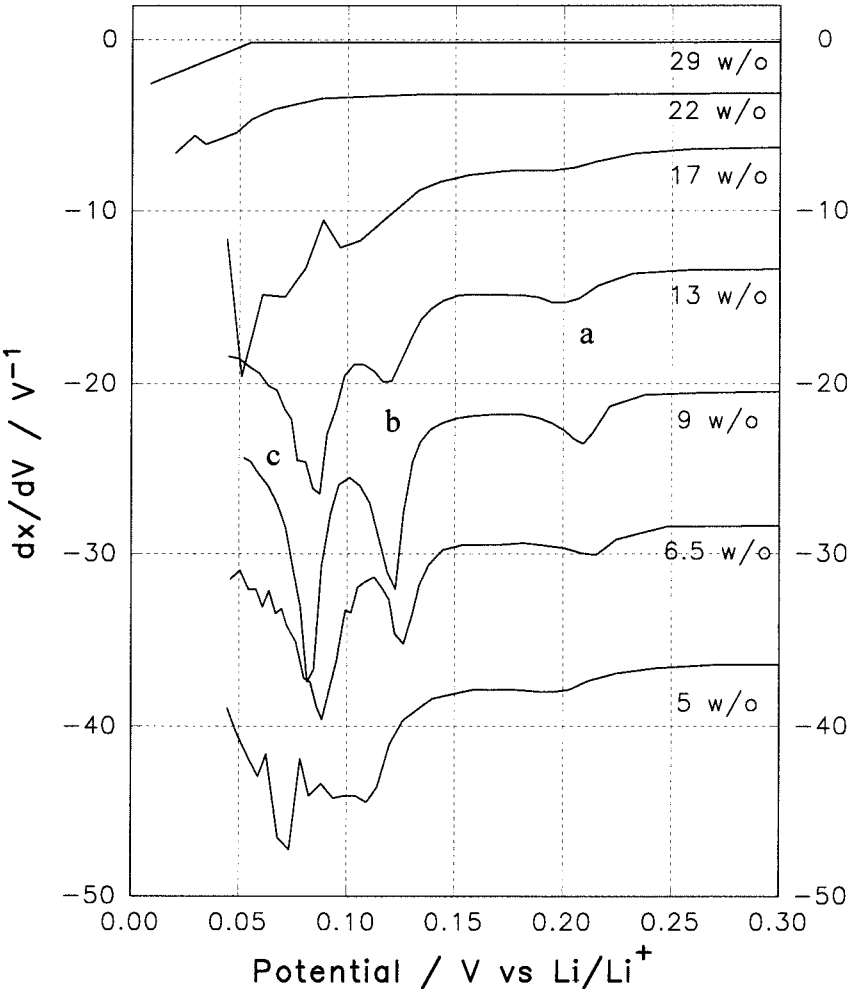

Figure 4.24 - dx/dV vs. V profiles for lithium insertion into graphite powder electrodes with varying binder concentrations from 5 w/o to 29 w/o. The traces have been offset along the y-axis by: 22 w/o, -3 V^{-1}; 17 w/o, -6 V^{-1}; 13 w/o, -13 V^{-1}; 9 w/o, -20 V^{-1}; 6.5 w/o, -28 V^{-1}; 5 w/o, -36 V^{-1}.

If the binder was considered to act by effectively isolating a proportion of the graphite particles whilst leaving the remainder in good electrical contact with the backing

foil (binder model I, Fig. 4.25) it would be expected that as the binder concentration was increased the proportion of the graphite that remained active would decrease. Thus for galvanostatic insertion at a given rate, the effective rate of insertion into the active electrode material would increase as the binder concentration was increased. Thus it may be anticipated that dx/dV plots for binder concentration dependence of a powder electrode (Fig. 4.24) would appear similar to plots for rate dependence of a monolithic electrode (Fig. 3.27)

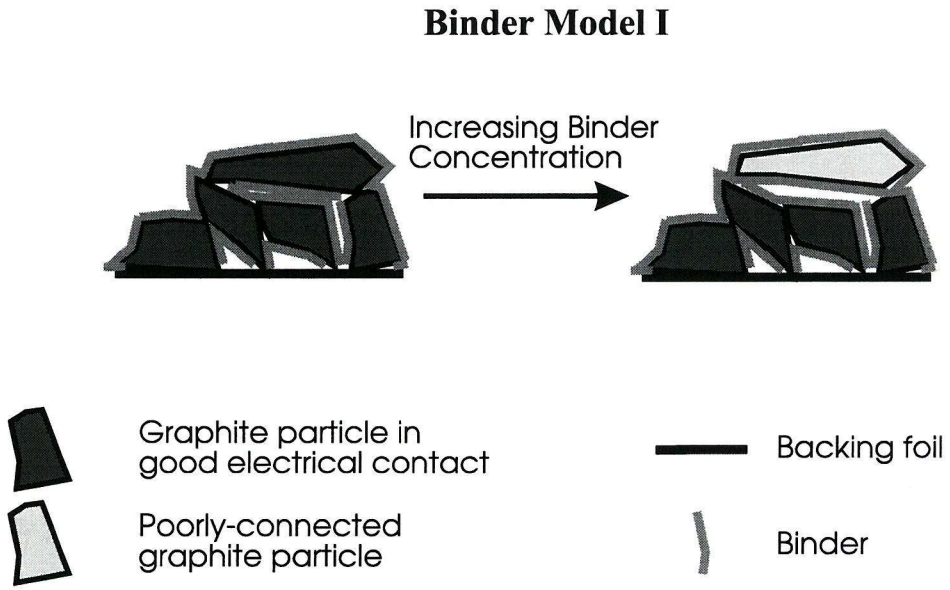

Figure 4.25 - Model I for the action of the electrode binder

From Fig. 4.24 it may be seen that the peak labelled b shifted to higher potentials as the binder concentration was decreased from 17 to 6.5 w/o. A similar trend was noted previously for monolithic graphite when the insertion rate was decreased (chap. 3.4). However, unlike the monolithic graphite the powder electrode the a peak also appeared to increase in potential with decreasing binder concentration to a maximum at 6.5 w/o EPM. It may also be seen that the area under peak c is larger than under peak b at binder concentrations of 17 w/o to 6.5 w/o, whereas the area under peak c only exceeds that of peak b at the lowest rate (C/126) for the monolithic electrode. Hence, it may be concluded that binder model I does not accurately reflect the behaviour of the bound electrodes.

A second model of the binder action was proposed (Fig. 4.26). Model II assumes that the binder acts to increase the resistance of the graphite particle-particle contacts and

the graphite particle-backing foil contacts in such a way as to produce a distribution of resistance pathways.

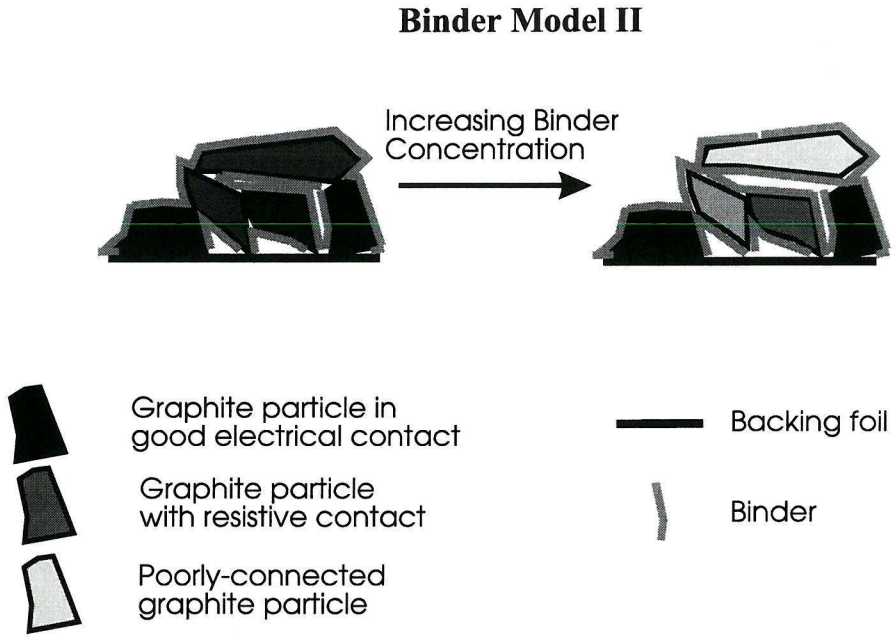

Figure 4.26 - - Model II for the action of the electrode binder

For the monolithic graphite it was proposed that a non-equilibrium distribution of surface Li-GIC phases may result after any given current pulse. Equilibration was expected to occur by lithium redistribution between the surface and bulk of the monolith. A similar processes would be predicted to occur to a similar extent within each 'good-contact' particle under the first binder model. However, under the second model the lithium activity on the surface of a given particle would be expected to depend on the resistance between the particle and the backing foil. An electrode with much binder would have a wide distribution of resistance pathways. It is then quite feasible that after an insertion pulse the extent of intercalation would vary widely between graphite particles. Inter-particle lithium diffusion may be expected to proceed less readily than intra-particle diffusion. Hence, after any given relaxation period a state of near-equilibrium may exist between the bulk and surface phases of any given particle, but the surface lithium activity of any two particles may be expected to differ. Hence each particle may be considered to possess a potential, $E_{particle}$, which is not necessarily the same as the measured electrode potential, E_{meas}, Fig. 4.27. In such a situation a mixed potential would be measured, E_{meas} which would be given by Eqn. 4.2.

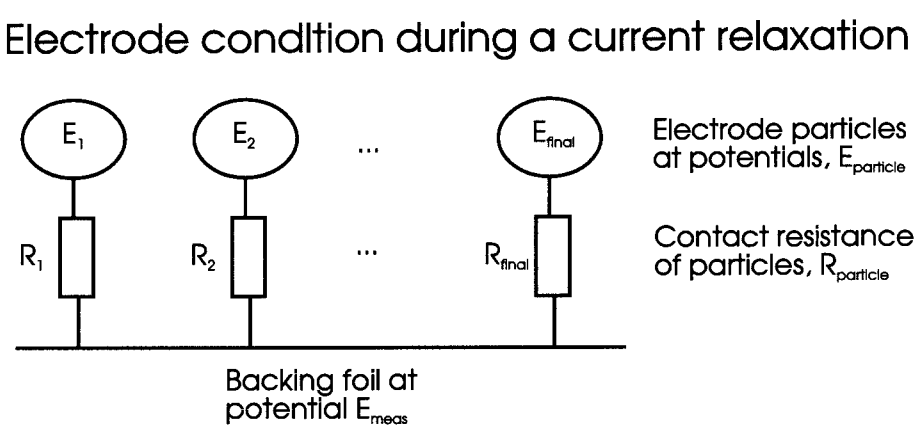

Figure 4.27 - Schematic representation of electrode during current relaxation

$$E_{meas} = \frac{\sum_{n=1}^{final} \frac{E_n}{R_n}}{\sum_{m=1}^{final} \frac{1}{R_m}} \qquad \textbf{Equation 4.2}$$

The dx/dV insertion peak positions would be determined by the particles with an 'average' contact resistance. However, at high binder concentrations the minority 'good-contact' particles would have a greater surface activity of lithium than the majority 'average-contact' particles at the end of any given insertion pulse. Assuming that the relaxation time was insufficient to reach an equilibrium in the inter-particle surface phase activities, the 'good-contact' particles would have lower values of E_n than the majority 'average-contact' particles. From Eqn. 4.2 it may be seen that this would cause E_{meas} to be lower than the potentials of the majority of the particles. As dx/dV would be expected to go through a maxima when the majority of particles are close to the true equilibrium potential of a given two-phase system, E_{meas} for a given dx/dV peak would be expected to be more negative than the true equilibrium potential.

Similarly, at low binder concentrations a positive shift in the peak positions may be produced by the minority of 'poor-contact' particles. This could occur if at the end of any given relaxation pulse the minority of 'poor-contact' particles exhibited lower lithium surface activities, and hence higher potentials, than the majority of 'good-contact' particles. At low binder concentrations the minority 'poor-contact' particles would have higher values of R_n than the average, whereas at high binder concentrations the minority of 'good-contact' particles would have lower values of R_n than the average. Therefore it may

be expected that the magnitude of the peak shift would be much smaller at low binder than at high binder concentrations, from Eqn. 4.2.

It appears that this model would account for the shift in peak positions observed in Fig. 4.24, for binder concentrations between 6.5 and 29 w/o. The profile of the 5 w/o electrode may be considered similar to that of the monolithic electrode at high rates (Fig. 3.27). This would be expected if some of the electrode material became detached in the cell, to leave an electrode with less than the original carbon loading.

At high binder concentrations the distribution of Li-GIC phases resulting from each current pulse may be expected to produce a peak broadening. Electrodes with 6.5 w/o - 9 w/o EPM were found to have the lowest peak widths (FWHM, 18 ± 4 mV).

4.5 Particle size

Three graphite powders with differing particle size distributions were used to form electrodes in an 8:1 ratio with lamp black, bound with 9 w/o EPM. The electrode loadings were 8.3 ± 1.5 mg cm^{-2} of carbon. The electrode capacities were determined by pulsed coulometric titration at a cycling rate of C/21, in EC/ DEC/ $LiCF_3SO_3$. The titration data has been summarised in Table 4.2, where n is the number of samples:

Table 4.2 - Summary of titration data for electrodes with different particle size distributions

Graphite type	Particle size / μm	First insertion charge / mAh g^{-1}	First extraction charge / mAh g^{-1}	n	Efficiency / %
KS6	< 6	415 ± 95	240 ± 55	2	58 ± 1
KS44	< 44	440 ± 85	255 ± 50	3	58 ± 1
KS75	< 75	385 ± 90	230 ± 55	2	59 ± 1

Under the cycling conditions employed there appeared to be little difference in the behaviour of the electrodes. However, practically it proved more difficult to obtain a uniform electrode loading with the KS6 graphite powder, because it tended to form macroscopic aggregates.

It was revealed by optical microscopy that grinding in an agate mortar broke up aggregates of graphite particles that were already present in the unbound powders, but did

not noticeably change the distribution of particle sizes. Grinding was found to improve the uniformity of electrode loadings but produced no distinct change in electrode capacity.

4.6 X-Ray Diffraction [14]

As stated previously, when lithium ions are inserted between the carbon layers in graphite, the stacking pattern changes from ABAB to AAAA (chap 1.2.2). This causes an increase in the average layer spacing [15 - 17]. X-ray diffraction (XRD) may been used to measure the average layer spacing and hence identify the Li-GIC phases.
XRD has been used in several studies to examine the equilibrium staging of electrochemically intercalated lithium in graphite (chap. 3.4.2) [3, 18].

It was decided to employ XRD to examine phase interconversion under non-equilibrium conditions in a graphite powder electrode. For these measurements a graphite powder electrode with 10 w/o lamp black conductivity additive was examined in EC/ DEC/ $LiCF_3SO_3$ electrolyte. Electrochemical measurements were made by using a MacPile II ™ cycling system. Concurrent X-ray measurements (CuK_α radiation) were made using the apparatus shown in chap. 2.

4.6.1 Calibration

Lithium was intercalated into the graphite powder electrode, by pulsed coulometric titration (Fig. 4.28 shows the full curve) at an overall rate of C/19. Four of the X-ray diffractograms that were recorded during the intercalation are shown in Fig. 4.29

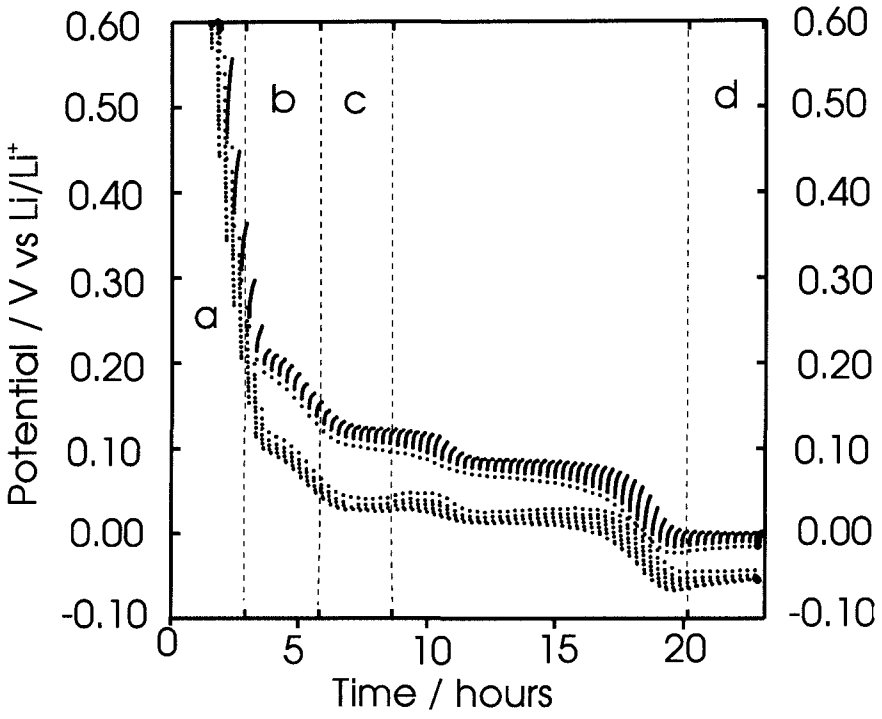

Figure 4.28 - Pulsed coulometric titration of lithium against graphite powder electrode. The upper and lower parts of the curve correspond to the insertion and relaxation periods respectively. The amount of charge passed corresponds to: (a) 0 - 56 mAh g^{-1} (b) 56 - 113 mAh g^{-1} (c) 113 - 169 mAh g^{-1}, and (d) 394 - 450 mAh g^{-1}.

The surface phases may be assigned, as before for monolithic graphite, from the plateau potentials (chap. 3.4), Table 4.3:

Table 4.3 - Li-GIC phase assignment from pulsed coulometric titration

Region	OCV range / mV vs. Li/Li^+	Dominant stage	Charge passed / mAh g^{-1}
(a)	2900 - 350	Pristine graphite, (1')	0 - 56
(b)	350 - 150	1', 4, (3)	56 - 113
(c)	150 - 120	(3), 2, 2L	113 - 169
(d)	0	1, plated lithium	394 - 450

A bracketed stage index indicates that it may be present as a minority component.

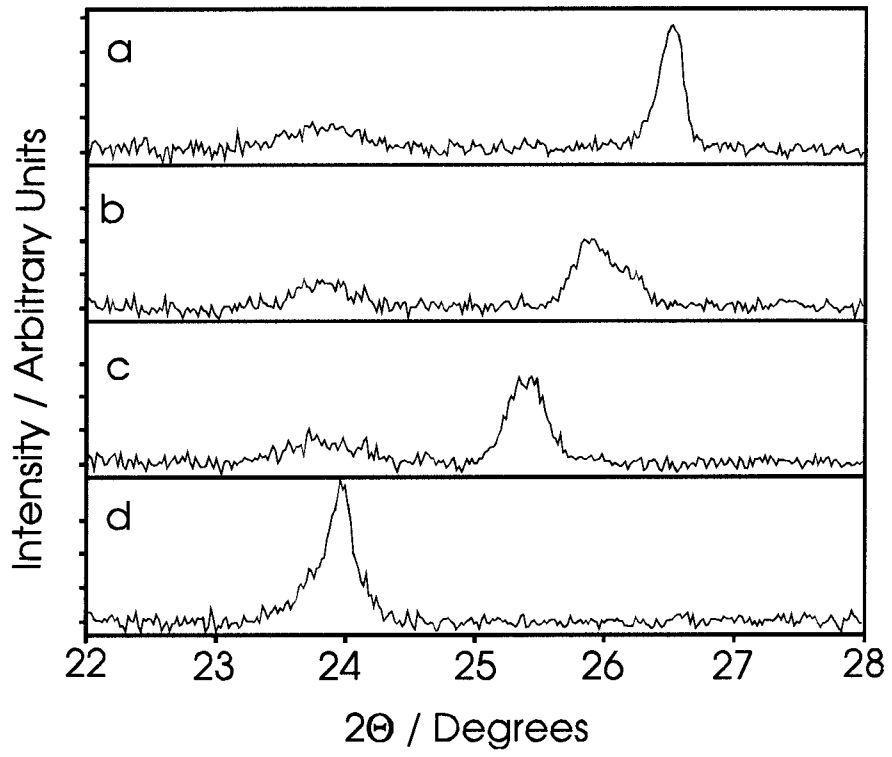

Figure 4.29 - X-ray diffractograms showing the 00*l* peak of graphite at various degrees of insertion. The amount of charge passed corresponds to: (a) 0 - 56 mAh g^{-1} (b) 56 - 113 mAh g^{-1} (c) 113 - 169 mAh g^{-1}, and (d) 394 - 450 mAh g^{-1}.

The broad peak at ~ 23.7° has been assigned to components of the aluminium-polymer laminate bag.

The positions of the graphite peaks (Fig. 4.29) were obtained by fitting curves (Pearson VII functions) using STOE software after baseline subtraction. Using the Bragg equation (Eqn. 2.8) the average layer spacing was obtained from the peak positions. The average layer spacings can be related to the stage of the Li-GIC by Eqn. 4.3, which is based on the assumption that there is no interaction between the lithiated layers, such that the separation of graphene layers may have one of only two distinct values.

$$d_{average} = \frac{d_{filled} + (n-1)d_{empty}}{n} \qquad \textbf{Equation 4.3}$$

Where $d_{average}$ is the average layer spacing, d_{empty} is the d_{002} spacing of pristine graphite and d_{filled} is the d_{001} spacing of the stage 1 compound. Using the accepted literature values of d_{empty} = 3.355 Å and d_{filled} = 3.705 Å, the XRD peaks in Fig. 4.29 may be readily assigned, Fig. 4.30.

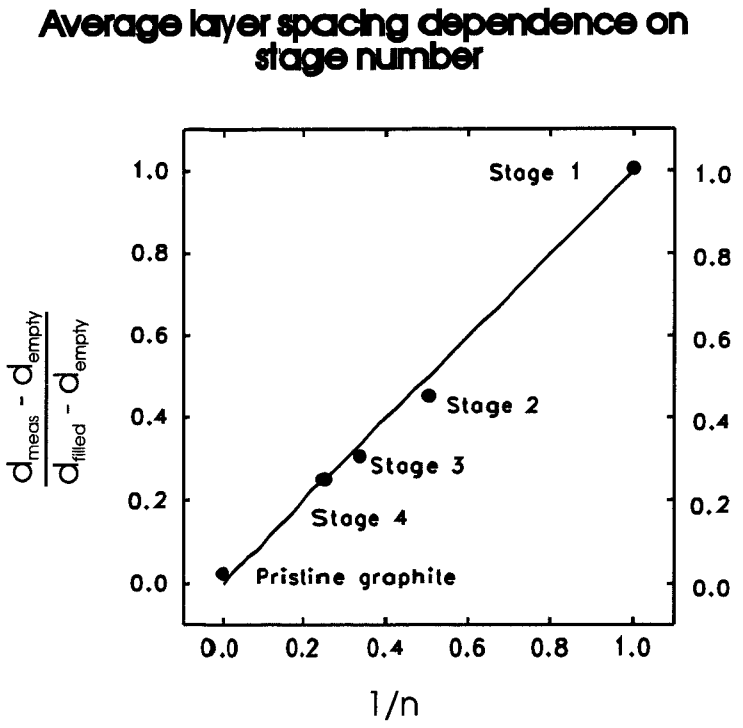

Figure 4.30 - Identification of Li-GIC stage from X-ray peak position using Eqn. 4.3

The phase assignments and areas under the peaks have been summarised in Table 4.4, where Method 2 consisted of fitting Pearson VII functions and Method 1 of integration between limits after baseline subtraction. The peak areas were normalised against the peak in region a. It may be noted that similar results were obtained by fitting Gaussian functions.

Table 4.4 - Summary of XRD parameters relating to Fig. 4.29

Region	Layer spacing / Å	Dominant stage [19, 20]	Method 1, normalised area	Method 2, normalised area
(a)	3.359	pristine graphite	1.00	1.00
(b)	3.44, 3.39	4 and 1'	0.99	1.03
(c)	3.513	2 and 2L	1.01	1.05
(d)	3.712	1	0.98	0.99

The XRD assignments are in good agreement with those made from the electrochemical measurements (Tables 4.3 and 4.4), indicating that under the insertion conditions employed the bulk and surface phases of the graphite particles were similar.

The area under the dominant peak (Fig. 4.29) is affected by the change in composition of the GIC and the change in the scattering angle, as well as any long term variations in the primary beam intensity. However, these effects appear to cancel out, as the area of this peak (Table 4.4) remained constant with GIC composition to within the accuracy of the above methods (± 0.04).

It was found, in accordance with theory [21] and transient K-GIC measurements [22], that there was little broadening of the graphite peaks during the following measurements; hence, it will be assumed that the proportion of graphite present in a given phase can be deduced using Eqn. 4.4.

$$proportion\ of\ stage\ x = \frac{(area\ under\ peak\ corresponding\ to\ stage\ x)}{\sum_{i=all\ stages} (area\ under\ peak\ corresponding\ to\ stage\ i)}$$

Equation 4.4

4.6.2 Lithium extraction

Lithium was extracted from the graphite powder electrode used above, at a rate of C/19, Fig. 4.31.

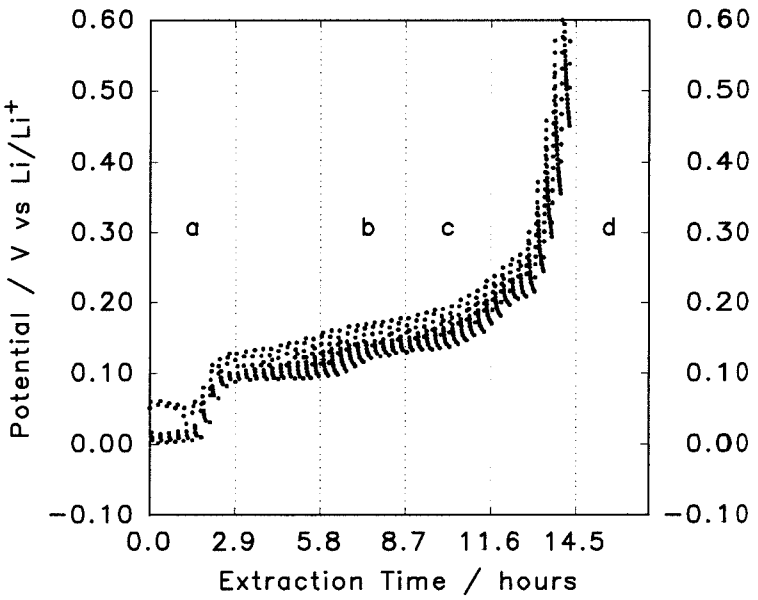

Figure 4.31 - Pulsed coulometric extraction from a graphite powder electrode, C/19 rate

Four of the X-ray diffractograms which were recorded at increasing degrees of lithium extraction from the graphite powder electrode are shown in Fig. 4.32.

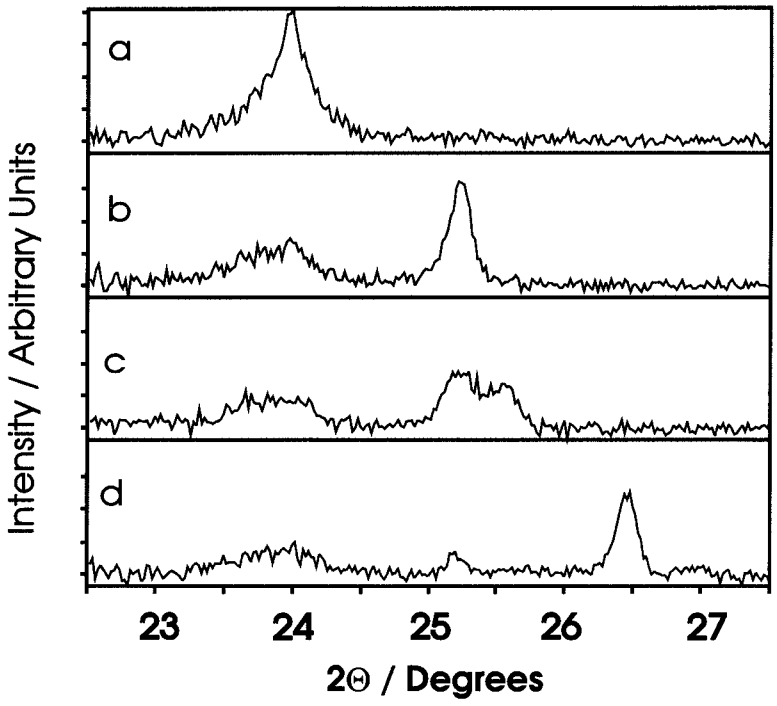

Figure 4.32- X-ray diffractograms showing the 00*l* peak of graphite at various degrees of extraction. The extent of 'inserted' charge corresponds to: (a) 450 - 394 mAh g^{-1} (b) 338 - 282 mAh g^{-1} (c) 282 - 225 mAh g^{-1}, and (d) 113 - 56 mAh g^{-1}

It was found that even after holding the cell at potentials > 0.5 V vs. Li/Li^+ for 8 hours the final X-ray diffractogram changed very little. The peaks that are apparent in Fig. 4.32 may be used to identify the Li-GIC stages present in the electrode, as before: a) - stage 1, b) - stages 1 and 2/ 2L, c) stages 2/ 2L and 3, d) stages 2/2L and pristine graphite.

That some low-order stage of Li-GIC remained present in the electrode with pristine graphite may be readily explained by the film formation model outlined previously (chap. 4.3). As the largest single contraction of the lithiated graphite particles occurs with the transition stage 1 → stage 2 (5.2 % perpendicular to the graphite planes) it is perhaps unsurprising that stage 2/ 2L Li-GIC remains in the electrode but undetectable (< 3 %) amounts of other phases.

4.6.3 Transient measurements

A cell, similar to the one used to calibrate the peak areas, was constructed. Lithium was inserted into the graphite powder electrode by means of a series of current pulses, Figs. 4.33, 4.35, 4.37, 4.39 and 4.41. The pulses were each of 300 s duration and conveyed 93 mAh g^{-1} of charge (3C charge rate). Following each pulse the cell was allowed to relax for at least 8 hours (until the rate of change of cell voltage was below 2 mV hr^{-1}). *In-situ* X-ray diffractograms were recorded every 150 s from the start of the current pulse (t = 0) for 2400 s, after which diffractograms were recorded every 450 s. The X-ray diffractograms were analysed as above (Eqn. 4.4), Fig. 4.34, 4.36, 4.38, 4.40 and 4.42. The proportion of a given phase was accurate to ± 0.05, except in the presence of >0.10 of stage 1, when it was accurate to ± 0.10. This was due to the inaccuracy incurred by separating the stage 1 peak from the broad background feature at ~ 23.7^{O}.

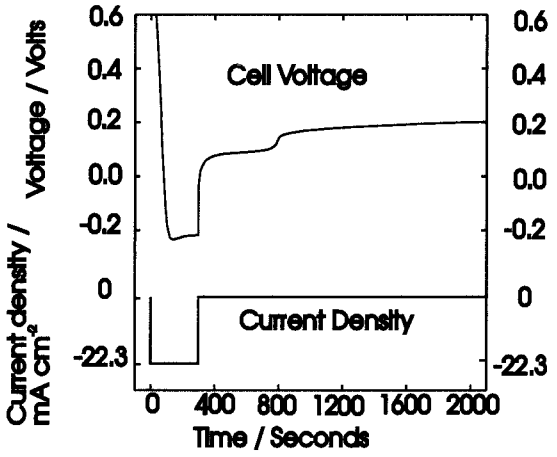

Figure 4.33 - Voltage variation on application of the first insertion pulse

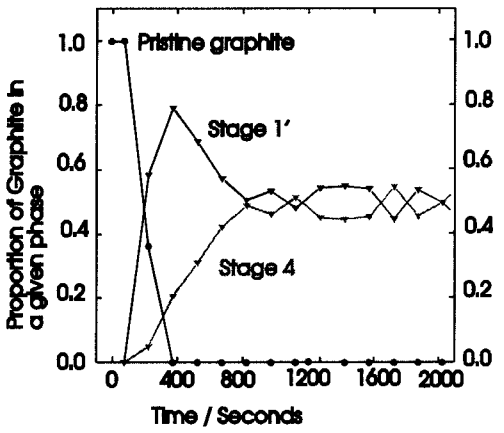

Figure 4.34 - Evolution of Li-GIC phases with time after the first insertion pulse

It may be seen that the amount of pristine graphite was found to become negligible (< 5 mol %) within 400 s of the start of the initial current pulse (Fig. 4.34). Thus, in excess of 95% of the electrode was accessible to lithium intercalation.

Following the first current pulse stage 1' Li-GIC was formed, which was then converted to a stage 4 phase. The growth of the stage 4 phase became negligible 500 s after the end of the current pulse.

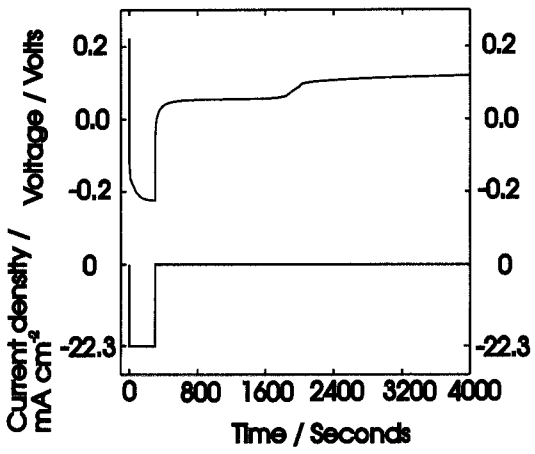

Figure 4.35 - As for Fig. 4.33, second pulse

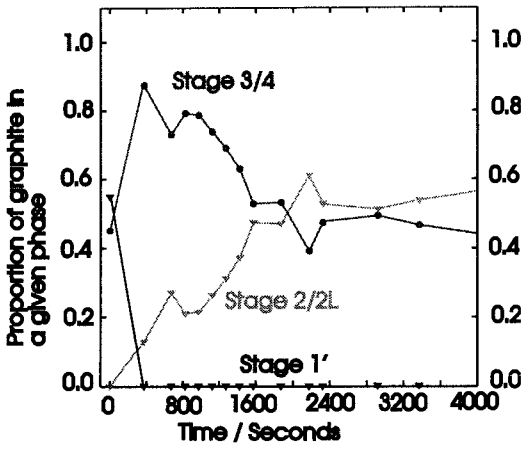

Figure 4.36 - As for Fig. 4.34, second pulse

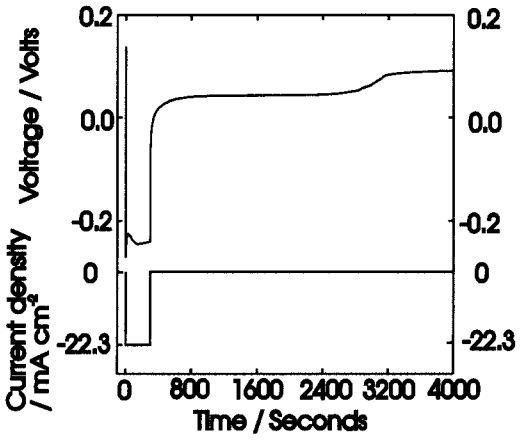

Figure 4.37 - as Fig. 4.33, third pulse

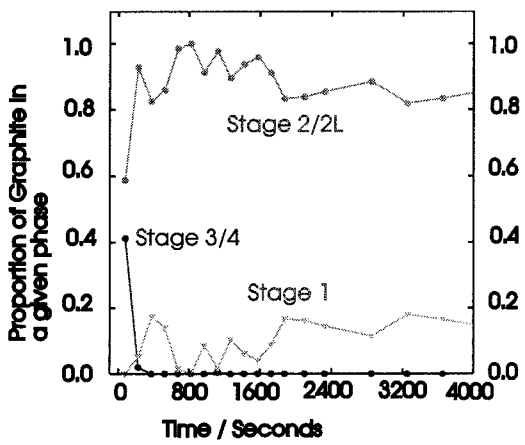

Figure 4.38 - as Fig. 4.34, third pulse

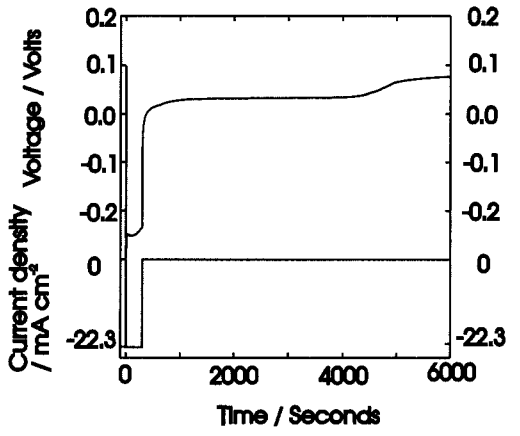

Figure 4.39- as Fig. 4.33, fourth pulse

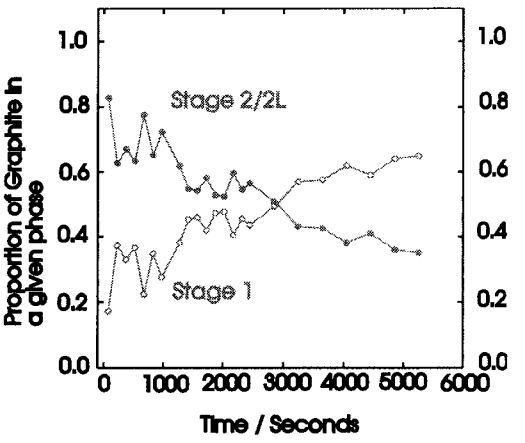

Figure 4.40- as Fig. 4.34, fourth pulse

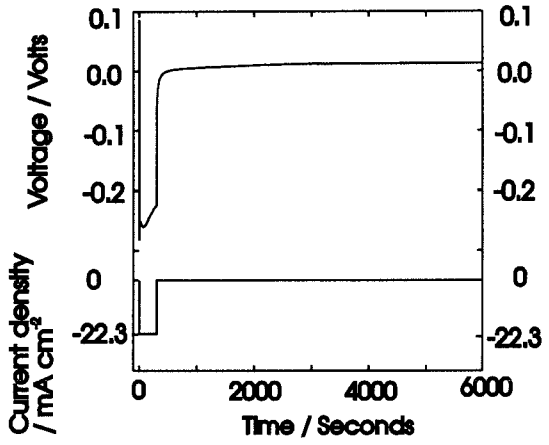

Figure 4.41 - as Fig. 4.33, fifth pulse

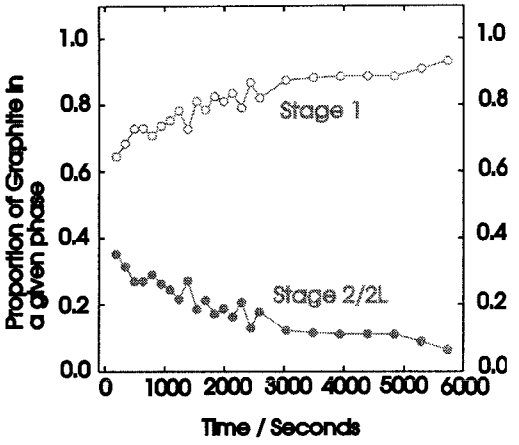

Figure 4.42 - as Fig. 4.34, fifth pulse

It can be seen (Figs. 4.34, 4.36, 4.38, 4.40 and 4.42) that phase interconversion continued during each relaxation period subsequent to each current pulse. The rate of phase interconversion decreased with charge passed until, after the final pulse (Fig. 4.42), phase interconversion continued for in excess of 5000 s. One apparent exception is the phase interconversion after the third pulse; however, it was not possible, from the X-ray data, to distinguish stage 2 from stage 2L. Hence, it may be expected that some phase interconversion, which was undetectable from the X-ray data, was proceeding, even though the sum of proportions of the two stage 2 phases remained virtually unchanged after 2000 s.

It can be seen (Fig. 4.33, 4.35, 4.37, 4.39 and 4.41) that, during the first four current relaxations ($t > 300$ s), the cell voltage passed through a final point of inflection. This reflects a sharp decrease in the surface activity of the graphite electrode. The time at which the inflection occurred, after the current pulse, (voltage relaxation time) was found to increase as the degree of lithium intercalation increased, Table 4.5. However, it should be noted that the faradaic yield of LiC_6 was approximately 80 % (Fig. 4.41).

Table 4.5 - Summary of the measurements shown in Figs. 4.33 to 4.41

Pulse number	Charge passed / mAh g^{-1}	Voltage relaxation time / s	Voltage at 6000 s / mV
1	93	500	216
2	186	1700	124
3	279	2600	93
4	372	4500	77
5	465	> 6000	12

The initial relaxation voltage plateau lay at a more negative potential than the final one, indicative that high-activity phases or metallic lithium were present at the graphite surface. The two voltage plateaux recorded in Fig 4.37, after the third pulse, were indicative of phase interconversions, which were not apparent from the X-ray data, as mentioned above. However, after the fifth pulse, the X-ray data revealed phase interconversions even though there was only a single voltage plateau. From these observations it is clear that chronopotentiometry and XRD are complementary techniques in the evaluation of phase interconversion in the Li-GIC system.

The presence of a minority concentrated phase may be inferred from the XRD peak positions identified after the first current pulse, (Fig. 4.43). Layer spacings, calculated for the dominant X-ray peaks, of > 3.45 Å were found at short times (t < 600 s). These spacings are indicative of a mixture of stage 3 and stage 4 Li-GICs, but stage 1' was also present (lower trace). Thus a mixture of at least three phases existed in the electrode [23]. At longer times, the layer spacing of the more concentrated phases (upper trace) decreased, implying a decrease in the ratio of stage 3 to stage 4.

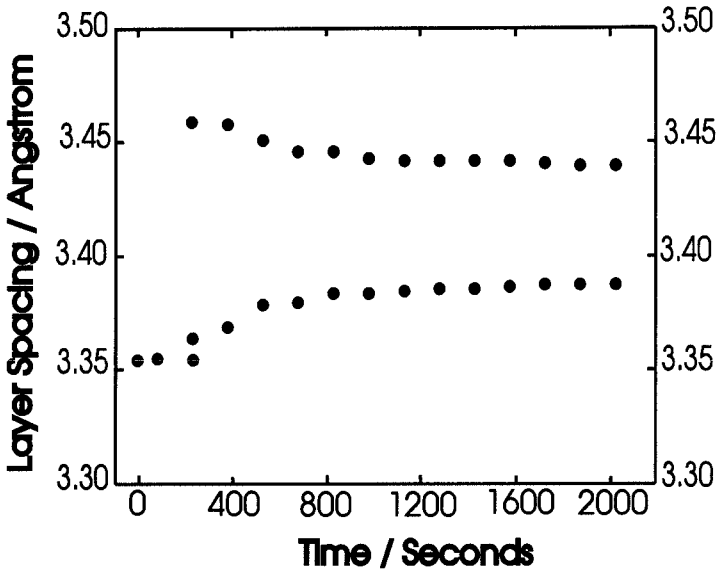

Figure 4.43 - $d_{average}$ layer spacings, following the first current pulse

Following the third, fourth and fifth pulses, the two dominant peaks, corresponding to stage 1 and stage 2 (or stage 2L), were found to vary little in position; $d_{average}$ = 3.700 ± 0.015 Å and 3.515 ± 0.005Å, respectively. It may also be noted that no intermediate phases (e.g. stage 1.5) were detected, even at short times. However, after the third pulse, the initial relaxation plateaux may indicate plated lithium rather than concentrated Li-GIC phases. This is almost certainly the case after the fifth pulse, where the voltage remained below 20 mV for more than 21 hours [24].

In the long-time limit (2 - 10 hours), after the first four pulses, the proportion of phases present and the cell voltage remained constant. In this limit, activity may be expected to differ little between the bulk and surface of the graphite particles. A model may be proposed that accounts for the observation above, for the two plateau situations, Fig. 4.44

i) The initial plateau corresponds to a dynamic system, in which concentrated lithium phases are present at the surface of the graphite particles. From these phases lithium diffuses to the more dilute bulk phases. As this happens, the ratio of high to low stage-order Li-GICs increases.

ii) The second voltage plateau extends for more than 10 hours after each pulse. In this region, the Li-GICs remain in almost constant ratio, indicating that the reservoir of lithium ions in concentrated surface phases has become depleted to an insignificant level.

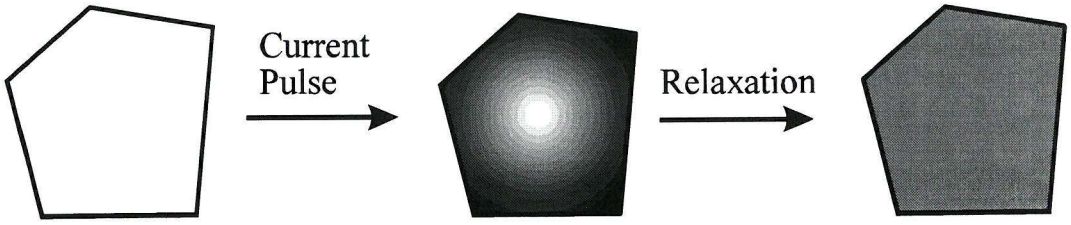

Figure 4.44 - Schematic representation of lithium activity in a graphite particle during intercalation. Depth of shading indicates lithium activity.

It may also be noted, from the data following the fifth pulse (Fig. 4.42), that lithium intercalated into the graphite particles from plated metallic deposits, although the mechanism for this process is unclear.

4.6 Above Ambient Temperature Intercalation

4.6.1 Electrolyte

It was expected that by heating the cell Li-GIC phase growth would be more rapid than at room temperature. Thus, it seemed plausible that by cycling a graphite powder electrode in a heated cell a similar capacity would be obtained to that in a room temperature cell at a lower cycling rate. In order to examine the behaviour of graphite powder in a heated cell an electrode with an 8:1 ratio of KS44:lamp black with 6 w/o PVDF binder, in a 1 M $LiCF_3SO_3$/ EC/ DEC electrolyte was subject to pulsed coulometric cycling at 60 ^{O}C. Fig. 4.45 shows the first cycle of the electrode at a rate of C/21 (note x is the theoretical degree of insertion, based on a charge efficiency of 100%, such that x = 1 is equivalent to $|Q| = 372$ mAh g^{-1}).

It may be noted that the insertion and extraction plateaux were distinct, but that there was an additional feature at ~ 0.3 V vs. Li/Li^+ on the extraction half-cycle. Similar features were observed with other electrodes under similar conditions, at apparently random potentials. As the electrodes were often found to have crumbled after cycling, it may be anticipated that the irregular features were due to an intermittent internal short-circuiting of the test-cell; this could also provide a mechanism for the >100 % cycling efficiency.

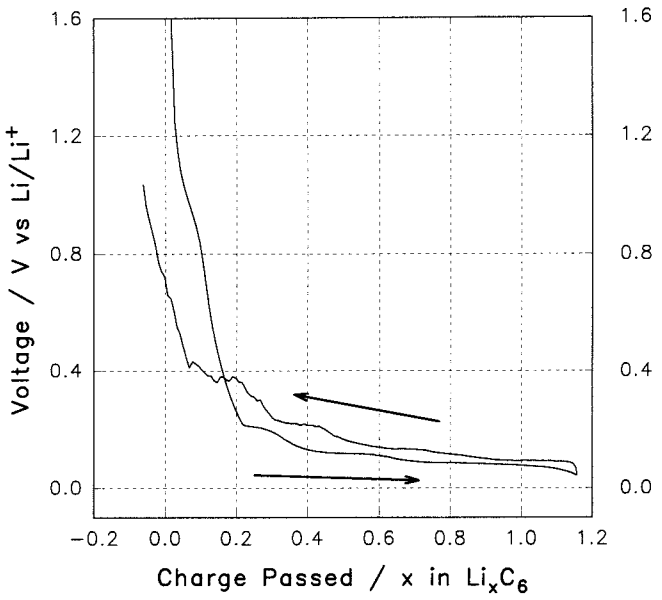

Figure 4.45 - The first cycle of a KS44 graphite powder electrode in EC/ DEC/ $LiCF_3SO_3$ at 60^{O}C

It has been noted previously (Chap. 2.1) that UV/ vis spectroscopy could be used to for qualitative analysis of solvent purity. Therefore, as the electrolyte was found to be slightly yellow after cycling at elevated temperatures, whereas room temperature cycling left it colourless, it was proposed that the elevated temperature of the cells may have increased the extent and possibly changed the products of the solvent decomposition reactions. Hence, It was decided to examine the behaviour of the electrodes in an alternative solvent.

Fig. 4.46 shows the first two and a half cycles of a KS44 electrode (as above) in a 1 M $LiCF_3SO_3$/ EC electrolyte at 60 ^{O}C, at a rate of C/21. It is clear by comparison of Fig. 4.46 and Table 4.1 that for the first cycle, both the extracted charge and cycling efficiency are greater in EC/ $LiCF_3SO_3$ at 60 ^{O}C than in EC/ DEC/ $LiCF_3SO_3$ at 25 ^{O}C. The first insertion profile in the EC electrolyte (Fig. 4.46) was similar to that in the heated EC/ DEC electrolyte (Fig. 4.45), but the extraction half-cycles showed no 'short-circuit' features. Therefore the crumbling of the electrodes in heated EC/ DEC may be attributed to the action of the DEC, or some impurity in the DEC.

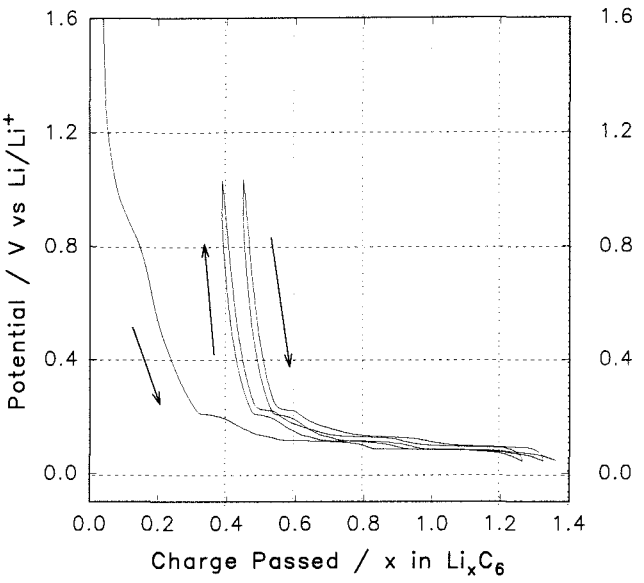

Figure 4.46 - First 2½ cycles of a KS44 graphite powder electrode in EC/ $LiCF_3SO_3$ at 60°C

It may also be seen from Fig. 4.46 that the cycling efficiency increases markedly from the first to second cycles of the electrode (71 % and 93 % respectively). Therefore, EC/ $LiCF_3SO_3$ was chosen as a suitable electrolyte to further explore the behaviour of the graphite powder electrodes .

4.6.2 Electrode capacity

Three ≤ 44 μm diameter graphite powders (KS44, MAA44 and SFG44) were used to make electrodes with the same concentrations of PVDF binder and lamp black as the electrode above (chap. 4.6.1). The electrodes were cycled as before. A summary of the cycling data, together with XRD parameters of the pristine powder has been made in Table 4.6.

Table 4.6 - Summary of coulometric titration and XRD data, for three graphite powders

Graphite type	d_{002} / Å	L_C / Å	First extraction charge/ mAh g^{-1}	Second extraction charge / mAh g^{-1}
KS44	3.361	350	326 ± 5	323 ± 5
MAA44	3.358	500	330 ± 5	325 ± 5
SFG44	3.363	500	302 ± 5	302 ± 5

The electrode capacities cited in Table 4.6 are based on the charge per unit mass of carbon. To accurately determine the amount of charge that was accommodated by the graphite it was considered necessary to independently evaluate the capacity of the lamp black. Fig. 4.47 shows the first two cycles of a lamp black electrode under similar cycling conditions to the graphite powder above.

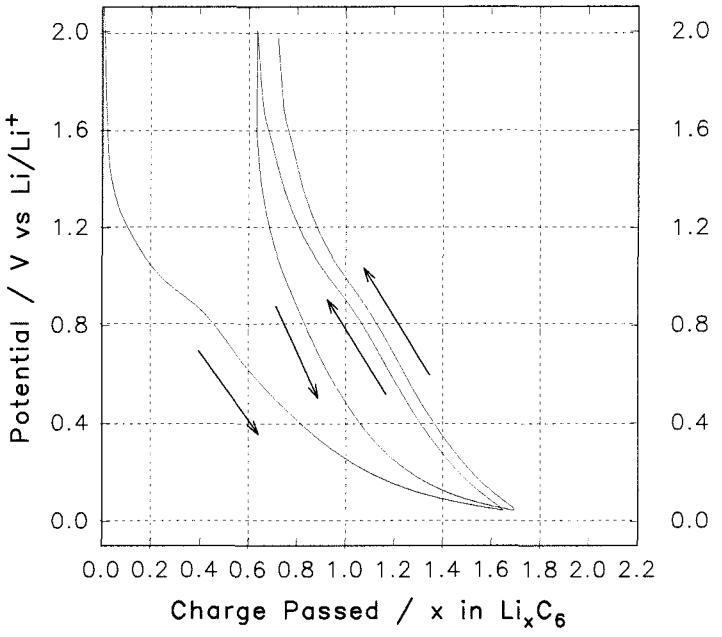

Figure 4.47 - First two cycles of a lamp black electrode in EC/ $LiCF_3SO_3$ at 60°C, C/21 rate

By considering the lamp black capacities between the appropriate cycling limits, the graphite capacities in the previous electrodes were calculated, Table 4.7. The values shown are close to the maximum literature values for graphite powder electrodes [25, 26].

Table 4.7 - Graphite-only extraction capacities and first cycle efficiencies

Graphite type	First extraction charge/ mAh g^{-1}	Second extraction charge / mAh g^{-1}	First extraction efficiency
KS44	331 ± 6	331 ± 6	73 ± 1 %
MAA44	336 ± 6	333 ± 6	78 ± 1 %
SFG44	305 ± 6	307 ± 6	83 ± 1 %

It has been postulated that slight differences in graphite capacities may arise from limited site availability at the edge of crystallites [27], and site-limitation due to

mixtures of rhombohedral and hexagonal graphite crystallites [25]. It has already be noted in Table 4.1 that there was a slight difference in crystallite size and layer spacing of the graphite samples. However, it is also possible that the slight differences in capacities arose from the different particle size distributions in the three samples (for example, the proportion of particles which were ≤ 10 μm was 12 w/o for SFG44, 30 w/o for KS44 [29]) or from the level of trace impurities (for example, 460 ppm silicon in SFG44, 90 ppm silicon in KS44 [29]).

4.6.3 Low potential features

Fig. 4.48 shows dx/dV vs. V traces for lithium insertion into graphite powder electrodes (SFG44 83.5 w/o, lamp black 10.5 w/o, PVDF 6 w/o) in EC/ $LiCF_3SO_3$ and EC/ DEC/ $LiCF_3SO_3$ electrolytes at 60 °C, C/21 rate.

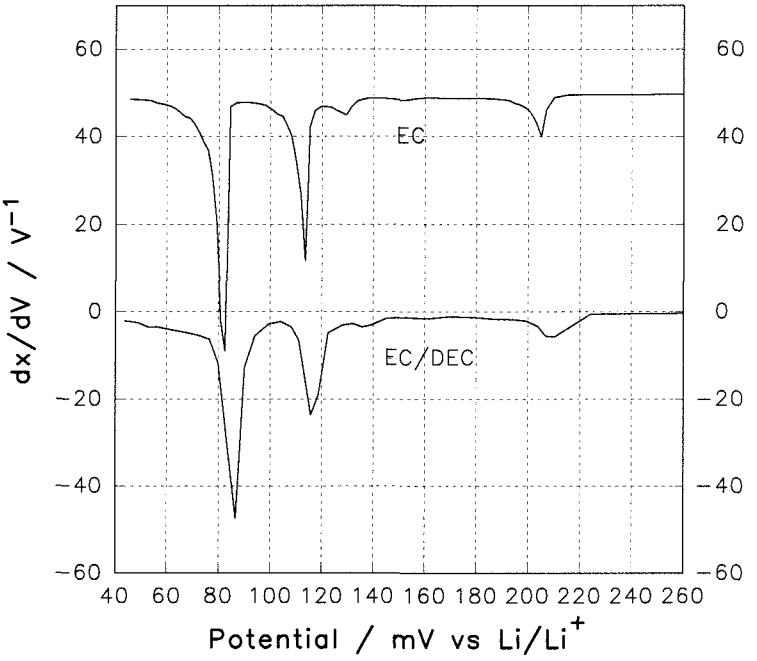

Figure 4.48 - dx/dV vs. V plots for lithium insertion into an SFG44 graphite powder electrode at 60°C in EC/ DEC and EC (offset by +50 V^{-1}) based electrolytes

It is clear from Fig. 4.48 that the dx/dV peaks are narrower and in the EC than EC/ DEC based electrolytes (FWHM ~5 mV in EC, ~8 mV in EC/ DEC). The peaks in both heated electrolytes are narrower than those observed at room temperature in powder electrodes (FWHM ~14 mV, EC/ DEC/ $LiCF_3SO_3$).

That cycling at a higher temperature produced a peak narrowing may have been anticipated, if it is supposed that the peak width results from incomplete relaxation of the surface lithium phases and that lithium diffusion (and phase re-arrangement) occurs more rapidly at elevated temperatures. However, the narrow 'sail-shaped' peaks in EC as opposed to broader 'bell-shaped' peaks in EC/ DEC (Fig. 4.48), are most probably attributable to the electrolyte or film rather than an intrinsic property of the graphite, as experimental parameters, other than the electrolyte, were kept constant.

Fig. 4.49 shows a dx/ dV vs. V plot for the first two cycles of a graphite powder electrode (MAA44) with EC/ $LiCF_3SO_3$ electrolyte at 60 ^{O}C at a rate of C/21.

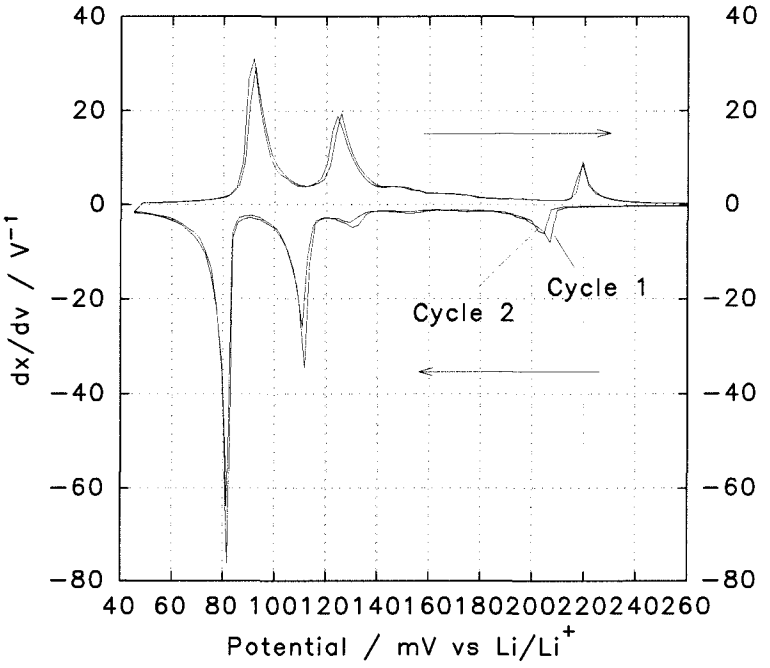

Figure 4.49 - First 2 cycles of a graphite powder electrode in EC/ $LiCF_3SO_3$ at 60^{O}C

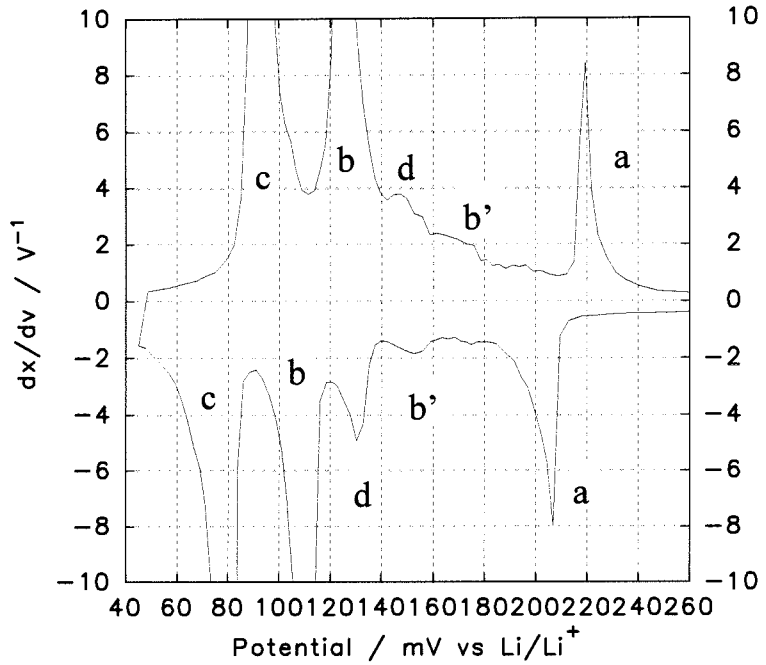

Figure 4.50 - The first cycle shown in Fig. 4.49 but with an expanded x-scale

From Fig. 4.50 it is apparent that five insertion and corresponding extraction peaks labelled a, b, b', c and d may be discerned in heated EC/ $LiCF_3SO_3$ electrolyte. Peaks a, b, b' and c are as for the monolithic graphite electrode at the lowest insertion rates (C/126). Peak d, at ~130 mV vs. Li/Li^+, has been reported for other graphite powder electrodes at room temperature, at low insertion rates (chap. 3.4).

It may be seen in Figs. 4.49 and 4.50 that the b, b', c and d extraction peaks were more symmetrical than the insertion peaks. This was found to be a reproducible effect, at least for the b peaks, over a range of cycle limits, Figs. 4.51 and 4.52. Following an initial conditioning cycle (OCV → 45 mV → 1 V vs. Li/Li^+), a KS44 electrode (as in chap. 4.6.1) was cycled between 145 mV and 100 - 125 mV vs. Li/Li^+. It may be noted that the positions of the peak maxima did not change, within experimental error, over the range of cycle-limits: the insertion peaks were located at 119 ± 2 mV and the extraction peaks 125 ± 2 mV vs. Li/Li^+.

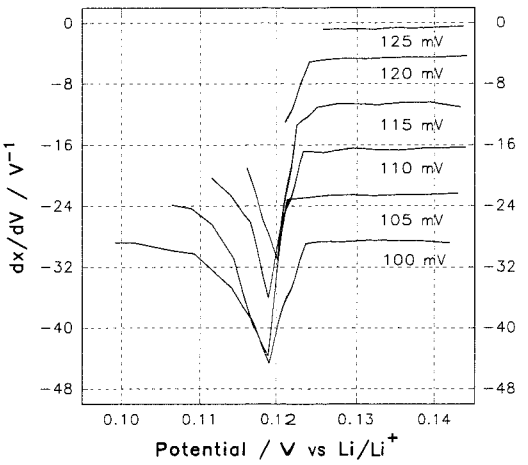

Figure 4.51 - Insertion into a KS44 electrode to the given potentials. Plots displaced along the y-axis by; 120 mV ,-4 V^{-1}; 115mV, -10 V^{-1}; 110 mV, -16 V^{-1}; 105 mV, -22 V^{-1}; 100 mV, -28 V^{-1}.

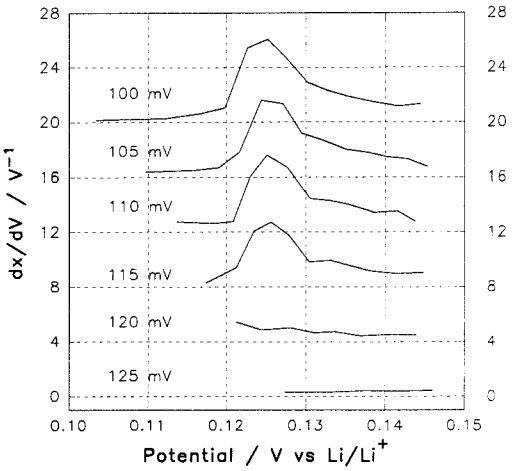

Figure 4.52 - Extraction from a KS44 electrode after insertion to the stated potentials, Fig. 4.51. Plots displaced along the y-axis by; 120 mV, +4 V^{-1}; 115mV, +8 V^{-1}; 110 mV, +12 V^{-1}; 105 mV, +16 V^{-1}; 100 mV, +20 V^{-1}.

In a system exhibiting a series of two-phase regions separated by vanishingly small single phase regions the ideal, equilibrium dx/dV vs. V plot (from chap. 1.2.1) would consist of a series of infinitely thin, infinitely high peaks (in practice both the height and width would be limited by the discriminator level or card resolution). However, in the real systems examined previously, at room temperature, a series of broad peaks were obtained. The peak broadening, and separation of the insertion and extraction peak maxima, were interpreted as being due to incomplete equilibration in the electrode. If the 'true two-phase' equilibrium potential of any given pair of adjacent phases is expected to lie between the insertion and extraction maxima, then it is clear that at a peak maximum the real electrodes were in a non-equilibrium state.

If the relaxation kinetics were increased or the relaxation time lengthened (i.e. a lower cycling rate was employed) it may be expected that the peak maxima would approach the 'true' equilibrium potential more closely. Additionally, the 'bell-shaped' peaks of the original system may remain 'bell-shaped' or become 'sail-shaped' depending on how the rate of potential relaxation $(\partial V/\partial t)_{x,\, t=t2}$, where t_2 is the final point of a given relaxation, varies with potential:

i) If $(\partial V/\partial t)_{x,\, t=t2}$ had a zeroth-order potential dependence for a given peak, the peak position may change, but the peak would retain its original width and shape.

ii) If $(\partial V/\partial t)_{x,\, t=t2}$ had a first-order potential dependence for a given peak, the peak width would change, but the peak shape would remain unchanged.

iii) If $(\partial V/\partial t)_{x,\, t=t2}$ had an n^{th}-order potential dependence, where $n \neq 0, 1$, the peak would be expected to change shape and possibly width and position.

It should be noted that $(\partial V/\partial t)_{x,\, t=t2}$ can only be used to assess the trend in peak evolution with decreasing insertion rate, because $(\partial V/\partial t)_{x,\, t=t2}$ would be expected to vary with cycling rate.

Fig. 4.53 shows the dx/dV vs. V and corresponding $-(\partial V/\partial t)_{x,\, t=t2}$ vs. V plots for an SFG44 electrode in EC/ $LiCF_3SO_3$ at 60 °C. The negative relaxation rate is plotted so that negative values were obtained for the insertion, enabling easier comparison with the corresponding dx/dV peaks.

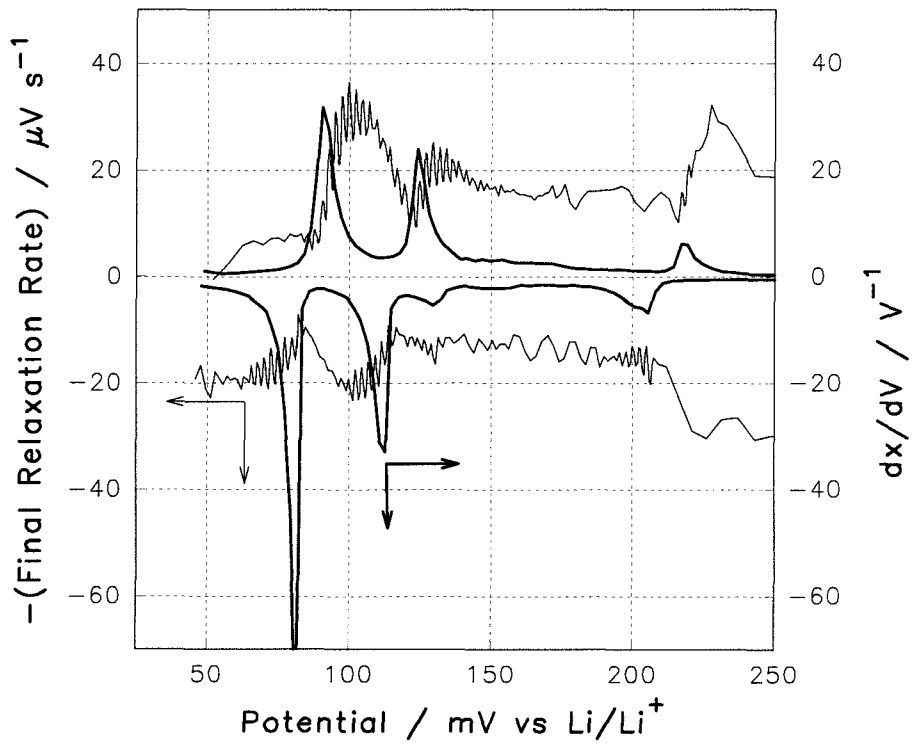

Figure 4.53 - $-(\partial V/\partial t)_{x,\, t=t2}$ vs. V and dx/dV vs. V plots for an SFG44 electrode at 60 °C in EC/ DEC electrolyte, C/21 rate

From the $(\partial V/\partial t)_{x,\, t=t2}$ in Fig. 4.53 it may be imagined that the insertion and extraction peaks would become narrower and that the peak separations would decrease

if a lower insertion rate were employed. It may also be noted that the minima in the $(\partial V/\partial t)_{x,\, t=t2}$ vs. V plots occur at the high-potential edge of the insertion peaks, but closer to the centre of the extraction peaks. Thus, it may be imagined that at lower rates the extraction peaks would also become asymmetrical. If this is so then the dx/dV vs. V peak shape, together with peak width and peak separation, may be used as a measure of the degree of relaxation kinetics of an electrode, at least in EC/ $LiCF_3SO_3$ at 60 °C.

On the assumption that the peak shape may be interpreted more generally, the insertion profiles in EC and EC/ DEC (Fig. 4.48) may be taken to indicate that the solvent had an influence on the relaxation kinetics of an electrode. This would imply that the maximum practical charge and discharge rates of a cell are, to an extent, dependent on the solvent. This complements an observation made previously (chap. 4.3.2) that the maximum cycling rates of a cell were not solely governed by the intrinsic diffusion rate of lithium in the graphite.

Chapter 5

Summary, Conclusions & Future Work

Initially it was shown that electrochemically, at room temperature, lithium did not readily form extensive alloys with either nickel or copper. Both metals were therefore considered suitable for negative electrode substrates and current collectors. However, the use of these metals as substrates for metallic lithium negative electrodes was not pursued due to poor cycling efficiencies and for safety considerations. In preference to metallic lithium, carbon-based insertion electrodes were examined.

Glassy carbon was used to model the behaviour of a carbon electrode without the complication of extensive insertion reactions. From impedance measurements it was concluded that a resistive film of electrolyte decomposition products appeared to be formed on the surface of the glassy carbon electrodes when polarised to +0.5 V vs. Li/Li^+. By fitting the impedance data to equivalent circuits it was possible to extract values of interfacial resistance and a modified capacitance term. The time-dependence of these parameters revealed that in PC and EC/ DEC solvents containing $LiAsF_6$ or $LiCF_3SO_3$, both the salt and solvent seemed to determine the rate of formation and constitution of the films. Further examination of these electrolytes revealed that in a softer (oriented pyrolytic carbon) electrode an iridescent film was formed from the EC/ DEC/ $LiCF_3SO_3$ electrolyte, but in the PC/ $LiCF_3SO_3$ gaseous decomposition products caused the electrode to fragment. A Fourier transform (FT) impedance technique was used to show that a graphite powder electrode also appeared to fragment in a PC/ $LiAsF_6$ electrolyte, but that a film grew on a coke powder electrode with no fragmentation. This demonstrates both the value of the FT impedance technique in being able to identify electrode processes *in situ*, with minimal disruption to the titration regime, and the detrimental effects of these PC-based electrolytes on soft, layered carbons.

It was also found by FT impedance that the addition of 12-crown-4 to an EC/ PC electrolyte appeared to facilitate intercalation and decrease electrode fragmentation. However, the toxicity of 12-crown-4 and $LiAsF_6$ made EC/ DEC/ $LiCF_3SO_3$ the preferred electrolyte.

Significant differences were observed in the pulsed coulometric titration profiles of graphite powder and graphite monolith electrodes. From these observations it was concluded that stack pressure was required to keep the particles in the graphite electrode from becoming electrically isolated by parasitic films formation during coulometric cycling. A model was also proposed to illustrate the electrical isolation of particles on contraction during lithium extraction. It was found that the addition of small conducting particles (copper or carbon blacks) helped to maintain contact between the graphite particles during extraction, although X-ray diffraction revealed that even with conductivity additives some lithiated particles remained isolated within a thick powder electrode, accounting for one source of 'charge loss'.

It was also found that the insertion and extraction capacities of a graphite powder electrode were critically dependent on the amount of binder. Based on dx/dV vs. V plots for electrodes with varying binder concentrations a model was proposed suggesting that the composition of surface phases present in the electrode at any given average state of charge was dependent on the distribution of conductivity pathways to individual graphite particles.

X-ray diffraction was used to investigate the evolution of phases in a graphite powder electrode during and after a series of large current pulses. Non-equilibrium distributions of phases were inferred to have been formed at the surface of the graphite particles during the pulses. During most of the current relaxations it was found that there was an inflection in the voltage curve which separated two distinct plateaux. The first plateau corresponded to a system in which lithium was diffusing from lithium-rich surface phases into the more dilute bulk phases. When the reservoir of lithium ions at the surface of the particles had been essentially exhausted the potential rose to the second plateau. The voltage relaxation times were found to increase by an order of magnitude as the average lithium concentration in the electrode increased.

In a heated EC/ $LiCF_3SO_3$ electrolyte, the extraction capacities of graphite powder electrodes were found to be markedly higher than in EC/ DEC/ $LiCF_3SO_3$ electrolyte at room temperature, at the same insertion rate. However, extraction from graphite powder electrodes in heated EC/ DEC/ $LiCF_3SO_3$ electrolyte was found to cause significant detachment of particles, often leading to internal short-circuits.

The use of dV/dt vs. V and $(\partial V/\partial t)_{x,\, t=t2}$ vs. V plots for lithium insertion into graphitic electrodes in heated EC/ $LiCF_3SO_3$ led to the prediction that as the electrode approached equilibrium more closely, due to faster kinetics or slower cycling rates, the dx/dV peaks would initially narrow and then become 'sail-shaped'. From this prediction it was suggested that the maximum practical charging rates for a given cell would, to some extent, be dependent on the electrolyte.

5.1 Future Work

Due to the large number of parameters which affect the cycling efficiency and extraction capacities of graphite powder electrodes it has clearly not been possible to optimise many of the experimental variables. However, it would clearly be of commercial interest to determine how the rate dependence of charge extraction depends on particle size, conductivity additive, temperature and electrode thickness. *in situ* X-ray diffraction and pulsed coulometric titration [1] may be expected to give valuable information in these regards.

Much work has recently focused on the development of novel 'high-capacity' carbon materials ($Q > 372$ mAh g^{-1}). The materials have been produced by pyrolysis of organic precursors under inert atmospheres or by ball-milling of 'low-capacity' carbons [2]. It would be of interest to use FT impedance and *in situ* X-ray diffraction, and pulsed coulometric titrations to examine the electrode processes and insertion kinetics of these materials in a range of solvents.

Appendix A

Power Supply Unit (PSU)

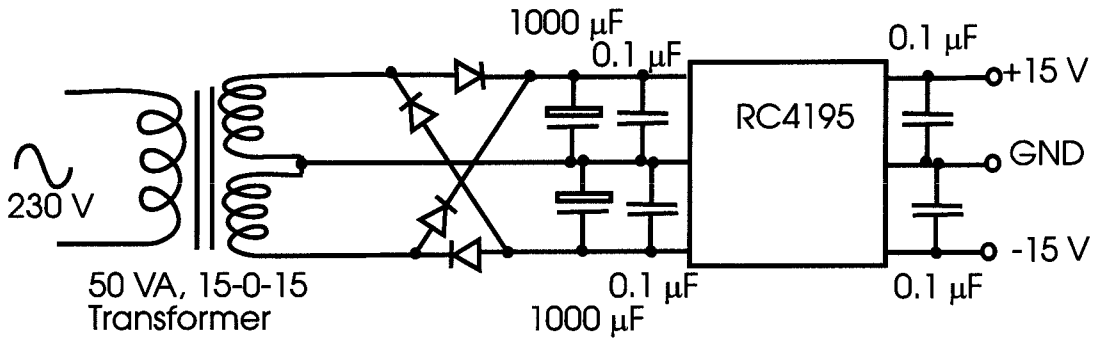

Galvanostat Circuit

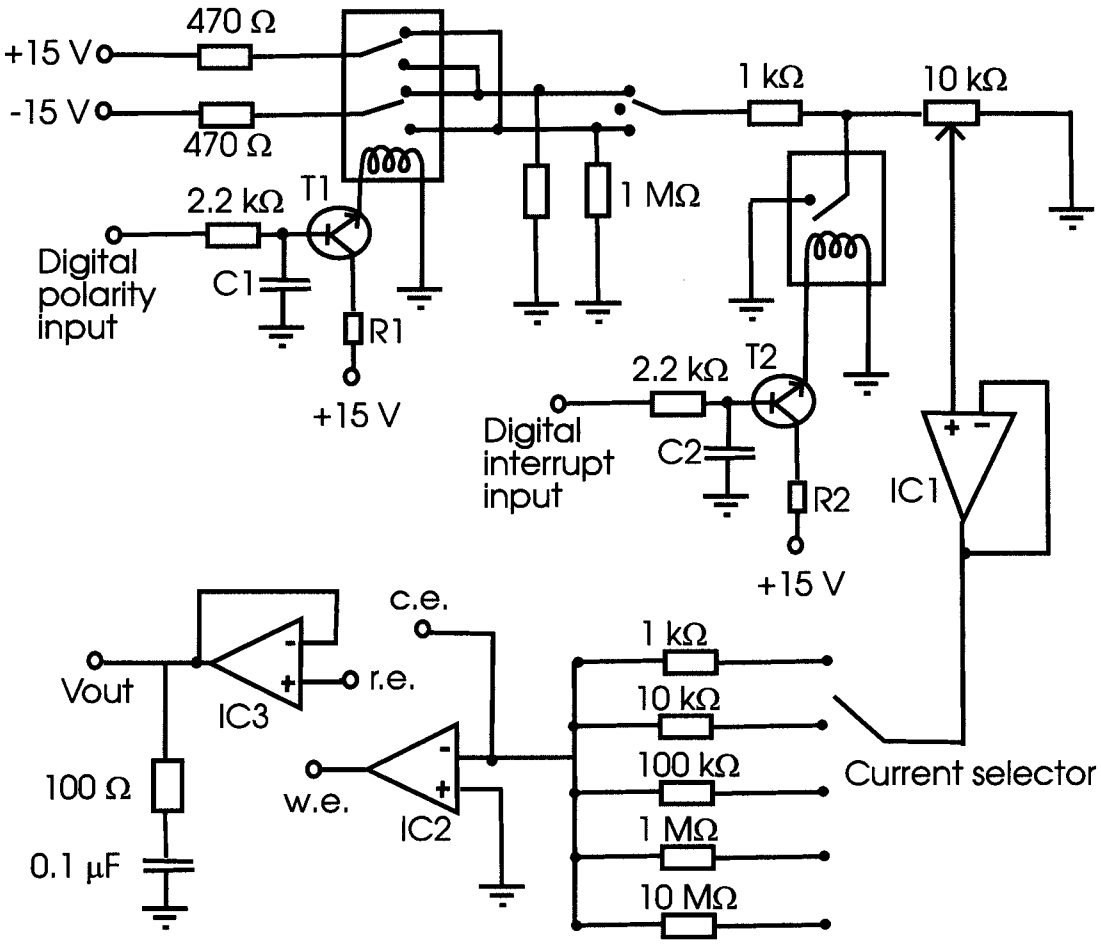

R1 = R2 = 270 Ω, C1 = C2 = 1 µF, T1 = T2 = BC109, IC1 = IC2 = IC3 = TL071CP

w.e. = working electrode, c.e. = counter electrode, r.e. = reference electrode

Appendix B

The following is software, written in QuickBasic, for controlling galvanostats via the PCL-812 I/O ADC card.

```
'
'          812 interface program
'            written 1994 by
'                 A.H.Whitehead
'
'            A/D Voltage logger * 2
'               4 channel input
'
'
' Important variables:  pnt = number of points
'          idir% = current direction per channel (1 = +ve)
'          sav$(r) = channel r file name
'          dout1 = digital output byte (polarity control)
'          ion% = current on period (# readings)
'          s = seconds between readings
'          itrue = current on/off (0 = off)
'          v(r) = channel r voltage / V
'          itime% = current switch time (# readings)
'          no% = 0 to 100 counter for readings
'          vneg(r) = channel r negative voltage limit / V
'          dy = vertical screen factor (vga monitors)
'
'
SCREEN 2: '              Big letters
CLS : LOCATE 1, 7: PRINT "Welcome to the Labcard 812 A/D data logger Version 4.0"
LOCATE 3, 9: PRINT "4 channel polarity switching and current enable/disable"
LOCATE 5, 10: PRINT "This should be run from QB not 'ordinary' Quickbasic"
LOCATE 7, 16: PRINT "Automatic averaging for long runs"
LOCATE 10, 21: PRINT "Qbasic version by A.H.W."
LOCATE 18, 2: PRINT "Press 't' to test the timer, analogue input and speaker"
LOCATE 16, 2: PRINT "press 'z' to adjust the screen size preferences"
'
WHILE a$ = "": a$ = INKEY$: WEND
IF a$ = "t" OR a$ = "T" THEN
FOR p = 4 TO .4 STEP -.6: FOR r = 100 TO 1 STEP -p: SOUND 250 + 200 * SIN(r) * COS(r * 1.2) + r * 5, .1: NEXT r, p
a$ = "": WHILE a$ = "": a$ = INKEY$: WEND: GOSUB a
END IF
vos = -.5: dy = 110
IF a$ <> "z" AND a$ <> "Z" THEN GOTO aa
PRINT : PRINT : PRINT "SCREEN PREFERENCES ..."
a1: INPUT " Min voltage (currently -.5) / V "; vos
IF vos < -5 OR vos > 5 THEN GOTO a1
a2: INPUT " Max voltage (currently 3.5) / V "; vup
IF vup = vos OR (vup < -5 OR vup > 5) THEN GOTO a2
dy = 440 / (vup - vos)
aa: '              Main Prog
'              variables
DIM l(100, 3), h(100, 3): '          voltage input array
DIM t(100): '                  timer array
l: s = 30: pnt = 5500        ' measurement times
dout1 = 0                ' digital outputs
idir% = 0                ' current directions
DIM v(4)                 ' cell voltages
DIM vneg(4), vpos(4)         ' voltage limits
DIM sav$(4)              ' save name
ion% = 10: ioff% = 10: itrue = -1
FOR r = 1 TO 4: sav$(r) = "chan" + RIGHT$(STR$(r), 1)
vneg(r) = .045: vpos(r) = 1                    'default settings
NEXT r
OUT (&H220 + 13), dout1: '          turn polarity switches off
```

```
OUT (&H220 + 4), 0: OUT (&H220 + 5), 0 '  current on
L0: CLS : '              Menu A
'
L0.5: LOCATE 2, 2: PRINT "Press the number to adjust the following:"
PRINT : PRINT "1> Time between readings "; s; " s   "
PRINT : PRINT "2> Total number of readings "; pnt; " = "; INT(pnt * s / 3600 + .5); " hours "
PRINT : PRINT "3> Help page"
PRINT : PRINT "4> Next menu"
PRINT : PRINT "5> Quit"
PRINT : PRINT : PRINT "Nb. Press 'q' to prematurely terminate run."
a$ = "": WHILE a$ = "": a$ = INKEY$: WEND
a = VAL(a$)
IF a < 1 OR a > 5 THEN GOTO L0                  'options
IF a = 3 THEN GOSUB z1: GOTO L0.5               'help
IF a = 5 THEN END                               'quit
IF a = 4 THEN GOTO L1                           'keep going
PRINT : INPUT "new value "; b
IF a = 1 AND (b < 4 OR b > 80000!) THEN GOSUB z2: GOTO L0    'range checks
IF a = 1 THEN s = b: GOTO L0
IF a = 2 AND (b < 2 OR b > 5000000!) THEN GOSUB z2: GOTO L0
IF a = 2 THEN pnt = INT(b)
GOTO L0
L1: CLS
LOCATE 2, 2: PRINT "Press the number to adjust the following:"
PRINT : PRINT "Nb. 1 reading = "; s / pnt; " seconds."
PRINT : PRINT "1> Current on duration "; ion%; " readings "
PRINT : PRINT "2> Open circuit duration "; ioff%; " readings "
PRINT : PRINT "3> Help page"
PRINT : PRINT "4> Next page"
PRINT : PRINT "5> Quit"
a$ = "": WHILE a$ = "": a$ = INKEY$: WEND
a = VAL(a$)
IF a < 1 OR a > 5 THEN GOTO L1
IF a = 3 THEN GOSUB z1: GOTO L1                 'help
IF a = 5 THEN END
IF a = 4 THEN GOTO L1.1
PRINT : INPUT "new value "; b
IF a = 1 THEN ion% = b: GOTO L1
IF a = 2 THEN ioff% = b: GOTO L1
L1.1: '          Voltage limits
isend% = 0: idir% = 0
FOR r = 1 TO 4
L1.2: CLS : PRINT : PRINT "Enter the following for cell "; r
PRINT : PRINT "1> Current initially ";
IF (idir% AND 2 ^ (r - 1)) > 0 THEN PRINT "positive  " ELSE PRINT "negative  "
PRINT : PRINT "2> Min. voltage "; vneg(r) * 1000; " mV     "
PRINT : PRINT "3> Max. voltage "; vpos(r) * 1000; " mV     "
PRINT : PRINT "4> exit program "
PRINT : PRINT "5> next cell setup "
PRINT : PRINT "6> Save file name: "; sav$(r)
PRINT : PRINT "reading length "; s; " seconds   "
L1.3: a$ = "": WHILE a$ = "": a$ = INKEY$: WEND
a = VAL(a$)
IF a > 6 THEN GOTO L1.3                 'options
IF a = 6 THEN PRINT : INPUT "new name"; sav$(r): GOTO L1.2
IF a = 4 THEN END                       'quit
IF a = 5 THEN GOTO L1.4                 'keep going
IF a = 1 THEN idir% = (idir% XOR 2 ^ (r - 1)): GOTO L1.3  'change current direction
PRINT : INPUT "new value "; b
IF a = 2 AND (b < -5000 OR b > 5000) THEN GOSUB z3: GOTO L1.2    'range checks
IF a = 2 THEN vneg(r) = b / 1000: GOTO L1.2
IF a = 3 AND (b < -5000 OR b > 5000) THEN GOSUB z3: GOTO L1.2    'range checks
IF a = 3 THEN vpos(r) = b / 1000: GOTO L1.2
GOTO L1.2
L1.4: itime(r) = ion%(r)
sav$(r) = "c:\" + sav$(r)
a% = 0
ON ERROR GOTO p2            'check file exists
```

```
OPEN sav$(r) FOR INPUT AS #1
ON ERROR GOTO 0
CLOSE
IF a% THEN GOTO L1.5
PRINT "This file already exists, do you wish to write over it (y/n)"
a$ = "": WHILE a$ = "": a$ = INKEY$: WEND
IF a$ = "n" THEN GOTO L1.2
KILL sav$(r)                'remove old file
L1.5: NEXT r
SCREEN 1: CLS
dx = 640 / pnt          '       graphics steps
'
L2: PRINT "press a key - do that thing"
WHILE INKEY$ = "": WEND
CLS : SCREEN 12
GOSUB v                             'timer reset
days = 0: q = TIMER
'
'                       READINGS
'
FOR n = 0 TO pnt
nh = INT(n / 100) * 100!            'split measurement counter into
no% = n - nh                        'high and low
IF itime% = INT(n + .01) THEN GOSUB M3          'current switch
'
FOR nn% = 1 TO 4
IF nn% = 1 THEN r = 3
IF nn% = 2 THEN r = 5                       ' A/D input channels
IF nn% = 3 THEN r = 6
IF nn% = 4 THEN r = 7
OUT (&H220 + 10), r                         'selects channel A/D
p = 0: a = 0: h = 0: l = 0
WHILE p < s * (n + .25 * nn%)
OUT (&H22C), 0                              'resets I/O
l = l + INP(&H224)
h = h + INP(&H225)
a = a + 1
p = TIMER - q + days                        'clock
WEND
h(no%, nn% - 1) = h / a
l(no%, nn% - 1) = l / a
NEXT nn%
IF TIMER + stp > 80000 THEN
days = days + TIMER             'another day, another night, another one night stand
GOSUB v                             'reset timer
END IF
t(no%) = p
FOR r = 1 TO 4
v(r) = (2048 - h(no%, r - 1) * 256 - l(no%, r - 1)) / 409.6
NEXT r
LOCATE 1, 2                         'Screen Header
PRINT "Cell 1 = "; v(1); " V,  "; INT(p + .5); " seconds ,   buffer capacity  "; (100 - no%); " %        "
PRINT " Cell 2 = "; v(2); " V,  Cell 3 = "; v(3); " V, Cell 4 = "; v(4); "V          "
IF itrue THEN PRINT "I on     " ELSE PRINT "I off     "

FOR r = 1 TO 4
PSET (no% * dx, 445 - (v(r) - vos) * dy), 9 + r         'Put dots on screen
NEXT r
IF no% = 99 THEN GOSUB fsr              'file save routine
a$ = INKEY$
IF a$ = "q" THEN n = pnt: pnt = no%     'quit
IF a$ = "Q" THEN n = pnt: pnt = no%
NEXT n
GOSUB fsr
d1: '               Display
'                       Menu B
'                    For six persons
'
```

```
IF pnt > 8000 THEN PRINT : PRINT "Too many points to manipulate in qbasic - data truncated": pnt = 8000
DIM temp(pnt, 1)                    'buffer for plots etc.
'
d1.1: SCREEN 2: CLS : PRINT : PRINT "Enter :"
PRINT : PRINT "1> View point data."
PRINT : PRINT "2> View line drawn data."
PRINT : PRINT "3> Exit."
PRINT : PRINT "4> Restart program"
PRINT : PRINT "5> View voltage data."
a$ = "": WHILE a$ = "": a$ = INKEY$: WEND
a = VAL(a$): IF a < 1 OR a > 6 THEN GOTO d1.1
IF a = 3 THEN END
IF a = 4 THEN CLEAR : RUN
INPUT "which cell number "; nn%
OPEN sav$(nn%) FOR INPUT AS #I
FOR r = 0 TO pnt
INPUT #1, temp(r, 0), temp(r, 1)
NEXT r
CLOSE #1
IF a = 1 THEN GOSUB D2: SCREEN 2: GOTO d1.1
IF a = 2 THEN GOSUB D3: SCREEN 2: GOTO d1.1
IF a = 5 THEN GOSUB M1: GOTO d1.1          'v out
D2: SCREEN 12: CLS : '              size 640x460
tmin = temp(0, 1)
tmax = temp(pnt, 1)
tdiv = (tmax - tmin) / 640
FOR r% = 0 TO pnt
t = (temp(r%, 1)) - tmin
v1 = temp(r%, 0)
PSET (INT(t / tdiv), 445 - (v1 - vos) * dy), 10   'draw dots
NEXT r%
WHILE INKEY$ = "": WEND: RETURN
D3: SCREEN 12: CLS : '              size 640x460
tmin = temp(0, I)
tmax = temp(pnt, 1)
tdiv = (tmax - tmin) / 640
FOR r% = 0 TO pnt - 1
t = (temp(r%, 1)) - tmin
v = temp(r%, 0)
t2 = (temp(r% + 1, 1)) - tmin
v1 = temp(r% + 1, 0)                    'draw lines
LINE (INT(t / tdiv), INT(445 - (v - vos) * dy))-(INT(t2 / tdiv), INT(445 - (v1 - vos) * dy)), 10 + nn%
NEXT r%
WHILE INKEY$ = "": WEND: RETURN
M1: '                       V output
CLS : PRINT
PRINT : INPUT "View every ith data point, i = "; stp
PRINT : PRINT "Audio output (y/n)";
a$ = "": WHILE a$ = "": a$ = INKEY$: WEND: PRINT
IF a$ = "y" THEN aud = 1 ELSE aud = 0
PRINT : PRINT "View all data on screen (y/n)";
a$ = "": WHILE a$ = "": a$ = INKEY$: WEND
IF a$ = "y" THEN GOTO M1.5
IF a$ <> "n" THEN RETURN
CLS : LOCATE 5, 5: PRINT "Point": LOCATE 5, 20: PRINT "V"
LOCATE 5, 40: PRINT "mV"
FOR r = 0 TO pnt STEP stp
LOCATE 7, I
PRINT TAB(5); r; "   "; TAB(20); temp(r, 0); "     ";
PRINT TAB(40); temp(r, 0) * 1000; "          "
IF aud = 1 THEN SOUND (temp(r, 0) + 6) * 40, .4
FOR q = 1 TO 5000: NEXT q
NEXT r
WHILE INKEY$ = "": WEND: RETURN
M1.5: CLS : LOCATE 1, 5: PRINT "Point": LOCATE I, 20: PRINT "V"
LOCATE 1, 40: PRINT "mV"
VIEW PRINT 2 TO 24
FOR r = 0 TO pnt STEP stp
```

```
PRINT TAB(5); r; "  "; TAB(20); temp(r, 0); "    ";
PRINT TAB(40); temp(r, 0) * 1000; "          "
IF aud = 1 THEN SOUND (temp(r, 0) + 6) * 40, .4
FOR q = 1 TO 5000
NEXT q
NEXT r
VIEW PRINT 1 TO 25
WHILE INKEY$ = "": WEND: RETURN
'
M3: ' Switch current on/off & check if extremes reached
'              Current TTL switch
IF itrue THEN
itime% = itime% + ioff%                ' turn current off
OUT &H224, &HFF: OUT &H225, &HF        ' output 5 V
END IF
IF itrue THEN itrue = 0: RETURN
itrue = -1
itime% = itime% + ion%                 ' turn current on
OUT &H224, 0: OUT &H225, 0             ' output 0 V
'
'                    Reverse current polarity

FOR nn% = 1 TO 4
bit = 2 ^ (nn% - 1)
IF (v(nn%) < vneg(nn%)) AND ((bit AND idir%) = 0) THEN idir% = bit + idir%: isend% = (isend% XOR bit)
IF (v(nn%) > vpos(nn%)) AND ((bit AND idir%) > 0) THEN idir% = idir% - bit: isend% = (isend% XOR bit)
NEXT nn%
OUT (&H220 + 13), isend%
RETURN
'
a: '                slow internal COUNTER
'              test for timer and A/D input
'
LOCATE 11, 1: PRINT "time :": PRINT : PRINT "Input :"
a = 3
WHILE INKEY$ = ""
OUT &H220 + 10, a   'selects channel A/D
OUT &H220 + 12, 0   'resets I/O
LOCATE 10 + a, 20: PRINT 5 * (1 - (INP(&H225) * 256 + INP(&H224)) / &H7FC); "      "
l = INP(&H221): h = INP(&H221): LL = INP(&H222): HH = INP(&H222)
t = TIMER
LOCATE 11, 20: PRINT TIME$; t - INT(t); "          "
IF a = 3 THEN a = 5 ELSE a = 3
WEND: RETURN
fsr:          '******** file save routine ************
t = 0                          'initial time
FOR nn% = 0 TO 3
ON ERROR GOTO p2
OPEN sav$(nn% + 1) FOR APPEND AS #1
ON ERROR GOTO 0
FOR r% = 0 TO no%
v = (h(r%, nn%) * 256! + l(r%, nn%))
a$ = STR$((2048 - v) / 409.6)          'voltage
b$ = STR$(t(r%) - t)                   'time
PRINT #1, a$ + "," + b$
NEXT r%
CLOSE #1
NEXT nn%
RETURN
p2:          '************Saving to disc error trapping*****************
SELECT CASE ERR
CASE 53: a% = -1
CASE 61: LOCATE 10, 35: PRINT "Disc full": a% = 1
CASE 64: LOCATE 10, 33: PRINT "Bad file name": a% = 1
CASE 71: LOCATE 10, 33: PRINT "Disc not ready": a% = 2
CASE 76: LOCATE 10, 30: PRINT "Path not found": a% = 1
CASE 55: LOCATE 10, 30: PRINT "File already open": a% = 1
CASE ELSE: ON ERROR GOTO 0
```

```
END SELECT
IF a% = -1 THEN RESUME NEXT
LOCATE 20, 28: PRINT "Press SPACE to continue"
DO: a$ = INKEY$: LOOP UNTIL a$ = " "
IF a% = 1 THEN RESUME NEXT ELSE RESUME
v: '          ********** Reset Counter *************
TIME$ = "00.00.00"
RETURN
z1: '              Help page
SCREEN 10: CLS : PRINT TAB(30); "Help Page"
PRINT : PRINT " This program was written to operate the PCL-812 LabCard as a voltage"
PRINT "logger. ie. it records voltage measurements with time. Assuming it is still"
PRINT "running on the Elonex 386, voltage is measured between the red and black wires"
PRINT "from the terminal board. Time is measured with an internal slow clock and"
PRINT "card-based fast counter."
PRINT : PRINT "Data is recorded at the fastest sampling rate (c. 0.3ms) and then"
PRINT "averaged to give the correct number of data points over the given time (8"
PRINT "to 2,000,000 seconds - 23 days). Channel 3 should be connected to cell 1 ,"
PRINT "channel 5 to cell 2, channel 6 to cell 3 and channel 7 to cell 4."
PRINT : PRINT "If the computer gets stuck in an endless loop, press Ctrl-Break to exit."
PRINT : PRINT " To perform analysis of the data, once aquired and saved, exit from this program"
PRINT "and run 'FTIMP1.BAS', 'DX_DV3.BAS' - if the data's in two columns"
PRINT : PRINT "Output from out1 at TTL levels (ie. 0 V for current on, 5 V for off.)"
PRINT "The Labcard won't give much current so feed into transistors prior"
PRINT "to relays."
WHILE INKEY$ = "": WEND
PRINT : PRINT "The V - t data may be saved after the run has finished. It will be saved as"
PRINT "two or four columns of data: V1, V2, V3 (counts) and t (seconds) which may be"
PRINT "imported into Sigma Plot. If too many data points have been recorded the"
PRINT "data may be averaged a number of times using this program . (400 points is"
PRINT "normally sufficient for a graph !)"
PRINT : PRINT "The run will finish after the time limit is reached, or may be stopped by"
PRINT "typing 'q' on the keyboard."
PRINT : PRINT "A file with data in the form channel 1, channel 2, channel 3, time will be"
PRINT "Saved automatically every 22 hours so that, if the computer crashes - or is"
PRINT "deprived of power, there is a fair chance that some data may be salvaged."
PRINT "The file will be entitled 'c:\temp.dat'."
PRINT : PRINT "If limits are set on the title screen a beep will be emitted during"
PRINT "normal readings when they are exceeded. The voltage is also displayed on"
PRINT "screen."
PRINT : PRINT TAB(30); "Press a key"
WHILE INKEY$ = "": WEND
SCREEN 2: RETURN
z2: '              error message
PRINT "Value out of range: ";
IF a = 1 THEN PRINT "4 to 80000 s."
IF a = 2 THEN PRINT "2 to 5,000,000 points."
WHILE INKEY$ = "": WEND: RETURN
z3: PRINT "Value out of range: 5000 to -5000 mV"
RETURN
```

Appendix C

The following is software, written in QuickBasic, is for the calaculation of dx/dV from coulometric titration data.

```
'
'     ****************** dx/dV calculation program ******************
'
SCREEN 0: CLS
a$ = CHR$(196)
FOR r = 1 TO 68: b$ = b$ + a$: NEXT
c$ = " " + CHR$(218) + b$ + CHR$(191)
d$ = " " + CHR$(192) + b$ + CHR$(217)
PRINT : PRINT c$
PRINT " "; CHR$(179); "                                                    "; CHR$(179)
PRINT " "; CHR$(179); "   This program will calculate dx/dV to allow plotting of graphs "; CHR$(179)
PRINT " "; CHR$(179); "                                                    "; CHR$(179)
PRINT " "; CHR$(179); "      New feature  *** Data saved in 3D plot format ****       "; CHR$(179)
PRINT " "; CHR$(179); "                                                    "; CHR$(179)
PRINT d$
r = 1000: WHILE r > 100: SOUND r, .05: r = r - 1000 / r: WEND
here: PRINT : INPUT "file source "; a$
IF RIGHT$(a$, 1) = "\" THEN a$ = a$ + "*.*": FILES a$: GOTO here
OPEN a$ FOR INPUT AS #1
PRINT : PRINT ".. reading disk"
DIM v(16000), t(16000)              'variables
DIM ov(16000), ot(16000)
DIM vv(4000), tt(4000)
DIM dx(4000), vo(4000), x(4000)
vmn = 5000: vmx = 0
WHILE EOF(1) = 0 AND no% < 15990
no% = no% + 1                       'number of points
INPUT #1, a$, b$
v(no%) = VAL(a$)
ov(no%) = v(no%)
IF v(no%) < vmn THEN vmn = v(no%)
IF v(no%) > vmx THEN vmx = v(no%)
t(no%) = VAL(b$)
ot(no%) = t(no%)
WEND
CLOSE
noo% = no%
vrg = vmx - vmn
xl% = 1
xh% = (no% / 10) + 1
xdiv = (t(xh%) - t(xl%)) / 638
q: PRINT : PRINT no%; " data points."
PRINT : PRINT "Do you wish to use every point when determining the dx/dV data?"
flag = 0
a$ = "": WHILE a$ = "": a$ = INKEY$: WEND
IF a$ = "y" THEN flag = -1
IF flag THEN GOTO p
CLS : PRINT : PRINT "Smartfinder: Place cursor over the first data point required and press"
PRINT "the space bar to select. Then select the next two points in chronolgical order,"
PRINT "from left to right. The program will auto-select points at equal spacings, to"
PRINT "the end of the data."
PRINT : PRINT "Nb. Maximum of 1000 points - or until your fingers drop off."
a$ = "": WHILE a$ = "": a$ = INKEY$: WEND
cnt% = 0
GOSUB D1
WHILE cnt% < 3                      'collect data
GOSUB D2
GOSUB D3
```

```
cnt% = cnt% + 1
IF tl% = no% THEN tl% = tl% - 1
IF cnt% = 2 THEN t1% = tl%
vv(cnt%) = v(tl%)
tt(cnt%) = t(tl%)
WEND
dt% = tl% - t1%
WHILE tl% < no%
tl% = tl% + dt%
cnt% = cnt% + 1
tt(cnt%) = t(tl%)
vv(cnt%) = v(tl%)
PSET (INT(t(tl%) / tdiv), INT((v(tl%) - vmn) * 225 / vrg + 5)), 11
WEND
no% = cnt% - 1
FOR r% = 1 TO no%
t(r%) = tt(r%)
v(r%) = vv(r%)
NEXT r%
WHILE INKEY$ = "": WEND
p: CLS
INPUT "How many volts is f.s.d. (4096 counts) equivalent to "; vscl
vscl = vscl / 4096
INPUT "How many counts is zero volts "; voff
PRINT : INPUT "At what time would x=1 "; tscl
PRINT : INPUT "Discriminator level (i.e. minimum |dv| ) "; mindv
PRINT : PRINT "Calculating ..."
dx2 = 0: dv2 = 0: p% = I
x2 = t(1)
FOR r% = I TO no% - 1
dx = dx2 + (t(r% + 1) - t(r%)) / tscl
dv = dv2 + (v(r% + I) - v(r%)) * vscl
x(p%) = x2 / tscl + dx / 2                    'x output
vo(p%) = ((v(r%) + v(r% + 1)) / 2 - voff) * vscl    'v output
IF ABS(dv) < mindv THEN dv2 = dv: dx2 = dx: GOTO s   'check min dv
dx(p%) = dx / dv                              'dx/dv output
p% = p% + I
dx2 = 0: dv2 = 0
x2 = t(r% + I)
s: NEXT r%
num% = p% - 1
no% = no% - 1
v: CLS : PRINT TAB(10); "dx/dv          v            x"
FOR r = 1 TO num%
PRINT TAB(10); dx(r); TAB(25); vo(r); TAB(40); x(r)
NEXT r
PRINT "Press a key"
a$ = "": WHILE a$ = "": a$ = INKEY$: WEND
w: CLS
PRINT : PRINT "Pick an option:"
PRINT : PRINT "1> View data."
PRINT : PRINT "2> Output to disk."
PRINT : PRINT "3> Quit."
PRINT : PRINT "4> Re-start."
PRINT : PRINT "5> Re-analyse."
PRINT : PRINT "6> Plot"
DO: a$ = ""
WHILE a$ = "": a$ = INKEY$: WEND
LOOP UNTIL VAL(a$) > 0 AND VAL(a$) < 7
a = VAL(a$): IF a = 1 THEN GOTO v
IF a = 5 THEN GOTO p
IF a = 4 THEN RUN
IF a = 3 THEN END
IF a = 6 THEN GOTO D5
IF a = 2 THEN GOTO D4
D1: SCREEN 12: CLS : '              size 639x460
'                          Top screen
tdiv = t(no%) / 638
```

```
FOR r% = 1 TO no%
PSET (INT(t(r%) / tdiv), INT((v(r%) - vmn) * 225 / vrg + 5)), 14
NEXT r%
LINE (0, 230)-(640, 230), 2, , 22982
RETURN
D1.5: FOR r% = 1 TO no% - 1
LINE (INT(t(r%) / tdiv), INT((v(r%) - vmn) * 225 / vrg + 5))-(INT(t(r% + 1) / tdiv), INT((v(r% + 1) - vmn) * 225 / vrg + 5)), 6
NEXT r%
RETURN
D2: xdv = (t(xh%) - t(xl%)) / 638        'bottom bits
LINE (0, 232)-(640, 460), 0, BF
FOR r% = xl% TO xh%
IF t(r%) < tt(cnt%) THEN spot = 11 ELSE spot = 14
PSET (INT((t(r%) - t(xl%)) / xdv), INT((v(r%) - vmn) * 225! / vrg + 235)), spot
NEXT r%
RETURN
D3: LINE (INT((t(tl%) - t(xl%)) / xdv), 460)-(INT((t(tl%) - t(xl%)) / xdv), 240), 4
LINE (INT(t(tl%) / tdiv), 0)-(INT(t(tl%) / tdiv), 4), 12
DO
a$ = "": WHILE a$ = "": a$ = INKEY$: WEND
LOOP UNTIL ASC(a$) = 32 OR LEN(a$) = 2
IF ASC(a$) = 32 THEN RETURN
a = ASC(RIGHT$(a$, 1))
IF a = 115 OR a = 116 THEN GOTO D3.1
IF a <> 75 AND a <> 77 THEN GOTO D3
D3.1: LINE (INT(t(tl%) / tdiv), 0)-(INT(t(tl%) / tdiv), 4), 0
LINE (INT((t(tl%) - t(xl%)) / xdv), 460)-(INT((t(tl%) - t(xl%)) / xdv), 240), 0
PSET (INT((t(tl%) - t(xl%)) / xdv), INT((v(tl%) - vmn) * 225! / vrg + 235)), 14
tl% = tl% + (a = 75) + 42 * (a = 115): IF tl% < 1 THEN tl% = 1
tl% = tl% - (a = 77) - 42 * (a = 116): IF tl% > (no% - 1) THEN tl% = no% - 1
IF tl% < (xl% + 1) AND xl% > 1 THEN xh% = xh% + tl% - xl% - 1: xl% = tl% - 1: GOSUB D2
IF tl% > (xh% - 1) AND xh% < no% THEN xl% = xl% + tl% - xh% + 1: xh% = tl% + 1: GOSUB D2
GOTO D3
D4: CLS : PRINT
PRINT "1> output dx/dv data"
PRINT "2> output all points selected"
PRINT "3> output 3D data points as x, t, V (no header line)"
back: a$ = "": WHILE a$ = "": a$ = INKEY$: WEND
a = VAL(a$): IF a < 1 OR a > 3 THEN GOTO back
nope: INPUT "Enter save name "; a$
GOTO zz
check: OPEN a$ FOR OUTPUT AS #1
IF a = 3 THEN GOTO D4.5
IF a = 1 THEN PRINT #1, "dx/dv , v , x" ELSE PRINT #1, "x , v"
IF a = 1 THEN N% = num% ELSE N% = no%
FOR r% = 1 TO N%
IF a = 1 THEN
PRINT #1, dx(r%); " , "; vo(r%); " , "; x(r%)
ELSE PRINT #1, (t(r%) / tscl); " , "; (voff - v(r%)) * vscl
END IF
NEXT r%
CLOSE
PRINT : PRINT "done"
WHILE INKEY$ = "": WEND
GOTO w
D4.5: '        x, t, V format for x, y, z plot
FOR r% = t1% TO noo% STEP dt%        'data from 2nd point to final point
a = (ot(r%) - t(I)) / tscl
FOR rr% = 0 TO dt% - 1
b = ot(rr% + t1%) - ot(t1%)
c = (ov(rr% + r%) - voff) * vscl
PRINT #1, a, b, c
NEXT rr%, r%
CLOSE
PRINT : PRINT "done"
WHILE INKEY$ = "": WEND
GOTO w
```

```
D5: SCREEN 12: CLS
dmin = 1000000!: dmax = -1000000!
vmin = 1000000!: vmax = -1000000!
FOR r% = 1 TO num%
IF dx(r%) < dmin THEN dmin = dx(r%)
IF dx(r%) > dmax THEN dmax = dx(r%)
IF vo(r%) < vmin THEN vmin = vo(r%)
IF vo(r%) > vmax THEN vmax = vo(r%)
NEXT r%
D5.1: CLS : xscl = 600 / (vmax - vmin)
yscl = 390 / (dmax - dmin)
FOR r% = 1 TO num% - 1
LINE ((vo(r%) - vmin) * xscl + 10, (-dx(r%) + dmax) * yscl + 10)-((vo(r% + 1) - vmin) * xscl + 10, (-dx(r% + 1) + dmax) * yscl +
10), 9
NEXT r%
LOCATE 27, 1: PRINT "voltage range "; vmin; " to "; vmax
PRINT "change range ?";
a$ = "": WHILE a$ = "": a$ = INKEY$: WEND
IF a$ <> "y" THEN GOTO w
LOCATE 27, 1: PRINT "                                                    "
PRINT "                                                    "
LOCATE 27, I: INPUT "vmin "; vmin
INPUT "vmax "; vmax
GOTO D5.1

z: END
zz: ON ERROR GOTO zzz
FILES a$
ON ERROR GOTO 0
INPUT "do you wish to right over this file ?"; b$
IF b$ = "Y" OR b$ = "y" THEN GOTO check
GOTO nope
zzz: IF ERR = 53 THEN RESUME check   ' file not present already on disk
```

Appendix D

The following is software, written in QuickBasic, is for the calculation of FT impedance data and Laplace transformed data from current or potential transients.

```
'
'          812 interface program
'            written 1994 by
'                A.H.Whitehead
'
'        - updated 4/10/95 for fast transforms -
'
'            Data Analysis
'
DIM t(16383), v(16383)
SCREEN 12: '              Little letters
CLS : LOCATE 2, 23: PRINT "Integral Data Analysis"
PRINT : PRINT " This program provides numerical analysis of data aquired using the 'ADCNOx.BAS'"
PRINT "series of programs."
a1: PRINT : PRINT " Enter filename of data file (or x:\ to dir drive x)"
INPUT a$
IF LEN(a$) > 2 AND RIGHT$(a$, 1) = "\" THEN GOSUB a2: GOTO a1
IF LEN(a$) = 1 THEN RUN
IF LEN(a$) < 4 THEN a$ = a$ + ".dat"              'add suffix
IF RIGHT$(a$, 4) <> ".dat" THEN a$ = a$ + ".dat"
GOSUB b: GOTO l           'load data
a2: a$ = a$ + "*.dat"
FILES a$: RETURN          'check drive
b: PRINT : PRINT "Data transfer ..."
OPEN a$ FOR INPUT AS #2   'input data
no% = 0: DO: no% = no% + 1
INPUT #2, a$
v(no%) = VAL(a$)
INPUT #2, a$
t(no%) = VAL(a$)
LOOP UNTIL EOF(2) = -1
CLOSE
RETURN
l: vmx = 0: vmn = 4096        'voltage limits
FOR r% = 1 TO no%
IF v(r%) > vmx THEN vmx = v(r%)
IF v(r%) < vmn THEN vmn = v(r%)
NEXT r%
vrg = (vmx - vmn) * 1.1
L1: '                     Menu A
'                   cheese on toast
CLS : PRINT : PRINT TAB(30); "Pick an option:"
PRINT : PRINT "1> Integrate peak area."
PRINT : PRINT "2> Laplace transform curve."
PRINT : PRINT "3> Fourier transform curve."
PRINT : PRINT "4> View curve."
PRINT : PRINT "5> Average data."
PRINT : PRINT "6> Point removal."
PRINT : PRINT "7> Exit."
PRINT : PRINT "8> temporal point removal."
PRINT : PRINT "9> Load new curve."
PRINT : PRINT "0> New Fourier transform."
a$ = "": WHILE a$ = "": a$ = INKEY$: WEND
a = VAL(a$)
IF a = 0 THEN GOTO L11
IF a = 9 THEN RUN
ON a GOTO L3, L4, L6, L2, L8, L9, z, L10
L2: GOSUB D1
```

```
WHILE INKEY$ = "": WEND: GOSUB D1.5
WHILE INKEY$ = "": WEND: GOTO L1
L3: CLS
PRINT : PRINT "Position time bars (low and high) and voltage baseline for the integration"
PRINT "by using the arrow keys to move the red bar cursors and space bar to accept"
PRINT "its position. The top display shows the whole trace, the lower display gives"
PRINT "an enlarged portion - to aid precision in positioning the cursor."
PRINT "Pg Up and Pg Dn can also be used for more rapid cursor movement. As can Ctrl"
PRINT "left or right."
WHILE INKEY$ = "": WEND
'
'               Obtain Limits
'
GOSUB D1
xl% = 1: xh% = INT(no% / 10 + .51): GOSUB D2    '10x expansion
tl% = 1: GOSUB D3
xh% = no%: xl% = INT(no% * .9 + .51): GOSUB D2    '10x expansion
th% = no%: GOSUB D4
vo% = 2044: GOSUB D5                    'Baseline (0 Volts)
GOSUB D5.5
'
'               Integration Bit
'
CLS : PRINT " Full scale deflection = 4095 counts"
INPUT " How many units (volts, amps etc.) is this equivalent to "; scl
scl = scl / 4095
i = 0
PRINT : PRINT "Counting squares ..."
FOR r% = tl% TO th% - 1
t = t(r% + 1) - t(r%)
v = (v(r% + 1) + v(r%)) / 2 - vo%
i = i + v * t
NEXT r%
i = -i * scl
FOR p = 1 TO 15: FOR r = 50 TO 200 STEP 5: SOUND r + (p * 30), .1: NEXT r, p
CLS
PRINT : PRINT "integration from :"; t(th%); " to "; t(tl%); " seconds"
PRINT : PRINT "Baseline at "; vo%; " counts"
PRINT : PRINT "Integrated area "; i; " unit seconds"
IF ABS(i) < .001 THEN PRINT TAB(10); " or "; i * 1000000!; " unit microseconds"
WHILE INKEY$ = "": WEND
END
L4: CLS
PRINT : PRINT "Position time bars (low and high) and voltage baseline for the transform"
PRINT "by using the arrow keys to move the red bar cursors and space bar to accept"
PRINT "its position. The top display shows the whole trace, the lower display gives"
PRINT "an enlarged portion - to aid precision in positioning the cursor."
PRINT "Pg Up and Pg Dn can also be used for more rapid cursor movement. As can Ctrl"
PRINT "left or right. Back Tab can be used to position baseline at the average level"
PRINT "of the last 10% of data points over the chosen interval."
WHILE INKEY$ = "": WEND
'
'               Obtain Limits
'
GOSUB D1
xl% = 1: xh% = INT(no% / 10 + .51): GOSUB D2    '10x expansion
tl% = 1: GOSUB D3
xh% = no%: xl% = INT(no% * .9 + .51): GOSUB D2    '10x expansion
th% = no%: GOSUB D4
vo% = 2044: GOSUB D5                    'Baseline (0 Volts)
GOSUB D5.5
'
'               Transform Bit
'
CLS : PRINT "Type of transient (i or v) ";
iv$ = "": WHILE (iv$ <> "i" AND iv$ <> "v"): iv$ = INKEY$: WEND
PRINT iv$
PRINT " Full scale deflection = 4095 counts"
```

```
IF iv$ = "i" THEN PRINT "How many amps is this equivalent to ";
IF iv$ = "v" THEN PRINT "How many volts is this equivalent to ";
INPUT scl
scl = scl / 4095
PRINT : PRINT "Transform limits:"
INPUT "Min s "; smn
INPUT "Max s "; smx
INPUT "Step s "; ds
PRINT
IF iv$ = "i" THEN PRINT "Voltage step (volts) ";
IF iv$ = "v" THEN PRINT "Current step (amps) ";
INPUT e
PRINT : PRINT "Transforming ..."
d% = INT(ABS(smx - smn) / ds + 1.5)
DIM s(d%), iv(d%), z(d%)
d% = 0
IF iv$ = "v" THEN GOTO L4.5
FOR r = smn TO smx STEP ds
d% = d% + 1
s(d%) = r
iv(d%) = 0
FOR p% = tl% TO th%: '                  current transient
t = t(p% + 1) - t(p%)
v = ((v(p% + 1) - vo%) * EXP(-r * (t(p% + 1) - t(tl%))) + (v(p%) - vo%) * EXP(-r * (t(p%) - t(tl%)))) / 2
iv(d%) = iv(d%) + v * t
NEXT p%
iv(d%) = -iv(d%) * scl
IF (r * iv(d%)) <> 0 THEN z(d%) = e / (r * iv(d%)) ELSE z(d%) = 0
PRINT "@";
NEXT r: PRINT : GOTO L4.8
L4.5: '                                 voltage transient
FOR r = smn TO smx STEP ds
d% = d% + 1
s(d%) = r
iv(d%) = 0
FOR p% = tl% TO th%
t = t(p% + 1) - t(p%)
v = ((v(p% + 1) - vo%) * EXP(-r * (t(p% + 1) - t(tl%))) + (v(p%) - vo%) * EXP(-r * (t(p%) - t(tl%)))) / 2
iv(d%) = iv(d%) + v * t
NEXT p%
iv(d%) = -iv(d%) * scl
IF (r * iv(d%)) <> 0 THEN z(d%) = (r * iv(d%)) / e ELSE z(d%) = 0
PRINT "@";
NEXT r: PRINT
L4.8: FOR p = 1 TO 20: FOR r = ABS(200 - p * 18) + 30 TO 200 STEP 5: SOUND r + (p * 30), .1: NEXT r, p
CLS
PRINT : PRINT "Transform from :"; t(th%); " to "; t(tl%); " seconds"
PRINT : PRINT "Baseline at "; vo%; " counts"
PRINT "s ", "F(s)", "Z(s)"
FOR r% = 1 TO d%
PRINT s(r%), iv(r%), z(r%)
NEXT r%
WHILE INKEY$ = "": WEND
flag = 0
L5: CLS : PRINT "Pick an option:"
PRINT : PRINT "1> Save data to a file"
PRINT : PRINT "2> View graph"
PRINT : PRINT "3> Exit"
PRINT : PRINT "4> Re-start"
PRINT : PRINT "5> View data"
a$ = "": WHILE a$ = "": a$ = INKEY$: WEND
a = VAL(a$): IF a < 1 OR a > 5 THEN GOTO L5
IF a = 1 THEN GOSUB p: SCREEN 12: GOTO L5
IF a = 3 THEN END
IF a = 4 THEN CLEAR : RUN
IF a = 5 THEN GOSUB D10: GOTO L5
GOSUB D6: GOTO L5
L6: CLS                 'fourier transform
```

```
PRINT : PRINT "Position time bars (low and high) and voltage baseline for the transform"
PRINT "by using the arrow keys to move the red bar cursors and space bar to accept"
PRINT "its position. The top display shows the whole trace, the lower display gives"
PRINT "an enlarged portion - to aid precision in positioning the cursor."
PRINT "Choose a baseline above the curve to obtain real impedance data. The last"
PRINT "10% of the data points are extrapolated if the minimum frequency is too short"
PRINT "for the fourier analysis."
PRINT "Pg Up and Pg Dn can also be used for more rapid cursor movement. As can Ctrl"
PRINT "left or right. Back Tab can be used to position baseline at the average level"
PRINT "of the last 10% of data points over the chosen interval."
WHILE INKEY$ = "": WEND
'
'               Obtain Limits
'
GOSUB D1
xl% = 1: xh% = INT(no% / 10 + .51): GOSUB D2    '10x expansion
tl% = 1: GOSUB D3
xh% = no%: xl% = INT(no% * .9 + .51): GOSUB D2    '10x expansion
th% = no%: GOSUB D4
GOSUB D11                               'Baseline
'
'               Transform Bit
'
CLS : PRINT "Type of transient (i or v) ";
iv$ = "": WHILE (iv$ <> "i" AND iv$ <> "v"): iv$ = INKEY$: WEND
PRINT iv$
CLS : PRINT " Full scale deflection = 4095 counts"
IF iv$ = "i" THEN PRINT "How many amps is this equivalent to ";
IF iv$ = "v" THEN PRINT "How many volts is this equivalent to ";
INPUT scl
scl = scl / 4095
PRINT : PRINT "Transform limits:"
t = t(th%) - t(tl%)
INPUT "min freq. "; smn
GOSUB L7                                'zero filling
IF smn > .5 / t THEN smn = .5 / t: PRINT "min freq. = "; smn
INPUT "Max freq "; smx
IF smx < 3 * smn THEN smx = 3 * smn             'check limit
ds = 2 * smn
PRINT
IF iv$ = "i" THEN PRINT "Voltage step (volts) ";
IF iv$ = "v" THEN PRINT "Current step (amps) ";
INPUT e
PRINT "Fast transform (y/n or ' ')": a$ = ""
WHILE a$ = "": a$ = INKEY$: WEND
IF a$ = "y" THEN fast = -1 ELSE fast = 0
PRINT : PRINT "Transforming ..."
d% = INT((smx / smn - 1) / 2 + 1.1)
DIM s(d%), z1(d%), z2(d%), z3(d%), z4(d%)
d% = 0: pi = 3.141592653589#
FOR rr = smn TO smx STEP ds
r = 2 * rr
d% = d% + 1
s(d%) = rr              'frequency
z1(d%) = 0: z2(d%) = 0
IF fast = 0 THEN GOTO La
'               fast integral
FOR p% = tl% TO th% - 1   'time range
t = t(p% + 1) - t(p%)
n = r * pi
i = ((v(p% + 1) - vo%) * SIN(n * (t(p% + 1) - t(tl%))) + (v(p%) - vo%) * SIN(n * (t(p%) - t(tl%)))) / 2
z1(d%) = z1(d%) + i * t
i = ((v(p% + 1) - vo%) * COS(n * (t(p% + 1) - t(tl%))) + (v(p%) - vo%) * COS(n * (t(p%) - t(tl%)))) / 2
z2(d%) = z2(d%) + i * t
NEXT p%: GOTO Lb
La: '               slow integral
n = r * pi
FOR p% = tl% TO th% - 1   'time range
```

```
t = t(p% + 1) - t(p%)
a = (v(p% + 1) - v(p%)) / t
i = (v(p%) - vo%) / n * COS(n * (t(p%) - t(tl%))) - (v(p% + 1) - vo%) / n * COS(n * (t(p% + 1) - t(tl%)))
i = i + a / (n ^ 2) * (SIN(n * (t(p% + 1) - t(tl%))) - SIN(n * (t(p%) - t(tl%))))
z1(d%) = z1(d%) + i
i = (v(p% + 1) - vo%) / n * SIN(n * (t(p% + 1) - t(tl%))) - (v(p%) - vo%) / n * SIN(n * (t(p%) - t(tl%)))
i = i + a / (n ^ 2) * (COS(n * (t(p% + 1) - t(tl%))) - COS(n * (t(p%) - t(tl%))))
z2(d%) = z2(d%) + i
NEXT p%
Lb: IF (t(th%) - t(tl%)) = .5 / smn THEN GOTO L6.5
t = t(th%) - t(tl%)                              'zero fill
i = (zo% - vo%) * (1 + COS(n * t)) / n           'exact integral
z1(d%) = z1(d%) + i
i = (zo% - vo%) * (SIN(n * t)) / n
z2(d%) = z2(d%) - i
L6.5: z1(d%) = z1(d%) * (n / e) * scl
z2(d%) = z2(d%) * (n / e) * scl
NEXT rr: GOTO Le
Lc: '                    current transient
FOR r% = 1 TO d%
z = z1(r%) - (zo% - vo%) * scl / e
q = 1 / (z ^ 2 + z2(r%) ^ 2)
z3(r%) = q * z: z4(r%) = -q * z2(r%)
NEXT r%
RETURN
Id: '                    voltage transient
FOR r% = 1 TO d%
z3(r%) = z1(r%) - (zo% - vo%) * scl / e
z4(r%) = z2(r%)
NEXT r%
RETURN
Le: FOR p = 1 TO 23: FOR r = ABS(500 - p * 20) + 30 TO 50 STEP -8: SOUND (r * p) / 3 + 30, .1: NEXT r, p
CLS
PRINT : PRINT "Transform from :"; tl%; " to "; th%; " seconds."
PRINT : PRINT "Baseline at "; vo%; " counts"
PRINT : PRINT "freq.", "Z'  ", "Z"  "
IF iv$ = "v" THEN GOSUB Id
IF iv$ = "i" THEN GOSUB Lc
FOR r% = 1 TO d%
PRINT s(r%), z3(r%), z4(r%)
NEXT r%
WHILE INKEY$ = "": WEND
flag = 1: GOTO L5
L7:              'end limit
zo% = v(th%): RETURN
L8: '                    averaging
CLS : PRINT : PRINT "1> average all data."
PRINT "2> average last half of data."
DO: a$ = "": WHILE a$ = "": a$ = INKEY$: WEND
LOOP UNTIL VAL(a$) > 0 AND VAL(a$) < 3
LOCATE 10, 7: PRINT "Amount done:"
IF VAL(a$) = 2 THEN GOTO L8.5
r% = 1: WHILE r% < no%
LOCATE 10, 20: PRINT INT(100 / no% * r% + .5)
p% = INT(r% / 2 + .51)
v(p%) = (v(r%) + v(r% + 1)) / 2
t(p%) = (t(r%) + t(r% + 1)) / 2
r% = r% + 2
WEND: no% = p%
GOTO LI
'              Half averaging
L8.5: r% = INT(no% / 2 + .501): rr% = INT(r% / 2 + .501)
WHILE r% < no%
LOCATE 10, 20: PRINT INT(200 / no% * r% - 99.5)
p% = INT(r% / 2 + .51 + rr%)
v(p%) = (v(r%) + v(r% + 1)) / 2
t(p%) = (t(r%) + t(r% + 1)) / 2
r% = r% + 2
```

```
WEND: no% = p%
GOTO L1
L9: '                Point removal
'
PRINT : PRINT "Place cursor over point to be removed and press space, 'x' to exit."
PRINT "Press a key"
WHILE INKEY$ = "": WEND
GOSUB D1
xl% = 1: xh% = INT(no% / 10 + .51): GOSUB D2     '10x expansion
tl% = 1: GOSUB D8
GOTO L1
L10:                 'temporal point removal
CLS : LOCATE 10, 10: PRINT "% thru'"
r% = 1: WHILE r% < no% - 1
LOCATE 10, 20: PRINT INT(100 / no% * r% + .5)
IF t(r% + 1) > t(r%) THEN GOTO L10a          'timer counts down
no% = no% - 1: FOR rr% = r% TO no%           'reshuffle data points
v(rr%) = v(rr% + 1)
t(rr%) = t(rr% + 1)
NEXT rr%
r% = r% - 1
L10a: r% = r% + 1: WEND
GOTO L1
L11: CLS : '                New Fourier Transform
PRINT : PRINT "Position time bars (low and high) and voltage baseline for the transform"
PRINT "by using the arrow keys to move the red bar cursors and space bar to accept"
PRINT "its position. The top display shows the whole trace, the lower display gives"
PRINT "an enlarged portion - to aid precision in positioning the cursor."
PRINT "The minimum frquency is dictated by the length of transient used."
PRINT "Pg Up and Pg Dn can also be used for more rapid cursor movement. As can Ctrl"
PRINT "left or right. Back Tab can be used to position baseline at the average level"
PRINT "of the last 10% of data points over the chosen interval."
WHILE INKEY$ = "": WEND
'
'                Obtain Limits
'
GOSUB D1
xl% = 1: xh% = INT(no% / 10 + .51): GOSUB D2     '10x expansion
tl% = 1: GOSUB D3
xh% = no%: xl% = INT(no% * .9 + .51): GOSUB D2     '10x expansion
th% = no%: GOSUB D4
GOSUB D11                                    'Baseline (initial V)
'
'                Transform Bit
'
CLS : PRINT "Type of transient (i or v) ";
iv$ = "": WHILE (iv$ <> "i" AND iv$ <> "v"): iv$ = INKEY$: WEND
PRINT iv$
CLS : PRINT " Full scale deflection = 4095 counts"
IF iv$ = "i" THEN PRINT "How many amps is this equivalent to ";
IF iv$ = "v" THEN PRINT "How many volts is this equivalent to ";
INPUT scl
scl = scl / 4095
PRINT : PRINT "Transform limits:"
t = t(th%) - t(tl%)
smn = .5 / t
PRINT "min freq. "; smn
GOSUB L7                                     'zero filling
INPUT "max step size "; ds
PRINT
IF iv$ = "i" THEN PRINT "Voltage step (volts) ";
IF iv$ = "v" THEN PRINT "Current step (amps) ";
INPUT e
WHILE a$ = "": a$ = INKEY$: WEND
PRINT : PRINT "Transforming ..."
ld% = INT((th% - tl%))
DIM s(ld%), z1(ld%), z2(ld%), z3(ld%), z4(ld%)
pi = 3.141592653589#
```

```
rr = smn
r = 2 * smn
d% = 0
t = t(tl%)
'                       subtract baseline + initial time
FOR p% = tl% TO th%
v(p%) = v(p%) - vo%
t(p%) = t(p%) - t
NEXT p%
WHILE th% > tl% + 2          'transform cycle
d% = d% + 1
s(d%) = .5 * r               'frequency
z1(d%) = 0: z2(d%) = 0
n = r * pi
FOR p% = tl% TO th% - 1      'time range
b = n * t(p%)
c = n * t(p% + 1)
a = (v(p% + 1) - v(p%)) / (t(p% + 1) - t(p%))
z1(d%) = z1(d%) + (a / n) * (SIN(c) - SIN(b))
z2(d%) = z2(d%) + (a / n) * (COS(c) - COS(b))
NEXT p%
z1(d%) = z1(d%) + v(tl%) + v(th%)
z1(d%) = z1(d%) * scl / e
z2(d%) = z2(d%) * scl / e
IF iv$ = "v" THEN GOSUB Lx
IF iv$ = "i" THEN GOSUB Ly
th% = th% - INT(ds * t(th%) * smn + 1)
r = 1 / t(th%)
LOCATE 10, 40: PRINT "thru' "; INT(100 * (1 - (t(th%) * 2 * smn)) + .5); " %  "
WEND: GOTO Lz
Ly: '                        current transient
z = z1(d%) - v(th%) * scl / e
q = 1 / (z ^ 2 + z2(d%) ^ 2)
z3(d%) = q * z
z4(d%) = -q * z2(d%)
RETURN
Lx: '                        voltage transient
z3(d%) = z1(d%) - v(th%) * scl / e
z4(d%) = z2(d%)
RETURN
Lz: FOR p = 1 TO 23: FOR r = ABS(500 - p * 20) + 30 TO 50 STEP -8: SOUND (r * p) / 3 + 30, .1: NEXT r, p
CLS
PRINT : PRINT "Transform "
PRINT : PRINT "Baseline at "; vo%; " counts"
PRINT : PRINT "freq.", "Z'  ", "Z"  "
FOR r% = 1 TO d%
PRINT s(r%), z3(r%), z4(r%)
NEXT r%
WHILE INKEY$ = "": WEND
flag = 1: GOTO L5
D1: SCREEN 12: CLS : '               size 639x460
'                           Top screen
tdiv = t(no%) / 638
FOR r% = 1 TO no%
PSET (INT(t(r%) / tdiv), INT((v(r%) - vmn) * 225 / vrg + 5)), 9
NEXT r%
LINE (0, 230)-(640, 230), 2, , 22982
RETURN
D1.5: FOR r% = 1 TO no% - 1
LINE (INT(t(r%) / tdiv), INT((v(r%) - vmn) * 225 / vrg + 5))-(INT(t(r% + 1) / tdiv), INT((v(r% + 1) - vmn) * 225 / vrg + 5)), 6
NEXT r%
RETURN
D2: xdv = (t(xh%) - t(xl%)) / 638        'bottom bits
LINE (0, 232)-(640, 460), 0, BF
FOR r% = xl% TO xh%
PSET (INT((t(r%) - t(xl%)) / xdv), INT((v(r%) - vmn) * 225! / vrg + 235)), 9
NEXT r%
RETURN
```

```
D3: LINE (INT((t(tl%) - t(xl%)) / xdv), 460)-(INT((t(tl%) - t(xl%)) / xdv), 240), 4
LINE (INT(t(tl%) / tdiv), 0)-(INT(t(tl%) / tdiv), 4), 12
DO
a$ = "": WHILE a$ = "": a$ = INKEY$: WEND
LOOP UNTIL ASC(a$) = 32 OR LEN(a$) = 2
IF ASC(a$) = 32 THEN RETURN
a = ASC(RIGHT$(a$, 1))
IF a = 115 OR a = 116 THEN GOTO D3.1
IF a <> 75 AND a <> 77 THEN GOTO D3
D3.1: LINE (INT(t(tl%) / tdiv), 0)-(INT(t(tl%) / tdiv), 4), 0
LINE (INT((t(tl%) - t(xl%)) / xdv), 460)-(INT((t(tl%) - t(xl%)) / xdv), 240), 0
PSET (INT((t(tl%) - t(xl%)) / xdv), INT((v(tl%) - vmn) * 225! / vrg + 235)), 9
tstep = no% / 20
tl% = tl% + (a = 75) + tstep * (a = 115): IF tl% < 1 THEN tl% = 1
tl% = tl% - (a = 77) - tstep * (a = 116): IF tl% > (no% - 1) THEN tl% = no% - 1
IF tl% < (xl% + 1) AND xl% > 1 THEN xh% = xh% + tl% - xl% - 1: xl% = tl% - 1: GOSUB D2
IF tl% > (xh% - 1) AND xh% < no% THEN xl% = xl% + tl% - xh% + 1: xh% = tl% + 1: GOSUB D2
GOTO D3
D4: LINE (INT((t(th%) - t(xl%)) / xdv), 460)-(INT((t(th%) - t(xl%)) / xdv), 240), 4
LINE (INT(t(th%) / tdiv), 0)-(INT(t(th%) / tdiv), 4), 12
DO
a$ = "": WHILE a$ = "": a$ = INKEY$: WEND
LOOP UNTIL ASC(a$) = 32 OR LEN(a$) = 2
IF ASC(a$) = 32 THEN RETURN
a = ASC(RIGHT$(a$, 1))
IF a = 115 OR a = 116 THEN GOTO D4.1
IF a <> 75 AND a <> 77 THEN GOTO D4
D4.1: LINE (INT(t(th%) / tdiv), 0)-(INT(t(th%) / tdiv), 4), 0
LINE (INT((t(th%) - t(xl%)) / xdv), 460)-(INT((t(th%) - t(xl%)) / xdv), 240), 0
PSET (INT((t(th%) - t(xl%)) / xdv), INT((v(th%) - vmn) * 225! / vrg + 235)), 9
tstep = no% / 20
th% = th% + (a = 75) + tstep * (a = 115): IF th% < tl% + 1 THEN th% = tl% + 1
th% = th% - (a = 77) - tstep * (a = 116): IF th% > no% THEN th% = no%
IF th% < (xl% + 1) AND xl% > 1 THEN xh% = xh% + th% - xl% - 1: xl% = th% - I: GOSUB D2
IF th% > (xh% - 1) AND xh% < no% THEN xh% = xh% + th% - xh% + 1: xh% = th% + 1: GOSUB D2
GOTO D4
D5: CLS                    'Baseline
'                    Top screen
tdiv = t(no%) / 638
FOR r% = 1 TO no%
PSET (INT(t(r%) / tdiv), INT(450 / 4096 * v(r%) + 5)), 9
NEXT r%
RETURN
D5.5: LINE (0, INT(450 / 4096 * vo% + 5))-(640, INT(450 / 4096 * vo% + 5)), 3
DO
a$ = "": WHILE a$ = "": a$ = INKEY$: WEND
LOOP UNTIL ASC(a$) = 32 OR LEN(a$) = 2
IF ASC(a$) = 32 THEN RETURN
a = ASC(RIGHT$(a$, 1))
IF a = 15 THEN GOSUB D9: GOSUB D5: GOTO D5.5      'auto baseline
IF a = 73 OR a = 81 THEN GOTO D5.6
IF a <> 72 AND a <> 80 THEN GOTO D5.5
D5.6: GOSUB D5
IF a = 73 THEN vo% = vo% - 40: IF vo% < 1 THEN vo% = 1
IF a = 72 AND vo% > 4 THEN vo% = vo% - 4
IF a = 81 THEN vo% = vo% + 40: IF vo% > 4097 THEN vo% = 4097
IF a = 80 AND vo% < 4093 THEN vo% = vo% + 4
GOTO D5.5
D6: CLS                    'Transform Display
imx = -1000000!: imn = 1000000!
IF flag = 1 THEN GOTO D7
FOR r% = 1 TO d%              'Laplace display
IF z(r%) < imn THEN imn = z(r%)
IF z(r%) > imx THEN imx = z(r%)
NEXT r%
IF imn > 0 THEN imn = 0
IF smn > 0 THEN smn = 0
di = (imx - imn) / 460
```

```
ds = (smx - smn) / 638
'                    axis
LINE (-smn / ds, 0)-(-smn / ds, 460), 2
LINE (0, 460 + imn / di)-(638, 460 + imn / di), 2
'                    data points
FOR r% = 1 TO d%
PSET ((s(r%) - smn) / ds, 460 + (imn - z(r%)) / di), 3
NEXT r%
WHILE INKEY$ = "": WEND
FOR r% = 1 TO d% - 1
LINE ((s(r%) - smn) / ds, 460 + (imn - z(r%)) / di)-((s(r% + 1) - smn) / ds, 460 + (imn - z(r% + 1)) / di), 14
NEXT r%
WHILE INKEY$ = "": WEND: RETURN
D7: FOR r% = 1 TO d%          'FT impedance diagram
IF z3(r%) < imn THEN imn = z3(r%)
IF -z4(r%) < imn THEN imn = -z4(r%)
IF z3(r%) > imx THEN imx = z3(r%)
IF -z4(r%) > imx THEN imx = -z4(r%)
NEXT r%
IF imn > 0 THEN imn = 0
dx = 450 / (imx - imn)
'                    axis
LINE (-imn * dx, 0)-(-imn * dx, 460), 2
LINE (0, 460 + imn * dx)-(460, 460 + imn * dx), 2
'                    impedance points
FOR r% = 1 TO d%
PSET ((z3(r%) - imn) * dx, 460 + (imn + z4(r%)) * dx), 3
NEXT r%
WHILE INKEY$ = "": WEND
FOR r% = 1 TO d% - 1
LINE ((z3(r%) - imn) * dx, 460 + (imn + z4(r%)) * dx)-((z3(r% + 1) - imn) * dx, 460 + (imn + z4(r% + 1)) * dx), 14
FOR p = 1 TO 2000: NEXT p       'slow draw
NEXT r%
WHILE INKEY$ = "": WEND: RETURN
D8: LINE (INT((t(tl%) - t(xl%)) / xdv), 460)-(INT((t(tl%) - t(xl%)) / xdv), 240), 4
LINE (INT(t(tl%) / tdiv), 0)-(INT(t(tl%) / tdiv), 4), 12
DO
a$ = "": WHILE a$ = "": a$ = INKEY$: WEND
LOOP UNTIL (ASC(a$) = 32 OR a$ = "x") OR LEN(a$) = 2
IF a$ = " " THEN GOTO D8.2
IF a$ = "x" THEN RETURN
a = ASC(RIGHT$(a$, 1))
IF a = 115 OR a = 116 THEN GOTO D8.1
IF a <> 75 AND a <> 77 THEN GOTO D8
D8.1: LINE (INT(t(tl%) / tdiv), 0)-(INT(t(tl%) / tdiv), 4), 0
LINE (INT((t(tl%) - t(xl%)) / xdv), 460)-(INT((t(tl%) - t(xl%)) / xdv), 240), 0
PSET (INT((t(tl%) - t(xl%)) / xdv), INT((v(tl%) - vmn) * 225! / vrg + 235)), 9
tl% = tl% + (a = 75) + 10 * (a = 115): IF tl% < 1 THEN tl% = I
tl% = tl% - (a = 77) - 10 * (a = 116): IF tl% > no% THEN tl% = no%
IF tl% < (xl% + 1) AND xl% > 1 THEN xh% = xh% + tl% - xl% - 1: xl% = tl% - 1: GOSUB D2
IF tl% > (xh% - 1) AND xh% < no% THEN xl% = xl% + tl% - xh% + 1: xh% = tl% + 1: GOSUB D2
GOTO D8
D8.2: IF tl% = no% THEN no% = no% - 1: a = 77: GOSUB D1: GOSUB D2: GOTO D8.1
FOR r% = tl% + 1 TO no%
t(r% - 1) = t(r%)
v(r% - 1) = v(r%)
NEXT r%
no% = no% - 1: GOSUB D1: GOSUB D2: a = 77: GOTO D8.1
D9: '                    Auto-Baseline
v = 0: rr = 0
IF (th% - tl%) < 10 THEN vo% = v(th%): RETURN
FOR r% = INT(th% - .1 * (th% - tl%)) TO th%
rr = rr + 1: v = v + v(r%)
NEXT r%
vo% = INT(v / rr + .501): RETURN
D10: '                    Data as text
CLS
a = 0
```

```
DO
PRINT "freq.", "Z'", "Z""
FOR r = 1 TO 20
a = a + 1
IF a <= d% THEN PRINT s(a), z3(a), z4(a)
NEXT r
WHILE INKEY$ = "": WEND
LOOP UNTIL a >= d%
WHILE INKEY$ = "": WEND: RETURN
D11: '                    Baseline
CLS : PRINT : PRINT "sloping baseline (y/n)"
a$ = "": WHILE a$ <> "y" AND a$ <> "n": a$ = INKEY$: WEND
IF a$ = "n" THEN vo% = (v(1) + v(2)) / 2: GOSUB D5: GOTO D5.5
'                    sloping baseline
PRINT : PRINT "For the sloping baseline position the cursor at the start and end points"
PRINT "of the baseline."
WHILE INKEY$ = "": WEND
GOSUB D1
xl% = 1: xh% = INT(no% / 10 + .51): GOSUB D2    '10x expansion
ath% = th%
atl% = tl%
th% = 2 * th% - tl% + 2: IF th% > no% THEN th% = no%
tl% = tl% - 1: GOSUB D3
xh% = th% + no% * .05: IF xh% > no% THEN xh% = no%
xl% = th% - no% * .05: GOSUB D2              '10x expansion
GOSUB D4
vo% = v(tl%): tt = t(tl%)                  'flat base
dv = (v(th%) - v(tl%)) / (t(th%) - t(tl%))    'slope
tl% = atl%: th% = ath%
FOR r% = tl% TO th%                        'subtract slope
v(r%) = v(r%) - dv * (t(r%) - tt)
NEXT r%
GOSUB D1: LOCATE 1, 10: PRINT "Gradient "; dv; " counts / sec"
WHILE INKEY$ = "": WEND: RETURN
z: END
p:   '**********Save data on disc**********
SCREEN 2: CLS : fp$ = "A:\"                  'drive  default
a% = 0
ON ERROR GOTO p2
OPEN "flag" FOR INPUT AS #1
ON ERROR GOTO 0
IF a% <> 0 THEN flag = 0 ELSE INPUT #1, fl$, fi$: flag = 1
CLOSE
IF flag = 0 THEN
fl$ = "FTIRUN"                             'default file
fi$ = "01"                                 'default number
END IF
LOCATE 22, 23: PRINT "Press ENTER to accept the default"
LOCATE 24, 23: PRINT "Press ESCAPE to return to the menu";
LOCATE 6, 8: PRINT "Please enter the path for the file in which data is to be saved"
LOCATE 8, 22: PRINT "Use BACKSPACE to modify the default"
b$ = fp$
GOSUB p1
IF ASC(a$) = 27 THEN RETURN
IF RIGHT$(b$, 1) <> "\" THEN b$ = b$ + "\"
fp$ = b$
LOCATE 12, 30 - LEN(fp$): PRINT fp$ + SPACE$(49)
LOCATE 6, 8: PRINT "      Please enter the file name (maximum 6 characters)      "
b$ = fl$
GOSUB p1
IF ASC(a$) = 27 THEN RETURN
fl$ = LEFT$(b$, 6)
LOCATE 12, 30 - LEN(fp$) - LEN(fl$): PRINT fp$ + fl$ + SPACE$(49)
LOCATE 6, 15: PRINT "    Please enter the index number (1 to 99)    "
LOCATE 17, 2: PRINT "The extension is added by the program - .DAT for data"
b$ = fi$
GOSUB p1
IF ASC(a$) = 27 THEN RETURN
```

```
DO WHILE LEN(b$) < 2: b$ = "0" + b$: LOOP
fi$ = LEFT$(b$, 2)
f$ = fp$ + fl$ + fi$ + ".DAT"
CLS : a% = 0
ON ERROR GOTO p2
OPEN f$ FOR INPUT AS #2
ON ERROR GOTO 0
IF a% = 1 THEN GOTO p
IF NOT a% THEN
CLOSE 2: CLS
LOCATE 10, 14: PRINT "A file with this name is already present on the disc"
LOCATE 12, 23: PRINT "Press  1 to overwrite"
LOCATE 14, 30: PRINT "2 to enter a new name";
DO: a$ = INKEY$: LOOP UNTIL a$ = "1" OR a$ = "2"
IF a$ = "2" THEN GOTO p
KILL f$
END IF
CLS
LOCATE 10, 32: PRINT "Saving data file"
th = th(1): tl = tl(1)                'initial time
OPEN f$ FOR OUTPUT AS #2
IF flag = 0 THEN PRINT #2, "s , F(s) , Z(s)"
IF flag = 1 THEN PRINT #2, "f , Z' , Z""
FOR i% = 1 TO d%
a$ = STR$(s(i%))
IF flag = 0 THEN b$ = STR$(iv(i%)) ELSE b$ = STR$(z3(i%))
IF flag = 0 THEN d$ = STR$(z(i%)) ELSE d$ = STR$(z4(i%))
c$ = a$ + "," + b$ + "," + d$
PRINT #2, c$
NEXT
CLOSE 2
CLS
LOCATE 6, 20: PRINT "Data saved as file "; f$
LOCATE 20, 30: PRINT "Press SPACE to continue"
DO: a$ = INKEY$: LOOP UNTIL a$ = " "
fi$ = LTRIM$(STR$(VAL(fi$) + 1))
DO WHILE LEN(fi$) < 2: fi$ = "0" + fi$: LOOP
ds% = -1
OPEN "flag" FOR OUTPUT AS #1
PRINT #1, fl$
PRINT #1, fi$
CLOSE
RETURN
p1: LOCATE 12, 30   '*************Enter file path, name and number*********
PRINT b$ + "_ "
DO
DO: a$ = UCASE$(INKEY$): LOOP UNTIL a$ <> ""
IF ASC(a$) = 13 OR ASC(a$) = 27 THEN EXIT DO
IF ASC(a$) = 8 THEN IF b$ = "" THEN GOTO p12 ELSE b$ = LEFT$(b$, LEN(b$) - 1): GOTO p11
IF a$ = "." THEN BEEP: GOTO p12
b$ = b$ + a$
p11: LOCATE 12, 30: PRINT b$ + "_ "
p12: LOOP
RETURN
p2:         '*************Saving to disc error trapping*****************
SELECT CASE ERR
CASE 53: a% = -1
CASE 61: LOCATE 10, 35: PRINT "Disc full": a% = 1
CASE 64: LOCATE 10, 33: PRINT "Bad file name": a% = 1
CASE 71: LOCATE 10, 33: PRINT "Disc not ready": a% = 2
CASE 76: LOCATE 10, 30: PRINT "Path not found": a% = 1
CASE ELSE: ON ERROR GOTO 0
END SELECT
IF a% = -1 THEN RESUME NEXT
LOCATE 20, 28: PRINT "Press SPACE to continue"
DO: a$ = INKEY$: LOOP UNTIL a$ = " "
IF a% = 1 THEN RESUME NEXT ELSE RESUME
```

References

Chapter 1

[1] M. Faraday, *"Experimental Researches in Electricity"*, Vol. I (1839) Taylor & Francis, Par. 989

[2] D.H. Doughty, *Sampe J.* 32 (1996) 75

[3] *RS Catalogue* 1 (1996) pp. 1-7

[4] Micron Communications Inc., literature (1996) (www.micron.com/mti/ir/financial/prod_pr/p5310.html)

[5] Wilson Greatbatch Ltd., literature 1996 (www.greatbatch.com/medprod.html #infosvo)

[6] J. Yamaki, *Prog. in Batteries and Solar Cells* 7 (1988) 363

[7] S.D. Jones, J.R. Akridge, *Sol. State Ionics* 53-56 (1992) 628

[8] R. Krause, *Pop. Sci.* 242 (1993) 64

[9] Duracell literature, 1996 (www.duracell.com/Product_lnfo/Big_Five/bigfive.html)

[10] J.R. Dahn, *Sol. State Ionics* 69 (1994) 284

[11] D. Brachio, *Natta document "Energy Storage"* 2 (1993)

[12] *Jap. Chem. Week* 1869 (1996) 2

[13] D. Thisdell, *New Scientist* 2011 (1996) 21

[14] D. Wood, *Oral Presentation, IEE Colloquium "Compact Power Sources"* (1996), London, UK

[15] C.A. Vincent, F. Bruno, M. Lazzari, B. Scrosati, *"Modern Batteries"* (1982) E. Arnold, pp. 59 - 62

[16] RS Components Ltd., product data sheet K 18786 (1994)

[17] C.A. Vincent, F. Bruno, M. Lazzari, B. Scrosati, *"Modern Batteries"* (1982) E. Arnold, pp. 75 - 76

[18] C.A. Vincent, F. Bruno, M. Lazzari, B. Scrosati, *"Modern Batteries"* (1982) E. Arnold, pp. 76 - 78

[19] US Naval document P-3676, chap. 8 (www.bmpcoe.org/knowhow/navp3676)

[20] A.R. Tilley, *Oral Presentation, "Electrochem '94"* (1994), Edinburgh UK

[21] P. Ruetschi, F. Meli, J. Desilvestro, *J. Power Sources* 57 (1995) 85

[22] F.R. Kalhammer, A. Kozawa, C.B. Moyer, B.B. Owens, *Interface* 5 (1996) 32

[23] E. Soragni, G. Davolio, *Power Sources* 15, Brighton, UK (1995) 458

[24] K. Brandt, *Sol. State Ionics* 69 (1994) 171

[25] G. Foley, *"The Energy Question"* 4th Ed. (1992) Penguin Books p. 272

[26] S. Nathan, *Chem. Industry* (1995) 1001

[27] F. Pearce, *New Scientist* 1969 (1995) 4

[28] D. Gaskell, *Chem. Britain* 32 (1996) 5

[29] B. Steele, *Oral Presentation,* May (1995), Southampton, UK

[30] P.R. Wolfe, *Oral Presentation, IEE Colloquium "Compact Power Sources"* (1996), London UK

[31] L. Bradnam, A. Moris, G. Preston, D. Thorpe, *"Solar Energy"* (1995) C.A.T.

[32] G. Foley, *"The Energy Question" 4th Ed.* (1992) Penguin Books, p. 164

[33] M. Bergey, *"A primer on Small Wind Generators"* (1996) Bergey Windpower Co. (www.bergey.com/primer.html)

[34] B.E. Conway, *Power Sources* 15, Brighton, UK (1995) 65

[35] S. Sarangapani, J.A. Kosek, A.B. LaConti, "*Handbook of Solid State Batteries and Capacitors"* (1995) Ed. M.Z.A. Munshi, World Scientific Publishing, pp. 601- 614

[36] A.J. Bard, L.R. Faulkner, *"Electrochemical Methods"* (1980) John Wiley & Sons, Inc.

[37] D. Guyomard, J.M. Tarascon, *Advanced Mater.* 6 (1994) 408

[38] K. Sawai, Y. Iwakoshi, T. Ohzuku, *Sol. State Ionics* 69 (1994) 273

[39] J.F. Revelli, F.J. DiSalvo, *Inorg. Synth.* 30 (1995) 155

[40] D. O'Hare, *3rd Year Lecture course,* Oxford University, October 1991

[41] R.F. Scarr, *J. Electrochem. Soc.* 117 (1970) 295

[42] K.I. Tikhonov, E.A. Belyakov, *Soviet Electrochem.* 16 (1980) 513

[43] L.A. Zyat'kova, V.N. Afanas'ev, G.A. Krestov, T.V. Ivanova, *Russ. J. Electrochem.* 29 (1993) 809

[44] B. Vuillemin, *Ph. D. Thesis* (1992) University of Franche-Compte, France

[45] M. Armand, *Ph. D. Thesis* (1978) INP Grenoble, France

[46] C. Deportes, M. Duclot, P. Fabry, J. Fouletier, A. Hammou, M. Kleitz, E. Siebert, J.-L. Souquet, *"Electrochimie des Solides"* (1994) University Press of Grenoble, pp.60 - 67

[47] J.M Tarascon, D. Guyomard, P.W. Warren, F.G. Alvarado, F. Shokoohi, G.L.

Baker, R.L. Denton, *6th Int. Meet. Lithium Batt.,* Münster (1992) 400

[48] D. Guyomard, J.M. Tarascon, *Sol. State Ionics* 69 (1994) 222

[49] T. Ohzuku, *Industrial Chem. Lib. 5 "Lithium batteries, New materials, Developments and Perspectives"* (1994) Ed. G. Pistoia, pp. 239 - 80

[50] D.H. Shen, G. Halpert, *6th Int. Meet. Lithium Batt.*, Münster (1992) 504

[51] C.R. Houska, B.E. Warren, *J. Appl. Phys.* 25 (1954) 1503

[52] A. Herold, *Bull. Soc. Chim. France* 187 (1955) 999

[53] J.E. Fischer, H.J. Kim, *Synth. Met.* 12 (1985) 137

[54] F.A. Cotton, G. Wilkinson, *"Advanced Organic Chemistrt",* 5th ed., Wiley Interscience, p. 238

[55] R. Yazami, M.Z.A. Munshi , *"Handbook of Solid State Batteries and Capacitors"* (1995) pp. 427 - 447

[56] R. Yazami, Ph. Touzain, *J. Power Sources* 9 (1983) 365

[57] I.T. Belash, O.V. Zharikov, A.V .Palnichenko, *Synth. Met.* 34 (1989) 47

[58] D. Guérard, A. Hérold, *Carbon* 13 (1975) 337

[59] G.S. Inorganic Products, pricelist March 1995

[60] J.R. Dahn, A.K. Sleigh, B.M. Way, W.J. Weydanz, J.N. Reimers, Q. Zhong, U. von Sacken, *Industrial Chem. Lib. 5 "Lithium batteries, New materials, Developments and Perspectives"* (1994) Ed. G. Pistoia, pp. 1 - 47

[61] J.R. Dahn, R. Fong, M.J. Spoon, *Phys. Rev.* B42 (1990) 6424

[62] Lonza Carbons Catalogue (1992) Lonza G + T Ltd.

[63] G. Foley, *"The Energy Question",* 4th Ed. (1992) Penguin Books, p. 65

[64] M.T. Weller, *"Inorganic Materials Chemistry",* Oxford University Press (1994) pp. 87 - 8

[65] Y. Chabre, D. Djurado, M. Armand, W.R. Rdmanow, N. Coustel, J.P. McCauley Jr., J.E. Fischer, A.B.Smith, *J. Am. Chem. Soc.* 114 (1992) 764

[66] Strem Chemical Inc. Catalog 16 (1995) 52-3

[67] R.H. Norman, *"Conductive Rubbers and Plastics"* (1970) Elsevier Publishing Co.

[68] K. Takei, N. Terada, K. Kumai, T. Iwahori, T. Uwai, T. Miura, *J. Power Sources* 55 (1995) 191

[69] K.Takei, K. Kumai, T. Iwahori, T. Uwai, M. Furusyo, *Denki Kagaku* 61 (1993) 421

[70] A. Watanabe, K. Mori, H. Ishikawa, Y. Nakamura, *J. Electrochem. Soc.* 134 (1987)

1318

[71] J. Vondrak, *Collect. Czech. Chem. Commun.* 60 (1995) 1158

[72] Cabot Carbon Ltd. European Technical Report S-136 (1995)

[73] Cabot Carbon Ltd. pricelist May 1995

[74] W.J. Weydanz, B.M. Way, T. van Buuren, J.R. Dahn, *J. Electrochem. Soc.* 141 (1994) 900

[75] S. Ito, T. Morata, M. Hasegawa, Y. Bito, Y. Toyoguchi, *8th Int. Meet. Lithium Batteries,* Ex. Abs., Nagoya, Japan (1996) 196

[76] B.M. Way, J.R. Dahn, *J. Electrochem. Soc.* 141 (1994) 907

[77] A.M. Wilson, J.N. Reimers, E.W. Fuller, J.R. Dahn, *Sol. State Ionics* 74 (1994) 249

[78] J.R. Dahn, J.S. Xue, W. Xing, A.M. Wilson, A. Gibaud, *8th Int. Meet. Lithium Batteries,* Ex. Abs., Nagoya, Japan (1996) 89

[79] M. Ishikawa, M. Morita, M. Asao, Y. Matsuda, *J. Electrochem. Soc.* 141 (1994) 1105

[80] M.W. Verbrugge, B.J. Koch, *J. Electrochem. Soc.* 143 (1996) 24

[81] M. Dohzono, H. Katsuki, M. Egashiro, *J. Electrochem. Soc.* 136 (1989) 1255

[82] N. Takami, A. Satoh, M. Hara, T. Ohsaki, *J. Electrochem. Soc.* 142 (1995) 2564

[83] M. Morita, N. Nishimura, Y. Matsuda, *Electrochim. Acta* 38 (1993) 1721

[84] J. Beard, *New Scientist* 1918 (1994) 18

[85] C. Franklin, *New Scientist* 1948 (1994) 25

[86] J. Webb, *New Scientist* 1775 (1991) 30

Chapter 2

[1] S. Tobishima, M. Arakawa, J. Yamaki, *Electrochim. Acta* 35 (1990) 383

[2] J.O. Besenhard, G. Eichinger, *J. Electroanal. Chem.* 68 (1976) 1

[3] S. Tobishima, M. Arakawo, J. Yamaki, *Electrochim. Acta* 33 (1986) 239

[4] M. Ishikawa, M. Morita, M. Asao, Y. Matsuda, *J. Electrochem. Soc.* 141 (1994) 1105

[5] V.R. Koch, J.L. Goldman, C.J. Mattos, M. Mulvaney, *J. Electrochem. Soc.* 129 (1982) 1

[6] D. Aurbach, Y. Gofer, *J. Electrochem. Soc.* 136 (1989) 3198

[7] D. Aurbach, M.L. Daroux, P.W. Faguy, E. Yeager, *J. Electrochem. Soc.* 135 (1988) 1863

[8] G. Nazri, R.H. Muller, *J. Electrochem. Soc.* 132 (1985) 2054

[9] K.J. Hanson, L.J. Antony, R.A. Holland, *J. Electroanal. Chem.* 234 (1987) 107

[10] D.Skoog, D.West, F.J.Holler, *"Fundamentals of Analytical Chemistry"* 5th ed. (1988) Saunders College Publishing. pp. 349-51

[11] A.I.Vogel, *"Vogel's Quantitative Chemical Analysis"* 5th ed. (1989) Longman Scientific & Technical, pp. 637-8

[12] D.Skoog, D.West, F.J.Holler, *"Fundamentals of Analytical Chemistry"* 5th ed. (1988) Saunders College Publishing. p. 347

[13] D.Skoog, D.West, F.J.Holler, *"Fundamentals of Analytical Chemistry"* 5th ed. (1988) Saunders College Publishing. p. 343

[14] T.Fujinaga, K.Izutsu, *"Recommended Methods for Purification of Solvents and Tests for Impurities"* (1982) Pergamon Press Ltd., pp. 19-30

[15] D. Aurbach, M.L. Daroux, P.W. Faguy, E.A. Yeager, *J. Electrochem. Soc.* 134 (1988) 1611

[16] E.Cattaneo, B.Dasch, W.Vielstich, *J. Appl. Electrochem.* 21 (1991) 885

[17] J.R.Dahn, *Solid State Ionics* 69 (1994) 284

[18] D. Aurbach, I. Weissman, A. Zaban, O. Chusid, *Electrochim. Acta* 39 (1994) 51

[19] J.G. Thevinin, R.H. Muller, *J. Electrochem. Soc.* 134 (1987) 273

[20] F. Croce, B. Scrosati, *J. Power Sources* 43-4 (1992) 9

[21] J.R. Dahn, A.K. Sleigh, H. Shi, B.M. Way, W.J. Weydanz, J.N. Reimers, Q. Zhong, U. von Sacken, *Industrial Chemistry Library, 5 "Lithium Batteries - New Materials, Developments and Perspectives"* Ed. G. Pistoia (1994) Elsevier, pp. 1 - 47

[22] M.T. Weller, *"Inorganic Materials Chemistry"* (1994) Oxford University Press, pp. 8 - 14

[23] M.T. Weller, *"Inorganic Materials Chemistry"* (1994) Oxford University Press, pp. 24 - 25

[24] F. Michalak, *Ph.D. Thesis* (1995) INP Grenoble, France, p. 140

[25] A.M. Mood, F.A. Graybill, D.C. Boes, *"Introduction to the theory of statistics"* 3rd Ed. (1974) McGraw-Hill Book Co., pp. 222 - 233

[26] Personal correspondence with Prof. J.O. Thomas

[27] University of Southampton Summer School, July 1994, Experiment 9 "Instrumental Artifacts in AC Impedance Measurements"

[28] A.A. Pilla, P. Schmukler, *J. Electrochem. Soc.* 129 (1982) 526

[29] J.R. Owen, C.G. Thurston, *6th int. meeting on lithium batteries*, Münster, Germany May (1992), Ex. Abs. II-A-13, p. 272

Chapter 3

[1] A.N. Dey, *Ex. Abs. 8th Int. Meet. Lithium Batteries,* Nagoya, Japan (June 1996) pp. 5 - 7

[2] J.L. Walker, M.R. Jackson, C.T. Sims, *"Alloying"* (1988) ASM International, pp. 141 - 3

[3] W.C. Maskell, J.R. Owen, *J. Electrochem. Soc.* 132 (1985) 1602

[4] D. Fauteaux, R. Koksbang, *J. Appl. Elect.* 23 (1993) 1

[5] M.C. Smith, *"Alloy series in physical metallurgy"* (1956) Harper & Brothers, pp. 118 - 9

[6] A.D. Pelton, *Bull. Alloy Phase Diag.* 7 (1986) 223

[7] J. Aragane, K. Matsui, H. Andoh, S. Suzuki, H. Fukuda, H. Ikeya, K. Kitaba, R. Ishikawa, *Ex. Abs. 8th Int. Meet. Lithium Batteries,* Nagoya, Japan (June 1996) 18 - 21

[8] R.P. Elliot, *"Constitution of Binary Alloys"* 1st Suppl. (1965) McGraw-Hill Book Co., p. 584

[9] R.P. Elliot, *"Constitution of Binary Alloys"* 1st Suppl. (1965) McGraw-Hill Book Co., p. 375

[10] N.N. Tomashova, A.B. Yekavmev, *Elektrokhimiya* 27 (1991) 937

[11] D. Aurbach, Y. Gofer, *J. Electrochem. Soc.* 138 (1991) 3529

[12] E. Cattaneo, B. Dasch, W. Vielstich, *J. Appl. Electrochem.* 21 (1991) 885

[13] D. Aurbach, Y. Gofer, J. Langzam, *J. Electrochem. Soc.* 136 (1989) 3198

[14] D.H. Shen, S. Subbarao, F. Deligiannis, G. Halpert, *The Electrochem. Soc. Proc. Vol. 89 - 4 "Materials & Processes for Lithium, Batteries"* (1989) pp. 223 - 236

[15] R. Fong, M.C. Reid, R.S. McMillan, J.R. Dahn, *J. Electrochem. Soc.* 134 (1987)

516

[16] F. Croce, B. Scrosati, *J. Power Sources* 43-4 (1992) 9

[17] J.G. Thevenin, R.H. Muller, *J. Electrochem. Soc.* 134 (1987) 273

[18] R.F. Scarr, *J. Electrochem. Soc.* 117 (1970) 295

[19] S.V. Sazhin, A.V. Gorodyskii, M.Y. Khimchenko, S.P. Kuksenko, V.V. Danilin, *J. Electroanal. Chem.* 344 (1993) 61

[20] I.E. Eweka, J.F. Rohan, J.R. Owen, A.G. Ritchie, *Power Sources 15 'Research and Development in Non-Mechanical Electrical Power Sources'* (1995) pp. 241 - 52

[21] D. Aurbach, A. Zaban, *J. Electroanal. Chem.* 348 (1993) 155

[22] J.G. Thevenin, R.H. Muller, *J. Electrochem. Soc.* 134 (1987) 273

[23] B. Simon, J.P. Boeuve, *J. Power Sources* 43-4 (1993) 65

[24] R. Yazami, D. Guérard, *J. Power Sources* 43-4 (1993) 39

[25] C. Deportes, M. Duclot, P. Fabry, J. Fouletier, A. Hammou, M. Kleitz, E. Siebert, J.-L. Souquet, *"Electrochimie des Solides"* (1994) University Press of Grenoble, pp. 271 - 91

[27] Y. Geronov, F. Schwager, R.H. Muller, *J. Electrochem. Soc.* 129 (1982) 1422

[28] E. Peled, C. Menachem, D. Bar-Tow, A. Melman, *J. Electrochem. Soc.* 143 (1996) L4

[29] D. Aurbach, M.L. Daroux, P.W. Faguy, E. Yeager, *J. Electrochem. Soc.* 134 (1987) 1611

[30] G. Eichinger, *J. Electroanal. Chem.* 74 (1976) 183

[31] Y. Matsuda, S. Wang, J. Mondori, *J. Electrochem. Soc.* 142 (1995) 2914

[32] H.J. Pain, *"The Physics of Vibrations and Waves"* 4th Ed. (1993) John Wiley & Sons, pp. 308 - 9

[33] M. Arakawa, J-I. Yamaki, *J. Electroanal. Chem.* 219 (1987) 273

[34] B. Jungblut, E. Hoinkis, *Phys. Rev. B* 40 (1989) 10810

[35] T. Tran, K. Kinoshita, *J. Electroanal. Chem.* 386 (1995) 221

[36] J.R. Dahn, *Phys. Rev.* B 44 (1991) 9170

[37] A.J. Bard, L.R. Faulkner, *"Electrochemical Methods"* (1980) John Wiley & Sons, Inc., pp. 265 - 6

[38] M. Morita, N. Nishimura, Y. Matsuda, *Electrochim. Acta* 38 (1993) 1721

[39] P. Liu, H. Wu, *Sol. State Ionics* 92 (1996) 91

[40] J.R. Dahn, R. Fong, M.J. Spoon, *Phys. Rev.* B 42 (1990) 6424

[41] T. Ohzuku, Y. Iwakoshi, K. Sawai, *J. Electrochem. Soc.* 140 (1993) 2490

[42] D. Billaud, F. Henry, P. Willman, *Mol. Cryst. Liq. Cryst.* 245 (1994) 159

[43] Z. Jiang, M. Alamgir, K.M. Abraham, *J. Electrochem. Soc.* 142 (1995) 333

Chapter 4

[1] Electrode prepared at Danionics A/S.

[2] J.M. Tarascon, D. Guyomard, *Electrochim. Acta* 38 (1993) 1221

[3] J.R. Dahn, R. Fong, M.J. Spoon, *Phys. Rev.* B 42 (1990) 9170

[4] J.M. Chen, C.Y. Yao, C.H. Chen, W.M.Hurng, T.H.Kao, *7th Int. Meeting on Lithium Batteries* (1994) pp. 229-31

[5] A.J. Bard, L.R. Faulkner, *Electrochemical Methods* (1980) John Wiley & Sons, p. 105

[6] Z.X. Shu, R.S. McMillan, J.J. Murray, *J. Electrochem. Soc.* 140 (1993) L101

[7] J.R. Dahn, A.K. Sleigh, H. Shi, B.M. Way, W.J. Weydanz, J.N. Reimers, Q. Zhong, U. von Sacken, *Industrial Chemical Library 5 "Lithium Batteries"* (1994) Ed. G. Pistoia, Elsevier, pp. 1 - 47

[8] P. Zelenay, M. Winnicka-Maurin, J. Sobkowski,*J. Electroanal. Chem.* 278 (1990) 361

[9] J.E. Fischer, H.J. Kim, *Synth. Met.* 12 (1985) 137.

[10] Z.X. Shu, R.S. McMillan, J.J. Murray, *J. Electrochem. Soc.* 140 (1993) 922

[11] Cabot Carbons Ltd., Company literature

[12] A.Watanabe, K.Mori, H.Ishikawa, Y.Nakamura, *J. Electrochem. Soc.* 134 (1987) 1318

[13] V. Manev, I. Naidenov, B. Puresheva, P. Zlatilova, G. Pistoia, *J. Power Sources* 55 (1995) 211

[14] A.H. Whitehead, K. Edström, N. Rao, J.R. Owen, *J. Power Sources* 63 (1996) 41

[15] J.C. Charlier, X. Gonze, J.P. Michenaud *Carbon* 32 (1994) 289

[16] C.R. Houska, B.E. Warren *J. Appl. Phys.* 25 (1954) 1503

[17] R. Juza, V. Wehle *Natw.* 52 (1965) 560

[18] D. Aurbach, Y. Ein-Eli *J. Electrochem. Soc.* 142 (1995) 1746

[19] Z. Jiang, M. Alamgir, K.M. Abraham *J. Electrochem. Soc.* 142 (1995) 333

[20] N. Takami, A. Satoh, M. Hara, T. Ohsaki *J. Electrochem. Soc.* 142 (1995) 371

[21] H. Miyazaki, C. Horie *Synth. Met.* 12 (1985) 149

[22] R. Nishitani, Y. Uno, H. Suematsu *Phys. Rev.* B27 (1983) 6572

[23] G. Kirczenow *Can. J. Phys.* 66 (1988) 39

[24] R. Yazami, Ph. Touzain *J. Power Sources* 9 (1983) 365

[25] H. Shi, J. Barker, M.Y. Saidi, R. Koksbang, *J. Electrochem. Soc.* 143 (1996) 3466

[26] T.D. Tran, J.H. Feikert, X. Song, K. Kinoshita, *J. Electrochem. Soc.* 142 (1995) 3297

[27] G. Li, Z. Lu, B. Huang, H. Huang, R. Xue, L. Chen, *Sol. State Ionics* 81 (1995) 15

[28] S. Atlung, K. West, *J. Power Sources* 26 (1989) 139

[29] Lonza Carbons Catalogue (1992) Lonza G + T Ltd.

Chapter 5

[1] A.H. Whitehead, M. Perkins, J.R. Owen, *J. Electrochem. Soc.* 144 (1997) L92

[2] F. Dismay, L. Aymard, L. Dupont, J-M. Tarascon, *J. Electrochem. Soc.* 143 (1996) 3959

Please note that internet addresses were correct at time of writing, but are liable to change.